ORSAY
Série A, n°
N° d'ordre :
1198

THÈSE

PRESENTEE

AU CENTRE D'ORSAY

UNIVERSITÉ PARIS-SUD

POUR OBTENIR

LE GRADE DE DOCTEUR ES-SCIENCES

PAR

Louis BIMBOT

Sujet de la thèse : Etudes de fonctions d'onde microscopiques par la diffusion inélastique de particules α de 166 MeV.

Soutenues le 30/11/1973 **devant la Commission d'examen**

MM. M. RIOU — Président.

B. TATISCHEFF
B. GIRAUD
H.D.HOLMGREN
} Examinateurs.

ORSAY
Série A, n°
N° d'ordre :

1198

THÈSE

PRESENTEE

AU CENTRE D'ORSAY

UNIVERSITÉ PARIS-SUD

POUR OBTENIR

LE GRADE DE DOCTEUR ES-SCIENCES

PAR

Louis BIMBOT

Sujet de la thèse : Etudes de fonctions d'onde microscopiques par la diffusion inélastique de particules α de 166 MeV.

Soutenues le 30/11/1973 **devant la Commission d'examen**

MM. M. RIOU — Président.

B. TATISCHEFF
B. GIRAUD
H.D.HOLMGREN
} Examinateurs.

Digitized by the Internet Archive
in 2026

https://archive.org/details/IA41548019_0029

REMERCIEMENTS

Je tiens à remercier vivement toutes les personnes qui m'ont permis de réaliser le travail de recherche qui fait l'objet du présent rapport :

Monsieur le Professeur M. RIOU tout d'abord qui m'a accueilli à Orsay dans la division de Physique Nucléaire et qui a toujours fait preuve à mon égard de compréhension et de bienveillance.

Messieurs I.BRISSAUD et B. TATISCHEFF qui m'ont constamment guidé pour que ces travaux puissent être menés à bien.

Madame N. WILLIS et Monsieur Y. LE BORNEC qui ont rendu le travail d'équipe particulièrement agréable et fructueux.

Messieurs M.K. BRUSSEL, V. COMPARAT et A. WILLIS et Mesdames G. DUHAMEL et N. FRASCARIA qui ont efficacement collaboré à la partie expérimentale.

Messieurs M. BOUTEN, V. GILLET, B. GIRAUD, M. RHO et A.P. ZUKER ainsi que Madame E.BARANGER et Mademoiselle M. SOYEUR qui nous ont communiqué avant leur publication des fonctions d'onde avec tous les éléments nécessaires pour en simplifier l'emploi dans nos calculs théoriques.

D'autre part la partie expérimentale ne s'est bien déroulée que grâce à l'habileté de Monsieur D. BOYER ; aux compétences de Messieurs M. BAYON, J.Y.MARTEL et F.REIDE pour l'électronique et à la coopération de toute l'équipe de conduite du Synchrocyclotron d'Orsay. Qu'ils trouvent ici l'expression de ma gratitude.

Des discussions fort intéressantes avec Messieurs B. GIRAUD, B. LORAZO, D. VAUTHERIN, M. VENERONI et A.P. ZUKER m'ont permis de lever très partiellement le voile cachant les secrets de la théorie. Je les en remercie bien vivement.

Pour la phase finale de présentation des résultats j'ai grandement apprécié les services de Madame S. BOUBY et Monsieur BRIEUGNE pour la réalisation des figures ; la frappe et l'impression ont été prises en charge par Mademoiselle M. PARE et effectuées par Mme PACALET et Monsieur GRISAUD avec soin et efficacité. Je leur exprime aussi toute ma reconnaissance.

Et enfin, à tous les amis oubliés par inadvertance mais qui ont joué un rôle dans l'accomplissement de ce travail j'adresse une pensée chaleureuse.

A tous un grand MERCI !

TABLE DES MATIERES

INTRODUCTION 3

I - TECHNIQUES EXPERIMENTALES 5

1 - Dispositif non achromatique 5

2 - Dispositif achromatique 6

3 - Calcul des sections efficaces absolues 6

4 - Choix des cibles étudiées 7

II - PRINCIPE DE L'ANALYSE DES SECTIONS EFFICACES DIFFERENTIELLES 9

1 - Détermination de l'interaction effective α-nucléon 10

2 - Effets d'échange 11

3 - Interaction coulombienne 11

4 - Discussion 11

III - DESCRIPTION SOMMAIRE DES METHODES DE CALCUL DES FONCTIONS D'ONDE UTILISEES 13

1 - Formalisme des quasi-particules 13

2 - Formalisme de diagonalisation exacte 17

3 - Interactions nucléon-nucléon des modèles utilisés 18

IV - RESULTATS EXPERIMENTAUX 21

1 - Résultats obtenus avec les isotopes de l'étain 23

2 - Résultats obtenus pour les niveaux 3^- du ^{40}Ca et du ^{208}Pb 35

3 - Ensemble des résultats obtenus avec les modèles de quasi-particules 39

4 - Résultats obtenus avec le modèle de diagonalisation exacte dans un espace de modèle en couche 63

CONCLUSION 65

REFERENCES BIBLIOGRAPHIQUES 69

AVERTISSEMENT

La présente thèse correspond à un travail de groupe échelonné sur plusieurs années. Les différentes publications des résultats obtenus sont réunies ici et accompagnées par une notice dégageant la ligne générale des recherches accomplies et les conclusions qui en découlent.

L'article n°1 (Phys. Rev. C Vol.6(1972) 595) montre dans le cas particulier des isotopes de l'étain les renseignements que l'on peut extraire de la diffusion élastique et inélastique de particules α .

L'article n°2 (Phys. Rev. C Vol.4(1971) 494) sert de justification à l'emploi de la diffusion inélastique de particules α de 166 MeV pour l'examen des fonctions d'ondes.

L'article n°3 (Nucl. Phys. A 210(1973) 397) présente un tableau presque complet des expériences réalisées et des résultats obtenus.

INTRODUCTION

La diffusion des particules α a toujours intéressé les physiciens nucléaires (1). Les caractéristiques quantiques simples (= 0, T = 0) de cette particule entrainent des simplifications de calcul. La grande énergie de liaison permet d'estimer, pour autant que l'on ne s'intéresse pas aux grands angles de diffusion, que le passage par des états intermédiaires complexes est peu probable. Les dimensions et la faible pénétrabilité qui en découle limitent les mécanismes mis en jeu aux effets de surface. Une des grandes difficultés de la physique des α reste le fait que c'est une particule composite et que son interaction avec les noyaux ou les nucléons du noyau est une moyenne des actions des quatre nucléons qui la composent. D'où des problèmes théoriques pour décrire l'interaction α-nucléon à partir de l'interaction nucléon-nucléon libre et pour traiter l'échange de nucléons entre la cible et le projectile.

La théorie de la DWBA microscopique (2) que nous utilisons pour les calculs des diffusions inélastiques nécessite la détermination d'un potentiel optique décrivant les voies d'entrée et de sortie de la particule α , d'un modèle nucléaire donnant les fonctions d'onde des différents états excités , et d'une interaction α-nucléon responsable de la transition étudiée. Les modèles nucléaires (3) existent depuis un certain temps et sont continuellement améliorés. Le potentiel optique utilisé se déduit de la diffusion élastique et il ne reste que l'interaction effective α-nucléon à déterminer.

Il est possible de rechercher, par la double convolution d'une interaction nucléon-nucléon avec des distributions de masse de la particule α et de la cible, un potentiel optique microscopique devant reproduire la diffusion élastique (4). Nous avons quant à nous utilisé une forme gaussienne de l'interaction α-nucléon et normalisé l'intensité pour décrire la diffusion élastique sur plusieurs noyaux avec des potentiels obtenus par convolution de cette interaction avec des densités de matière des noyaux cibles. Ensuite, ayant tous les éléments du calcul en DWBA, nous avons testé les fonctions d'onde par comparaison directe des sections efficaces mesurées et des prédictions théoriques.

Cette étude s'est déroulée parallèlement à celles de Schaeffer (5) pour des protons, Satchler (6) pour des α et des ^{3}He et plus récemment de Terrien (7) pour des protons et des particules composites. Les points importants et originaux de notre étude sont : la grande énergie des particules α (166 MeV soit 42 MeV par nucléon environ) ce qui diffère des expériences citées et présente l'avantage de diminuer les effets d'échanges ; l'analyse simultanée de la diffusion élastique (qui permet d'ajuster l'interaction effective pour l'énergie incidente considérée) et inélastique ; et enfin la systématique sur un grand nombre de noyaux et de modèles différents.

En plus des analyses de nos propres expériences, nous avons calculé les taux de transition électromagnétiques et les facteurs de forme de diffusion inélastique d'électrons, en approximation de Born,

pour les comparer aux valeurs expérimentales disponibles et tester séparément le modèle pour les protons. La diffusion inélastique de particules α fournit alors un renseignement supplémentaire sur les configurations de neutrons pour les noyaux $N > Z$.

Dans les chapitres qui suivent nous allons d'abord donner brièvement la description des dispositifs expérimentaux utilisés (I) puis exposer le formalisme de la méthode d'analyse utilisée (II). Viendra ensuite la description des modèles nucléaires microscopiques que nous avons pu introduire dans nos calculs (III), partie qui n'est jamais développée dans les articles inclus. La comparaison entre les résultats et l'expérience est par contre bien traitée dans ces publications et nous n'avons donc repris ici que les résultats nouveaux obtenus depuis. Enfin l'apport constitué par ce travail est résumé dans la conclusion et les possibilités d'améliorations ultérieures sont définies.

I - TECHNIQUES EXPERIMENTALES

Toutes les expériences ont été réalisées avec le faisceau externe de particules α de 166 MeV du Synchrocyclotron de l'Institut de Physique Nucléaire d'Orsay. Le faisceau était focalisé sur la cible au centre de la chambre à réaction. Les alphas diffusés étaient déflé-chis par un spectromètre magnétique pour analyser les impulsions donc les énergies. La mise en place d'un système achromatique a permis d'amé-liorer la résolution en énergie et de séparer les niveaux étudiés pour quelques noyaux supplémentaires. Pour les cibles très oxydables (Ca,Sr) un système de sas perfectionné a permis un montage sur le porte-cible sous vide évitant toute détérioration.

I.1 - DISPOSITIF NON ACHROMATIQUE

Une description circonstanciée des conditions expérimentales est donnée dans la thèse de 3ème cycle de Le Bornec (8). Je ne donnerai donc ici que les caractéristiques techniques essentielles :

a) Faisceau :

- Tache sur la cible 15 mm de haut x 8 mm de large
- Intensité $\approx$ 10 nA sur la cible
- Résolution $\approx$ 0.6 MeV avant la cible

b) Analyseur :

- Aimant horizontal de 120°, indice 1/2
- Rayon moyen 170 cm
- Objet à 260 cm de l'entrée des pièces polaires
- Dispersion $y = \frac{\Delta E(E+M)}{E(E+2M)} \times D$ $\qquad D = 707$

  (M et E étant la masse et l'énergie de la particule diffusée et ΔE la différence d'énergie entre 2 particules séparées par une distance y (en cm) dans un plan perpendiculaire à l'axe optique.)
- Diaphragme d'entrée donnant une résolution angulaire de 0°.7

c) Multidétecteur :

- Ensemble de 17 scintillateurs de sections 3,5 x 2,8 mm
- Plage couverte dans le plan focal 6 MeV (soit 22,5 cm)
- Photomultiplicateurs type 52 AVP de Radiotechnique
- Alimentation et amplification des signaux de chaque photomultiplicateur par plaquettes séparées interchan-geables
- Discriminateur à seuil sur chaque voie pour éliminer les autres particules diffusées traversant le spectro-mètre
- Grand scintillateur de 20 cm relié à un photomultipli-cateur double chaine (56 AVP) en coïncidence avec chacun des 17 petits scintillateurs pour éliminer le "bruit" de la salle.

d) Monitorage :

- Cylindre de Faraday pour $\theta_{Lab} \geq 9°$
- Mesureur à induction pour $\theta_{Lab} < 9°$

I.2 - DISPOSITIF ACHROMATIQUE

L'utilisation de deux spectromètres à dispersions compensées permet d'améliorer de façon appréciable la résolution des mesures. Le dispositif implanté à Orsay est décrit dans la thèse 3ème cycle de N. Frascaria (9). Je rappellerai les caractéristiques dans les conditions où nous l'avons employé.

a) Faisceau :

- Tache sur la cible 2cm x 2cm après analyse par le premier spectromètre magnétique
- Intensité $\approx$ 10 nA sur la cible
- Résolution 0.450 MeV au niveau de la détection dans le plan focal

b) Spectromètre magnétique de refocalisation :

- Aimant horizontal de 127°, indice 1/2
- Rayon moyen 125 cm
- Dispersion $y = \frac{\Delta E(E+M)}{E(E+2M)} \times D$ $\qquad D = 500$
- Diaphragme d'entrée pour ajuster la résolution angulaire à 0°9

c) Détecteur :

- Chambre à étincelles à localisation par distribution de courant
- Plage couverte : plus de 10 MeV (80 cm dans plan focal)
- Déclenchement par deux scintillateurs plastiques de 30cm x 2mm placés perpendiculairement au faisceau, reliés à des photomultiplicateurs double chaine (56 AVP) et dont les signaux sont mis en coïncidence pour identifier les particules
- Utilisation d'un diviseur digital pour corriger les variations éventuelles du courant total passant dans l'étincelle.

d) Monitorage :

- Cylindre de Faraday pour $\theta_{Lab} \geq 15°$
- Mesureur à induction pour $\theta_{Lab} < 15°$

I.3 - CALCUL DES SECTIONS EFFICACES ABSOLUES

Lors de l'emploi de l'hodoscope à 17 scintillateurs, le faible nombre de points définissant les pics et la perte éventuelle entre les scintillateurs a nécessité un planimétrage des courbes obtenues. Avec la chambre à étincelles une simple intégration du nombre de coups dans un pic donnait le même renseignement. Les valeurs absolues de $d\sigma/d\Omega$ ont été déduites d'une comparaison des sections efficaces de la réaction (α,α) sur l'hydrogène et de la réaction inverse $p + {}^4He$ pour une même énergie totale dans le centre de masse. Cette section efficace $p + {}^4He$

a été extrapolée de résultats à 40 MeV (10) et 55 MeV (11). Les erreurs obtenues sur les sections efficaces absolues de diffusion inélastique sont de l'ordre de 15% compte tenu des incertitudes de monitorage, d'étalonnage et de décomposition.

I.4 - CHOIX DES CIBLES ETUDIEES

L'étude systématique a été entreprise pour les noyaux légers et les noyaux lourds ayant au moins une couche ou sous-couche fermée en protons ou en neutrons, ou les deux. En dehors des limitations techniques le choix a été guidé par la possibilité de disposer de fonctions d'onde et de résultats expérimentaux de diffusion inélastique d'électrons. La liste est donnée dans le tableau n°1 avec les caractéristiques de chaque cible. Leurs dimensions minimales étaient d'environ 20 mm x 10mm.

Tableau n°1

Elément	Epaisseur de Cible $mg.cm^{-2}$	Pureté Isotopique %
^{12}C	29.08	98.9
^{24}Mg	15.40	99.9
^{28}Si	218.43	92.2
^{32}S	124.90	95.0
^{40}Ca	44.30	97.0
^{44}Ca	0.930	98.5
^{48}Ca	0.945	96.2
^{48}Ti	19.55	99.4
^{56}Fe	39.70	91.7
^{59}Co	47.55	100.
^{58}Ni	23.04	-
^{60}Ni	39.65	99.8
^{62}Ni	30.48	98.7
^{68}Zn	20.59	97.6
^{88}Sr	40.90	99.8
^{89}Y	47.50	100.
^{90}Zr	40.00	97.7
^{94}Zr	29.99	96.5
^{92}Mo	38.77	98.3
^{116}Sn	25.40	95.7
^{118}Sn	25.40	96.6
^{120}Sn	12.40	98.1
^{124}Sn	11.86	94.7
^{140}Ce	70.86	88.5
^{208}Pb	23.55	99.1

Caractéristiques des cibles utilisées dans l'étude systématique de la réaction (α, α') à 166 MeV.

II - PRINCIPE DE L'ANALYSE

DES SECTIONS EFFICACES DIFFERENTIELLES

Les particules α accélérées ayant 166 MeV (soit ≃ 42 MeV par nucléon) la DWBA est le formalisme le mieux adapté pour le calcul théorique des sections efficaces différentielles. Les conditions d'application de l'approximation de Born sont bien connues et se résument comme suit : l'interaction perturbe peu la cible ; la diffusion élastique est prépondérante par rapport à toutes les voies ouvertes et le recouvrement entre les fonctions d'onde décrivant la cible et le noyau résiduel est important. Ces conditions sont toujours remplies dans le cas des réactions de diffusion inélastique étudiées ici. Pour les cibles de spin 0 on a alors(2) :

$$\frac{d\sigma}{d\Omega}(\theta) = \left(\frac{\mu}{2\pi\hbar^2}\right)^2 \times \frac{k_f}{k_i} \sum_{M_f} |T_{if}^{M_f}|^2 \qquad (1)$$

et l'amplitude de transition se calcule suivant la formule :

$$T_{if}^{M_f} = \int d\vec{r}\ \chi_f^-(\vec{k}_f,\vec{r}) < f\ |V(\vec{r},\vec{r}')|\ i > \chi_i^+(\vec{k}_i,\vec{r}) \qquad (2)$$

$|i>$ et $|f>$ sont les fonctions d'onde des états initial et final du noyau cible ; χ_i^+ et χ_f^- sont les fonctions d'onde entrante et sortante solutions de l'équation de Schrödinger pour le potentiel optique ; $\vec{k}_i$ et $\vec{k}_f$ sont les vecteurs d'onde des particules incidentes et diffusées ; $\vec{r}$ est la distance entre le centre de masse de l'alpha et celui du noyau ; μ est la masse réduite du système α-noyau cible et $<f|V(\vec{r},\vec{r}')|i>$ est le facteur de forme de diffusion inélastique associé à l'interaction $V(\vec{r},\vec{r}')$.

Trois points apparaissent alors importants : la valeur de l'interaction effective alpha-nucléon (et une grande partie de notre travail a porté sur ce sujet), la détermination du potentiel optique (donc des ondes distordues) et enfin la description du noyau par le calcul de fonctions d'ondes nucléaires.

Ce dernier point fera l'objet d'un chapitre spécial et nous allons montrer maintenant que les deux autres points peuvent être reliés et traités simultanément.

II.1 - DETERMINATION DE L'INTERACTION EFFECTIVE α - NUCLEON.

Dans les approches microscopiques de description des réactions nucléaires le potentiel optique responsable de la diffusion peut se calculer à partir d'une interaction nucléon-nucléon et des distributions de masse des noyaux cible et projectile. Cela donne la partie réelle du potentiel optique à laquelle il est indispensable d'ajouter (surtout pour les alphas de 166 MeV) une partie imaginaire, celle-ci pouvant être postulée proportionnelle à la partie réelle ; une telle proportionnalité étant approximativement vérifiée dans les analyses par les potentiels phénoménologiques de Woods-Saxon.

Pour notre part, nous avons repris l'idée de Glendenning et Vénéroni (12) d'une interaction α-nucléon obtenue par la convolution d'une interaction effective nucléon-nucléon de forme gaussienne rendant compte de la diffusion à basse énergie et d'une distribution de masse de l'α supposée gaussienne afin de donner une interaction α-N de forme gaussienne également. Les paramètres ont été recalculés par Bernstein(1) qui obtient les valeurs numériques : $V_0 = -37$ MeV et $\lambda_D = 2{,}0$ fm pour une interaction

$$V_{\alpha\text{-}N} = V_0 \, e^{-(r/\lambda_D)^2}$$

Cette interaction a été utilisée pour calculer, pour différents noyaux dont les densités de masse sont supposées connues, un potentiel optique microscopique par application de la relation :

$$V_{opt} = (U_R + iU_I) \int_0^\infty \rho(\vec{r}\,') \, V_{\alpha\text{-}N}(|\vec{r}-\vec{r}\,'|) \, d\vec{r}\,'$$

et une recherche de U_R et U_I par une méthode de moindres carrés sur les calculs des sections efficaces de diffusion élastique.

$\vec{r}\,'$ est le rayon vecteur coordonnée interne dans le noyau cible

$\rho(\vec{r}\,')$ la densité de matière nucléaire et $V_{\alpha\text{-}N}$ dépend de la distance entre la particule α et un point du noyau donc de $|\vec{r}-\vec{r}\,'|$.

Cette procédure sert essentiellement à relier globalement les phénomènes de diffusion à une interaction alpha-nucléon sans prétendre décrire le comportement exact de l'alpha au voisinage du noyau. Les valeurs obtenues pour U_R et U_I sont données dans le tableau n°2. Ces valeurs sont très proches quel que soit le noyau et valent en moyenne pour notre énergie :

$$\bar{U}_R = 0.70 \quad \text{et} \quad \bar{U}_I = 0.35.$$

Tableau n°2

Cible	Densité	U_R	U_I	x^2/N
^{12}C	S.M.	0.71	0.32	24.0
^{28}Si	Fermi	0.66	0.27	13.8
^{120}Sn	Fermi	0.75	0.39	29.0
^{120}Sn	H.F.	0.69	0.36	32.5
^{208}Pb	Fermi	0.72	0.39	24.0
^{208}Pb	H.F.	0.61	0.33	24.0
$\bar{U}_R = 0.70$			$\bar{U}_I = 0.35$	

Coefficients de renormalisation de l'interaction effective α-nucléon déduits de l'étude de la diffusion elastique.

Ces coefficients peuvent être interprétés comme une renormalisation de l'interaction effective α-nucléon tenant compte des processus complexes de la diffusion (échanges, diffusions multiples). L'utilisation de cette interaction pour l'étude de la diffusion inélastique suppose de plus que les mécanismes estimés par l'intermédiaire de $\bar{U}_R$ et $\bar{U}_I$ sont globalement les mêmes dans les deux processus de diffusion.

II.2 - EFFETS D'ECHANGE

Parmi les effets négligés, l'échange entre un nucléon de la cible et un nucléon de l'α peut être calculé de façon approchée suivant une méthode proposée par R. Schaeffer (13). Il faut pour cela ajouter à l'interaction α-nucléon un pseudopotentiel qui dépend de l'énergie incidente pour tenir compte de la non-localité de l'effet d'échange. Ce calcul fait intervenir l'approximation de Perey-Saxon et est explicité en détail dans la réf.13, dans laquelle il est estimé que les échanges plus complexes de plusieurs nucléons sont peu probables et que l'approximation ainsi faite est suffisante, tout au moins dans son ordre de grandeur.

Dans notre cas, l'interaction directe étant $V_D = -37\ e^{-(r/2)^2}$, l'interaction d'échange est donnée par $V_E = -40\ e^{-(r/1{,}31)^2}$. La nouvelle interaction $V_{\alpha\text{-}N} = V_D + V_E$ est alors renormalisée par un nouveau calcul de $\overline{U}_R$ et $\overline{U}_I$ pour obtenir les distributions angulaires de diffusion élastique sur les noyaux étalons. Les nouvelles valeurs sont $\overline{U}_R = 0.64$ et $\overline{U}_I = 0.34$ assez proches des anciennes valeurs. Cette première correction au terme direct se fait surtout sentir aux grands angles puisque le pseudopotentiel est de plus faible portée mais l'importance reste partout assez faible n'atteignant qu'un maximum de 35%, pour le 2^+ du ^{12}C, dans l'augmentation des sections efficaces.

II.3 - INTERACTION COULOMBIENNE

Pour les protons, l'interaction $V_{\alpha\text{-}N}$ est améliorée par l'addition de la répulsion coulombienne. Dans l'hypothèse d'une sphère uniformément chargée il faut ajouter un terme, constant jusqu'à 1 fm, et égal à 2.88 MeV/r au-delà. Cette interaction, incluse dans notre calcul, n'entraîne qu'une faible diminution des sections efficaces calculées.

II.4 - DISCUSSION

Nous avons donc ainsi calculé l'interaction $V_{\alpha\text{-}N}$ la plus apte à rendre compte de la diffusion élastique de particules α de 166 MeV sur un noyau quelconque.

Les calculs faits avec des interactions N-N différentes, en particulier celles de Wong (30) et de Tang (31) ne présentent que des patites variations sur les valeurs des profondeurs (10%) et des portées (7%) de l'interaction α-nucléon. Notre méthode de renormalisation compense les variations de profondeur par des variations de $\overline{U}_R$ et $\overline{U}_I$. L'influence de la portée a été examinée et les incidences sur les résultats sont négligeables dans les limites des forces envisagées. Les incertitudes sur nos résultats proviennent donc principalement de l'utilisation de $\overline{U}_R$ et $\overline{U}_I$ pour tous les noyaux. La faiblesse relative des écarts observés pour les noyaux étalons par rapport aux valeurs moyennes entraîne pour notre méthode une précision globale de l'ordre de 20%.

La signification exacte des coefficients $\overline{U}_R$ et $\overline{U}_I$ et la nature des grandeurs cachées que ces paramètres renferment dépassent le cadre de cet ouvrage car cela pose entre autre le problème théorique ardu de l'interprétation microscopique de la partie imaginaire du potentiel optique. Nos efforts n'ont pas porté sur l'étude précise de ces coefficients mais plutôt sur la détermination d'une interaction α-nucléon permettant de tester des fonctions d'onde. La solution cohérente adoptée pour l'étude de la diffusion élastique et inélastique s'est rapidement révélée satisfaisante dans la restitution des formes des distributions angulaires et nous n'avons pas poussé plus loin l'investigation des

différentes solutions pouvant apporter des résultats identiques telles que par exemple l'utilisation d'une partie imaginaire de l'interaction donnée par la dérivée d'un potentiel optique macroscopique phénoménologique, bien que cette procédure se soit révélée efficace à plus basse énergie (6,7). Un problème reste posé car cette deuxième méthode donne des facteurs de forme plus à l'extérieur du noyau. Peut-être alors les tests portent-ils sur deux parties légèrement différentes des fonctions d'ondes? Cependant nous gardons une bonne continuité avec les résultats à plus basse énergie pour les noyaux de référence. Nous avons donc poursuivi notre étude systématique dans le cadre microscopique pour avoir des comparaisons directes et sûres des différents modèles.

Tableau n°3

	V(MeV)	r_R (fm)	a_R (fm)	W(MeV)	r_I (fm)	a_I (fm)	χ^2/N
^{12}C	100.9	1.21	0.76	14.7	1.86	0.48	2.50
^{24}Mg	97.7	1.30	0.77	26.5	1.63	0.53	6.40
^{28}Si	109.7	1.25	0.81	24.6	1.63	0.51	0.55
^{32}S	116.8	1.22	0.82	20.4	1.67	0.52	2.57
^{40}Ca	112.9	1.24	0.79	20.7	1.62	0.55	4.15
^{48}Ca	106.9	1.29	0.77	21.5	1.59	0.65	0.70
^{58}Ni	107.4	1.27	0.75	22.6	1.59	0.50	3.72
^{60}Ni	103.8	1.28	0.71	25.3	1.51	0.63	2.08
^{62}Ni	115.7	1.20	0.80	21.6	1.53	0.64	2.70
^{88}Sr	116.0	1.27	0.76	22.6	1.50	0.76	1.35
^{90}Zr	118.4	1.24	0.79	21.7	1.54	0.59	1.88
^{92}Mo	120.5	1.22	0.81	21.1	1.54	0.60	2.20
^{116}Sn	121.5	1.21	0.84	21.9	1.51	0.63	5.07
^{118}Sn	125.6	1.19	0.86	21.6	1.52	0.62	4.35
^{120}Sn	119.4	1.26	0.76	30.7	1.43	0.70	6.10
^{124}Sn	119.3	1.26	0.77	28.8	1.45	0.67	3.88
^{208}Pb	119.9	1.26	0.74	21.3	1.45	0.80	1.32

Paramètres des potentiels optiques de Woods-Saxon

$V_{opt} = -V[1+\exp(r-r'_R)/a_R]^{-1} - i\, W[1+\exp\ (r-r'_I)/a_I]^{-1}$

avec $r'_R = r_R A^{1/3}$ et $r'_I = r_I A^{1/3}$. Les profondeurs des potentiels sont en MeV, les rayons et les diffusivités sont en fm. La quantité

$\frac{\chi^2}{N} = \frac{1}{N} \sum_N \{ |(\frac{d\sigma}{d\Omega})_{exp} - (\frac{d\sigma}{d\Omega})_{th.}|^2 / (\Delta \frac{d\sigma}{d\Omega})^2_{exp.} \}$ traduit la qualité du fit.

L'interaction effective sert au calcul du facteur de forme nucléaire de diffusion inélastique ainsi qu'au calcul du potentiel par le procédé de convolution (potentiel optique que nous appellerons microscopique). On peut aussi rechercher indépendamment un potentiel optique macroscopique de type Woods-Saxon à 6 paramètres à partir des données expérimentales de diffusion élastique. Cela a été fait avec notre code JIB 4 (extension de JIB 3) et les résultats sont portés dans le Tableau n°3.

Le travail préliminaire à l'étude des fonctions est terminé. Il ne reste plus qu'à introduire dans les formules (1) et (2) les fonctions d'onde de différents modèles pour calculer les sections efficaces différentielles de diffusion inélastique et les comparer directement aux résultats expérimentaux.

III - DESCRIPTION SOMMAIRE DES METHODES DE CALCUL DES FONCTIONS D'ONDE UTILISEES

III.1- FORMALISME DES QUASI-PARTICULES (Méthode BCS)

Les fonctions d'onde que nous avons utilisées sont pour la plupart calculées dans un formalisme de quasi-particule, généralisation du modèle trou-particule, et utilisent les approximations des phases aléatoires (RPA) ou de Tamm-Dancoff (TDA). Rappelons ici le principe de ce genre de calcul (3).

Dans les noyaux à une couche fermée la force d'appariement constitue l'interaction résiduelle principale entre les particules de la couche incomplète. La transformation de Bogolioubov-Valatin appliquée aux états de la couche non fermée permet de définir des états de "quasi-particules" qui apparaissent comme des combinaisons linéaires des états de particules et de trous du champ de Hartree-Fock. La méthode permet d'interpréter les premiers niveaux des noyaux pair-impairs comme états à une quasi-particule indépendante. Les états des noyaux pair-pair que nous étudions sont alors décrits par l'introduction d'une interaction entre les quasi-particules indépendantes préalablement déterminées.

En seconde quantification l'hamiltonien nucléaire phénoménologique peut s'écrire

$$H = \sum_{jm} \varepsilon_j : \eta^+_{jm}\eta_{jm} : + \frac{1}{4} \sum_{\substack{j_1m_1j_2m_2 \\ j_3m_3j_4m_4}} \langle j_1m_1j_2m_2|V|j_3m_3j_4m_4\rangle : \eta^+_{j_1m_1}\eta^+_{j_2m_2}\eta_{j_4m_4}\eta_{j_3m_3} :$$

L'énergie E_0 de l'état Hartree-Fock dans lequel tous les niveaux sont remplis jusqu'au niveau de Fermi a été négligé ce qui entraîne que les énergies sont relatives. Les énergies de Hartree-Fock (ε_j) n'ont de signification physique simple que pour les noyaux à double couche fermée plus ou moins un nucléon où il s'agit des énergies de particules ou trous indépendants et peuvent alors être déduites des mesures expérimentales. Dans les autres cas ces énergies sont des paramètres. L'interaction résiduelle nucléon-nucléon V peut être effective ou réaliste selon les modèles et doit satisfaire à des conditions d'invariance simples. Sa description fera l'objet d'un chapitre séparé.

Les opérateurs de création (η^+_{jm}) ou de destruction (η_{jm}) d'un nucléon dans l'état $|jm\rangle$ sont définis par rapport au vide $|0\rangle$ tel que :

$$\eta_{jm}|0\rangle = 0 \quad \forall\ j \text{ et } m$$

Pour décrire l'appariement des nucléons Bogolioubov et Valatin ont proposé la transformation canonique suivante :

$$\eta^{+}_{jm} = u_j \, \xi^{+}_{jm} - (-)^{j-m} v_j \, \xi_{j-m}$$

$$\eta_{jm} = u_j \, \xi_{jm} - (-)^{j-m} v_j \, \xi^{+}_{j-m}$$

définissant des opérateurs de création (ξ^{+}_{jm}) et de destruction (ξ_{jm}) de "quasi-particules" mélange de particule et de trou de même moment angulaire.

Le vide relatif à ces nouveaux opérateurs est donné selon Bardeen-Cooper-Schiffer par :

$$|BCS> = \pi_{jm} \, [u_j + (-)^{j-m} v_j \eta^{+}_{jm} \eta^{+}_{j-m}] |0>$$

telle que $\xi_{jm}|BCS> = 0 \quad \forall \; j \text{ et } m$

Le problème est de déterminer u_j et v_j pour que l'énergie de l'état $|BCS>$ soit minimale compte tenu de la normalisation et d'une condition de conservation du nombre moyen de particules. Cela conduit aux équations du "gap" :

$$2(\tilde{\varepsilon}_j - \lambda) u_j v_j + (u_j^2 - v_j^2) \Delta j = 0$$

$$u_j^2 + v_j^2 = 1$$

avec : $\tilde{\varepsilon}_j = \varepsilon_j + \sum_{ij} \frac{2J+1}{2J_j+1} <(ji)J|V|(ji)J> v_i^2$

$$\Delta_j = -\frac{1}{2} \sum_j \left(\frac{2J_i+1}{2J_j+1} \right)^{1/2} <(jj)0|V|(ii)0> u_i v_i$$

Le choix des phases est tel que $<(ii)0|V|(jj)0> \geq 0$

Ce système d'équations conduit à :

$$u_j^2 = \frac{1}{2} \left(1 + \frac{\tilde{\varepsilon}_j - \lambda}{\sqrt{(\tilde{\varepsilon}_j - \lambda)^2 + \Delta_j^2}} \right) \qquad v_j^2 = \frac{1}{2} \left(1 - \frac{\tilde{\varepsilon}_j - \lambda}{\sqrt{(\tilde{\varepsilon}_j - \lambda)^2 + \Delta_j^2}} \right)$$

Si l'on considère l'Hamiltonien nucléaire dans la représentation de Bogolioubov-Valatin

$$H' = H - \lambda N = H'_{00} + H'_{11} + H'_{20} + H'_{int}$$

on peut le décomposer en 4 termes :

H'_{00} qui ne dépend pas de ξ ni de ξ^{+} donne l'énergie du fondamental :

$$\langle BCS|H'_{00}|BCS\rangle = E_{BCS}$$

H'_{11} qui est diagonal et donne les énergies de quasi-particules

$$H'_{11} = \sum_j E_j \xi_j^+ \xi_j \quad \text{avec} \quad E_j = \sqrt{(\tilde{\varepsilon}_j - \lambda)^2 + \Delta_j^2}$$

H'_{20} est identiquement nul si les équations du gap sont satisfaites.

$H'_{int.}$ correspond à l'interaction résiduelle entre quasi-particules et est négligé dans l'approximation des quasi-bosons ou quasi-particules indépendantes.

En faisant abstraction des couches fermées un calcul BCS consiste donc à calculer un spectre des énergies E_j des quasi-particules indépendantes après avoir choisi les paramètres de l'interaction effective nucléon-nucléon et un ensemble d'énergies propres ε_j, ce choix étant modifié jusqu'à reproduire les valeurs expérimentales connues des E_j. Dans la méthode d'inversion des équations du Gap (14) (IGE) on calcule l'intensité V_0 de l'interaction nucléon-nucléon et les valeurs des $\tilde{\varepsilon}_j$ en déduisant ces quantités des résultats connus donnant les énergies de quasi-particules indépendantes et des différences de masse des noyaux pair-impairs.

Le passage aux noyaux pair-pairs à une couche fermée se fait par l'introduction d'une interaction résiduelle entre les quasi-particules. On pose donc $H = H' + \nu$ et l'on prend comme fonction d'onde le ket $|\psi^n\rangle$ donné par :

$$|\psi^n\rangle = \sum_i \chi_i^n \, |\phi_i\rangle \qquad |\phi_i\rangle \text{ étant fonction d'onde propre de } H'.$$

Les χ_i^n sont solutions du problème séculaire

$$\sum_k (E_i \delta_{ik} + \langle\phi_i|\nu|\phi_k\rangle) \chi_k^n = E^n \chi_i^n$$

Les problèmes qui se posent sont :

- le choix de l'interaction
- la détermination de l'espace de configurations
- la diagonalisation de l'interaction résiduelle.

Ces trois problèmes sont liés mais dans les noyaux de Z élevé étudiés par ce modèle (Z>20) la diagonalisation exacte de l'interaction résiduelle est impossible. Deux méthodes d'approximation sont donc utilisées correspondant à des descriptions différentes des structures nucléaires du fondamental et des états excités.

L'approximation de Tamm-Dancoff consiste à décrire les états excités comme des structures de deux quasi-particules construites sur l'état de référence $|BCS\rangle$. D'une façon générale, ces configurations sont notées :

$$|\phi_{\alpha\beta}^{JM}\rangle = \sum_{\substack{m_\alpha \\ m_\beta}} \langle j_\alpha j_\beta m_\alpha m_\beta | JM\rangle \, \xi_\alpha^+ \xi_\beta^+ |BCS\rangle$$

et le problème séculaire devient :

$$\sum_{\gamma\delta} \left\{ [E_\alpha + E_\beta]\delta_{\alpha\gamma}\ \delta_{\beta\delta} + \langle \phi^{JM}_{\alpha\beta} | v | \phi^{JM}_{\gamma\delta} \rangle \right\} \chi^{nJ}_{\gamma\delta} = E^{nJ}_{\alpha\beta}\ \chi^{nJ}_{\alpha\beta}$$

où $E_\alpha + E_\beta$ est l'énergie de la configuration à deux quasi-particules,

E^{nJ} et χ^{nJ} les valeurs propres et les amplitudes de la fonction d'onde $|\psi^n\rangle$ correspondante. Les éléments de matrice $\langle \phi^{JM}_{\alpha\beta} | v | \phi^{JM}_{\gamma\delta} \rangle$ prennent dans ce cas une forme simple permettant la résolution du problème séculaire et la détermination des fonctions d'ondes.

L'approximation des Phases Aléatoires suppose que les états excités diffèrent de l'état fondamental par des paires de quasi-particules en plus ou en moins. L'état fondamental est alors redéfini comme l'état orthogonal à tous les états excités et ne contient par suite qu'un nombre pair de paires de quasi-particules. Pour traiter le problème on définit des opérateurs de création et d'annihilation de paires de quasi-particules.

$$\Omega^+_{JM}(\alpha\beta) = \sum_{m_\alpha m_\beta} \langle j_\alpha j_\beta m_\alpha m_\beta | JM \rangle \xi^+_{j_\alpha m_\alpha} \xi^+_{j_\beta m_\beta}$$

$$\Omega_{JM}(\alpha\beta) = \sum_{m_\alpha m_\beta} \langle j_\alpha j_\beta m_\alpha m_\beta | JM \rangle \xi_{j_\alpha m_\alpha} \xi_{j_\beta m_\beta}$$

et les opérateurs de création et de destruction d'un état sont donnés par :

$$Q^+_{nJM} = \sum_{\alpha\ \beta} \chi^n_{\alpha\beta}\ \Omega^+_{JM}(\alpha\beta) - (-)^{J+M}\ Y^n_{\alpha\beta}\ \Omega_{J-M}(\alpha\beta)$$

$$Q_{nJM} = \sum_{\alpha\ \beta} \chi^n_{\alpha\beta}\ \Omega_{JM}(\alpha\beta) - (-)^{J-M}\ Y^n_{\alpha\beta}\ \Omega^+_{J-M}(\alpha\beta)$$

tels que $|nJM\rangle = Q^+_{nJM}|f\rangle$ et $Q_{nJM}|f\rangle = 0 \qquad \forall |nJM\rangle$

Le traitement analogue du problème séculaire dans ce formalisme mène à la résolution d'équations couplées pour le calcul de $\chi^n_{\alpha\beta}$ et $Y^n_{\alpha\beta}$:

$$(E_\alpha + E_\beta)\chi^n_{\alpha\beta} + \sum_{\gamma\delta} \langle \alpha\delta | v | \beta\gamma \rangle \chi^n_{\gamma\delta} - \sum_{\gamma\delta} \langle \alpha\gamma | v | \beta\delta \rangle Y^n_{\gamma\delta} = E^n \chi^n_{\alpha\beta}$$

$$(E_\alpha + E_\beta)Y^n_{\alpha\beta} + \sum_{\gamma\delta} \langle \alpha\delta | v | \beta\gamma \rangle Y^n_{\gamma\delta} - \sum_{\gamma\delta} \langle \alpha\gamma | v | \beta\gamma \rangle \chi^n_{\gamma\delta} = -E^n Y^n_{\alpha\beta}$$

où E^n est l'énergie mesurée à partir de $E^f = 0$ et E_α et E_β sont les énergies de quasi-particules indépendantes.

La RPA introduit donc des corrélations dans le fondamental par l'intermédiaire des $Y^n_{\alpha\beta}$ qui correspondent à l'existence de paires de quasi-particules exclues de $|BCS>$, l'effet de cohérence de ces configurations amenant une amélioration nette des phénomènes collectifs que l'on cherche à décrire ($B(E\lambda)$, diffusion d'électrons et diffusion inélastique de particules en interaction forte) et des autres propriétés nucléaires.

Les modèles trou-particule utilisés pour les noyaux à double couche fermée correspondent au même formalisme et sont calculés avec les mêmes approximations mais en limitant les états possibles à des états de quasi-particules d'un type bien déterminé formé par une particule couplée à un trou ce qui donne $u_\alpha = 1$, $v_\alpha = 0$ pour la "particule" et $u_\beta = 0$ $v_\beta = 1$ pour le "trou".

III.2- FORMALISME DE DIAGONALISATION EXACTE

Pour des noyaux relativement légers des méthodes de calcul permettent une diagonalisation exacte, dans un espace restreint mais souvent très acceptable, de la matrice hamiltonienne donnant les fonctions d'onde d'un très grand nombre de niveaux. Un champ moyen sert à calculer les couches de l'espace que l'on doit considérer. Une interaction résiduelle entre les nucléons emplissant les orbites est aussi définie. Les propriétés du noyau considéré sont alors déterminées par un choix du nombre de nucléons "actifs" et des orbites disponibles. Un formalisme général dû à French (15) permet d'exprimer simplement les quantités apparaissant dans ces calculs à partir des coefficients de parentage fractionnels. Cela fait appel à l'algèbre des opérateurs tensoriels irréductibles et à la représentation des opérateurs en seconde quantification. Les opérateurs à un corps et deux corps vont donner lieu à des transferts de nucléons entre couches définies par des nombres quantiques différents. Il est intéressant de les représenter à partir des opérateurs de création et d'annihilation de particules (A et B) ce qui les factorise en opérateurs agissant sur une seule couche.

Plus généralement on peut ainsi développer couche par couche tout opérateur tensoriel irréductible en introduisant un nombre quantique supplémentaire dans chaque couche représentant la différence entre le nombre d'opérateurs de création et d'annihilation.

Le calcul des éléments de matrice à plusieurs couches peut alors se simplifier par une factorisation d'éléments de matrice à une couche reliés, pour les opérateurs à un ou deux corps, aux coefficients de parentage fractionnels, donc aisément calculables. Le programme utilisé pour ces calculs a été mis au point à Oakridge par S.S.M.Wong et al. et est décrit dans la référence 15.

Les calculs que nous avons faits : $B(E_L)$, facteur de forme de diffusion inélastique d'électrons et sections efficaces de diffusion inélastique de particules α ne font intervenir que des opérateurs à un corps et ne nécessitent que la connaissance des éléments de matrice réduits de produits d'opérateurs élémentaires A et B entre les deux états considérés : $<JT||A^iB^j||J'T'>$ $\forall i$ et j servant à décrire $|JT>$ et $|J'T'>$ et renfermant toutes les caractéristiques du modèle. Ces valeurs nous ont été données par M.Soyeur et A.P.Zuker pour certains noyaux des couches (sd) et (fp).

III.3- L'INTERACTION NUCLEON-NUCLEON DANS LES MODELES NUCLEAIRES

Les calculs que nous venons de décrire nécessitent l'emploi d'une interaction résiduelle nucléon-nucléon. Celle-ci peut être choisie égale à l'interaction entre nucléons libres et doit alors reproduire les déphasages de diffusion nucléon-nucléon. De ce type de forces dites "réalistes" le potentiel de Tabakin donne de très bons résultats si l'on tient compte des corrections du second ordre (16). Il est donc fréquemment employé(16,25). Mais il est aussi possible d'utiliser une interaction indépendante des propriétés des nucléons libres, déterminée en essayant de traduire les propriétés expérimentalement observées des noyaux (énergie de particule, tailles nucléaires) à partir d'une forme analytique paramétrisée dont on calcule les coefficients. C'est la famille des potentiels "effectifs". Les conditions d'invariances imposent à cette force une certaine forme à trois termes : force centrale, force spin-orbite et force tenseur (3). Les deux derniers termes sont toujours négligés dans les calculs que nous considérons et la force centrale est exprimée en fonction de plusieurs paramètres. Une des formes généralement utilisée est la suivante :

$$V_{central} = V_0 F(r/\mu)\{a_0 + a_\sigma \vec{\sigma}_1.\vec{\sigma}_2 + a_\tau \vec{\tau}_1.\vec{\tau}_2 + a_{\sigma\tau}\, \vec{\sigma}_1.\vec{\sigma}_2\, \vec{\tau}_1.\vec{\tau}_2\}$$

r est la distance entre les nucléons
μ est la portée de l'interaction en fermi
$\vec{\sigma}$ et $\vec{\tau}$ sont les spin et isospin des nucléons,

Différentes formes peuvent être choisies pour le facteur de forme $F(r/\mu)$ et les valeurs des paramètres de mélange a_0, a_σ, a_τ et $a_{\sigma\tau}$ varient d'un auteur à l'autre. Le tableau n°4 donne les valeurs correspondant aux différents modèles que nous avons utilisés. Le tableau n°5 d'autre part récapitule les caractéristiques essentielles de ces modèles et sera une bonne référence pour les interprétations des comparaisons avec les résultats expérimentaux.

Tableau n°4

Modèle	F(r/μ)	V_0	a_0	a_σ	a_τ	$a_{\sigma\tau}$
G.G.R. (14)	Gaussien μ=1.7fm	IGE	0.26	-0.25	-0.31	-0.10
G.V.M. ^{12}C (26)	Gaussien	-40	0.00	-0.20	-0.30	-0.10
Eisenberg (24)	Gaussien	-40	0.012	-0.14	-0.29	-0.09
G.G.S. (17)	Gaussien					
	CAL	-40	0.15	-0.02	-0.22	-0.14
	COP	-40	0.60	0.10	-0.30	-0.30
Bouten (27)	2 Gaussiennes	-60	0.19	-0.16	-0.16	-0.16
Perez (23)	Yukawa	-40.8	0.0	0.12	-0.26	-0.01

C.B. (18) : Potentiel de Tabakin renormalisé
Dieperink (21) : Potentiel de Tabakin
Zuker (19) : Potentiel de Tabakin renormalisé.

Caractéristiques des interactions nucléon -nucléon utilisées dans les modèles

$$V_c = V_0 F(r/\mu)\{a_0 + a_\sigma \vec{\sigma}_1.\vec{\sigma}_2 + a_\tau \vec{\tau}_1.\vec{\tau}_2 + a_{\sigma\tau} \vec{\sigma}_1.\vec{\sigma}_2 \vec{\tau}_1.\vec{\tau}_2\}$$

Tableau n°5

Noyau	Modèle	réf.	Fonctions d'onde de particule individuelle	Force	Approximation	Résultats	
						J^π	λ
^{208}Pb	G.G.S.	17	O.H. b = 2.32 fm	C.O.P.(gaussienne)	R.P.A.	3^-	2.4
	G.G.R.	14	O.H. b = 2.50 fm	I.G.E.(gaussienne)	R.P.A.	3^-	1.0
$^{116,118,120,124}Sn$	C.B.	18	O.H. b = 2.22 fm	Tabakin renormalisé	T.D.A.	2^+ 3^-	1.5 1.3
	G.G.R.	14	O.H. b = 2.27 fm	I.G.E.(gaussienne)	R.P.A.	2^+ 3^-	2.0 1.7
$^{88}Sr, ^{90}Zr, ^{92}Mo$	G.G.R.	14	O.H. b = 2.13 fm	I.G.E.(gaussienne)	R.P.A.	2^+ 3^-	2.9 1.3
$^{58,60,62}Ni$	G.G.R.	14	O.H. b = 2.00 fm	I.G.E.(gaussienne)	R.P.A.	2^+ 3^-	2.1 1.5
	Zuker	19	O.H. b = 1.97 fm	Tabakin renormalisé	Diagonalisation	2^+	2.2
^{40}Ca	Dieperink	21	O.H. b = 1.87 fm	Tabakin	R.P.A.	3^-	0.8
	G.S.	20	O.H. b = 1.89 fm	C.A.L.(gaussienne)	R.P.A.	3^- 5^-	1.3 1.7
	S.M.	22	W.S.1 potentiel	Yukawa (1.25 fm)	R.P.A.	3^-	1.8
	Perez	23	W.S. plusieurs potentiels	Yukawa (1.54 fm)	T.D.A.	3^-	2.4
^{32}S	Einsenberg	24	O.H. b = 1.70 fm (b = 1.87 fm)	gaussienne	T.D.A.	2^+	5.5
^{28}Si	Einsenberg	24	O.H. b = 1.70 fm	gaussienne	T.D.A.	2^+	3.2
	Z.S.	25	O.H. b = 1.79 fm	Tabakin renormalisé	Diagonalisation	2^+	1.0
^{24}Mg	Z.S.	25	O.H. b = 1.78 fm	Tabakin renormalisé	Diagonalisation	2^+	1.0
^{12}C	G.V.M.	26	O.H. b = 1.66 fm	gaussienne	R.P.A.	2^+ 3^-	1.4 1.2
	Bouten	27	O.H. b = 1.64 fm	Volkov (2 gaussiennes)	H.F. projeté	2^+	1.0

Caractéristiques générales des modèles utilisés et résultats obtenus en diffusion inélastique de particules α de 166 MeV ($\lambda = [(d\sigma/d\Omega)_{exp.} / (d\sigma/d\Omega)_{th.}]^{1/2}$ est pris en valeur moyenne quand l'étude a porté sur plusieurs isotopes ou isotones).

IV - RESULTATS EXPERIMENTAUX
ET COMPARAISON AUX PREDICTIONS THEORIQUES

Les résultats expérimentaux sont donnés dans les articles ci-joints qui servent de base à la thèse. L'étude essentielle des modèles à particule-trou ou quasi-particules y est présentée en détail ; nous allons donc inclure ces articles ici en recommandant de porter attention aux chapitres des résultats expérimentaux.

Nous donnerons ensuite les résultats nouveaux obtenus par de récents calculs concernant le modèle de diagonalisation dans les couches (sd) et (fp) . Dans la conclusion nous essayerons de résumer l'ensemble des remarques qui se sont imposées lors de la comparaison des résultats expérimentaux avec les grandeurs calculées.Les valeurs numériques obtenues dans notre analyse systématique des sections efficaces de diffusion inélastique de particule α sont portées sur le Tableau 5 et résument clairement l'ensemble des résultats.

IV.1 - RESULTATS OBTENUS AVEC LES ISOTOPES DE L'ETAIN

PHYSICAL REVIEW C VOLUME 6, NUMBER 2 AUGUST 1972

Study of Some Properties of Tin Isotopes Through High-Energy Alpha-Particle Scattering

I. Brissaud, B. Tatischeff, L. Bimbot, V. Comparat, and A. Willis
Institut de Physique Nucléaire, 91 Orsay, France

and

M. K. Brussel
University of Illinois, Urbana-Champaign, Illinois 61801

(Received 23 July 1971)

Angular distributions of 166-MeV α particles scattered from the Sn isotopes 116, 118, 120, and 124 have been measured. An analysis of the elastic scattering data was performed using an optical potential calculated from an effective interaction between the α particle and a nuclear-matter distribution. The variation of nuclear sizes among the isotopes is considered. Assuming charge densities derived from the results of elastic electron scattering and/or mesonic atom data, values of neutron-matter radii for the tin isotopes are deduced which agree well with theoretical values. An analysis of the inelastic α-particle scattering to the first 2^+ and 3^- levels for each isotope was effected using the optical potentials calculated from the elastic scattering, the distorted-wave Born-approximation, and quasiparticle wave functions for the excited states. Electromagnetic transition rates and form factors for electron scattering were calculated with the same wave functions, and a comparison of the calculations to the experimental results provides information about the proton and neutron configurations in these isotopes.

I. INTRODUCTION

In a previous paper[1] the real part of the optical potential for 166-MeV α particles was calculated for several nuclei (from ^{12}C to ^{208}Pb) using an α-particle nuclear-matter effective interaction, $V^R_{\text{eff}}(\vec{r}, \vec{r}_\alpha)$, and a nuclear-matter distribution, $\rho(\vec{r})$. Thus,

$$V^R_{\text{opt}}(r_\alpha) = \int V_{\text{eff}}(\vec{r}, \vec{r}_\alpha)\rho(\vec{r})\, d\vec{r}\,. \tag{1}$$

The present work, in which we discuss α-particle scattering on the tin isotopes of mass number 116, 118, 120, and 124, is an extension, with experimental improvements, of the work of Ref. 1.

The nuclear-matter distribution, $\rho(\vec{r})$, is determined in the process of constructing an optical potential [Eq. (1)] from the α-nucleus elastic scattering cross sections. Our aim has been to study the precision of this determination in order to examine the feasibility of obtaining precise rms nuclear radii for the tin isotopes. With such radii at our disposal, electron elastic scattering data, which yield the charge densities of nuclei, are used to determine the radii corresponding to the neutron-matter densities. Little is known about these neutron densities at the present time.

Because the optical potentials used in the analysis are predetermined by the elastic scattering, and because the α–nuclear-matter effective interaction employed is the same in both the elastic and inelastic scattering calculations, the analysis made of inelastic scattering data in this work allows various microscopic wave functions which have been employed to describe the relevant excited states to be tested in a rather self-consistent framework. It has been our hope that such an analysis will finally permit comparisons with the experimental results to be made which will be sensitive enough to allow one to distinguish between

proposed theoretical wave functions.

In addition to the inelastic α-particle scattering data presented here, inelastic electron scattering data and electromagnetic transition rates are employed to define the neutron and proton contributions to the wave functions.

Experimental data for the elastic and inelastic scattering of α particles on tin exist at lower energies.[2,3] These data were analyzed with either phenomenological form factors in a distorted-wave Born approximation (DWBA) so as to extract the deformation parameters, β_l,[3] or with the Austern-Blair model so as to extract the deformation lengths, δ_l.[2] Recently, several authors[4] have calculated strong absorption radii of several nuclei via an analysis of α-particle elastic scattering. Scattering experiments on the tin isotopes using other projectiles also exist and have been analyzed with standard phenomenological methods. An extensive bibliography may be found in the work of Bruge *et al.*[2]

2. EXPERIMENTAL DETAILS

The 166-MeV α-particle beam of the Orsay synchrocyclotron was used in this experiment. The experimental layout is basically that described in Ref. 1, but was improved by use of a hodoscope containing 15 plastic scintillation detectors (each 3.5 mm wide) placed in the focal plane of the Orsay magnetic spectrometer. A 20-cm-wide scintillation detector placed behind the hodoscope array was required to be in time coincidence with the individual detectors for each event. An appreciable background, due mainly to tritons from (α, t) reactions, was observed for angles greater than 30°. This background was eliminated by use of electronic pulse-height discrimination. With this system a 4-MeV range of excitation energy could be covered in a single run. A sample spectrum (for ^{116}Sn) is shown in Fig. 1.

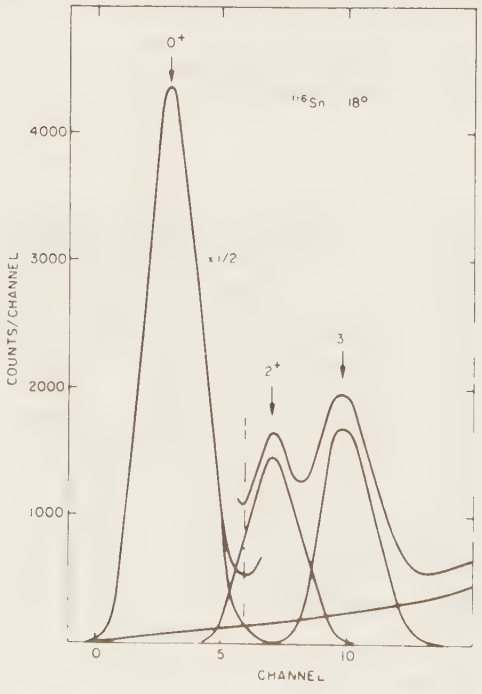

FIG. 1. Spectrum of α particles scattered from ^{116}Sn. The 2^+ state and 3^- state lie at 1.27 and 2.24 MeV, respectively.

The incident beam intensity was monitored with a Faraday cup except at scattering angles less than 9° (lab) when a secondary electron chamber was used. The isotopically pure targets of mass numbers 116, 118, 120, 124, had target thicknesses equal to 25.4, 25.4, 12.4, and 11.86 mg/cm^2, respectively. The total angular resolution was about 0.7°, and the measurements were taken at 1° increments between 5 and 44° (lab).

The absolute values of cross sections were determined by normalization of the reaction $H(\alpha, \alpha)H$ to the results of the inverse reaction $^4He(p, p)^4He$ of Brussel and Williams[5] and Hayakawa *et al.*[6] Estimates of the absolute experimental errors are indicated by bars on representative points of the cross-section curves. They vary between 5 and 10% for the elastic scattering, and between 15 and 20% for the inelastic scattering. The energy resolution during the experiment was about 900 keV full width at half maximum.

3. ELASTIC SCATTERING

The optical potential generated from Eq. (1) was calculated with an α–nuclear-matter effective interaction having a Gaussian form: $V_{eff}(\vec{r}, \vec{r}_\alpha) = V_0 \exp(-|\vec{r} - \vec{r}_\alpha|^2/\mu^2)$. As a starting point the values $V_0 = 37$ MeV and $\mu = 2.0$ fm were chosen, but the strength of the interaction was in fact renormalized by a factor U_R in order to help account for exchange and higher-order corrections not explicitly included in Eq. (1). Thus V_{eff} is replaced by $U_R V_{eff}$ in Eq. (1). U_R was determined by considering the matter density $\rho(r)$ of selected nuclei to be fixed, either from the phenomenological analysis of electron scattering measurements on $N = Z$ nuclei, or from Hartree-Fock calculations on heavy nuclei which yield charge distributions accurately consistent with electron scattering. [Since the Hartree-Fock calculations yield proton densities, it was necessary to fold in a proton size factor in order to obtain the charge (or proton matter) distributions.] Having made α-particle elastic scat-

tering measurements at 166 MeV on such selected nuclei,[1] U_R was adjusted so that an optimum least-squares fit to the measured differential cross sections was obtained. It was found[1] that the resultant values of U_R were approximately constant for the nuclei studied (from C to Pb), allowing one to meaningfully use an average value, $\bar{U}_R$, as characteristic of U_R. With the values of V_0 and μ given above, it was determined that $\bar{U}_R = 0.7$. Our previous experience[1] and the recent work of Batty, Friedman, and Jackson[4] show that there exists a correlation between $U_R V_0$ and μ, so that only one of these parameters needs to be adjusted in fitting the data.

Batty, Friedman, and Jackson[4] have indicated that the effective α-nucleon interaction cannot describe the free α-nucleon interaction data. For 166-MeV α-nucleus scattering, the α particles can penetrate beyond the outer surface of the nucleus and interact with nucleons in the nuclear interior which cannot be considered free. Consequently, conclusions derived from a comparison of the α-nucleon effective interaction with one which describes the free α-nucleon interaction are likely to be spurious at these energies. One would expect a coalescence of the two interactions only for low-energy α particles which scatter elastically from the outer skirts of the nucleus. U_R may be regarded as a parameter which normalizes our interaction so as to make it conform to the actual situation. Clearly, it will have an energy dependence which is related to that obtained from a phenomenological Woods-Saxon optical potential.[1] Bernstein and Seidler[7] have found, for example, in an analysis very similar to the one reported here that $U_R = 0.815$ for 104-MeV α particles.

The imaginary part of the optical potential W_I is assigned the same form as the real part, so that $W_I = (U_I/U_R)V_{\text{eff}}$. The average value of U_I, obtained as was U_R, has been found[8,9] to be $\bar{U}_I = 0.35$.

Figure 2 shows the differential cross sections

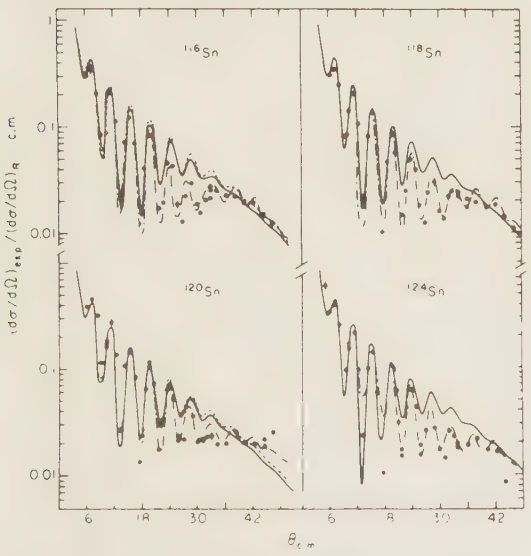

FIG. 2. Cross sections for the elastic scattering of 166-MeV α particles from isotopes of tin. The curves indicate cross sections generated from (a) Fermi distribution, ———; (b) Hartree-Fock distribution, - - - -; (c) six-parameter Woods-Saxon potential, — — — .

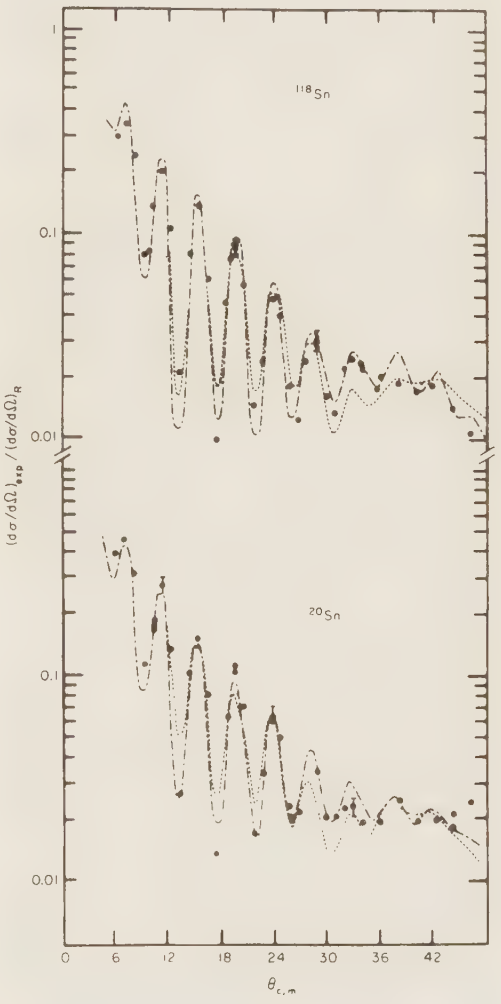

FIG. 3. Cross sections for the elastic scattering of 166-MeV α particles from isotopes of tin. The curves indicate cross sections generated from (a) six-parameter Woods-Saxon potential, — — — —; (b) four-parameter potential whose imaginary part has a Woods-Saxon (three-parameter) form , ····· .

TABLE I. Optical-model parameters for the six-parameter Woods-Saxon optical potential.

A	V_R (MeV)	r_R (fm)	a_R (fm)	W_I (volume) (MeV)	r_I (fm)	a_I (fm)
116	121.5	1.21	0.84	21.9	1.51	0.63
118	125.6	1.19	0.86	21.6	1.52	0.62
120	119.4	1.26	0.76	30.7	1.43	0.70
124	119.3	1.26	0.77	28.8	1.45	0.67

(the continuous line) calculated with an optical potential derived from a matter distribution having a Fermi shape, $\rho(r) = \rho_0[1 + e^{(r-c)/a}]^{-1}$, and the average effective interaction quoted above. Good agreement with experiment is obtained up to a scattering angle of 20°, but the agreement is relatively poor between 20 and 30°. Curves calculated with a Hartree-Fock matter distribution,[10] also plotted in Fig. 2 for ^{116}Sn and ^{120}Sn, are similar to those obtained with the Fermi distribution. (The Hartree-Fock distribution was generated[11] with a Brink-Boeker interaction.) It had been noted in Ref. 1 also that the optical-model analysis did not distinguish between the Fermi of the Hartree-Fock matter distributions in the case of tin: The two matter distributions were almost identical. Consequently, we consider here only the Fermi distribution whose analytical form is more convenient in applications where systematic parameter variations are made.

An arbitrary assumption of our method has been to take $W_I(r_\alpha)$ proportional to $V_R(r_\alpha)$. Alternately, one can modify the imaginary potential by using for it alone a Woods-Saxon potential of three parameters, retaining the real potential calculated by Eq. (1). The cross-section curve obtained with such a (four-parameter) potential is shown in Fig. 3, and it agrees with the experimental data throughout the angular range. For comparison purposes a conventional six-parameter Woods-Saxon potential was also used to fit the data (see Fig. 2). Its parameters are given in Table I. In Table II are given the parameters obtained (which are average values from the best fits to 166-MeV α-particle scattering data from 10 nuclei between carbon and lead) using the four-parameter form. The value of U_R obtained with the four-parameter form (0.66) is close to the value obtained (0.70) when the imaginary potential was given the same form as the real potential.

TABLE II. Average values of optical-model parameters for the four-parameter potential used to describe 166-MeV α-particle elastic scattering from tin.

U_R	W_I (volume) (MeV)	r_I (fm)	a_I (fm)
0.66	21.18	1.50	0.74

A comparison of the four experimental angular distributions (Figs. 2 and 3) shows that they are nearly the same except in the angular range 15–30°, where, although they have in-phase oscillations, their amplitudes vary. One reason for these differences appears in Fig. 4, which shows the Woods-Saxon potentials for the four isotopes together with the potentials constructed from a Fermi density function for ^{120}Sn in the 5–9-fm range (the important range for 166-MeV α particles). (The potentials for the other three isotopes are practically identical to those of Fig. 4.) The real components of both constructed and Woods-Saxon potentials all have the same shape, but the imaginary Woods-Saxon potentials differ appreciably from isotope to isotope. Thus, it appears that the addition of neutrons for the isotopes

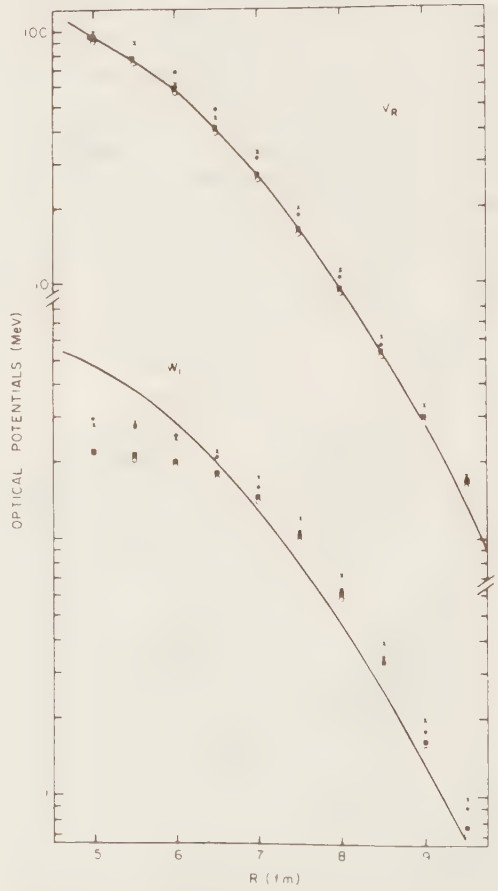

FIG. 4. Six-parameter Woods-Saxon optical potentials: ○, ^{116}Sn; ■, ^{118}Sn; ●, ^{120}Sn; ×, ^{124}Sn. The full lines correspond to the potentials calculated for ^{120}Sn from a Fermi distribution.

$A = 116$ to 124 does not affect the real potential appreciably, but does affect the imaginary potential, and this causes the fluctuations observed in the cross section. This may imply that the added neutrons lead to a larger number of inelastic channels. The disagreement of calculations and experiment at larger scattering angles thus probably indicates that other reaction mechanisms (for instance the transition through intermediate states) are involved which are not accounted for in a simple two-parameter model.

Determination of Neutron and Matter Radii

Charge distributions (assumed here to be synonymous with proton matter) are assumed to be known from electron scattering experiments or studies of muonic atoms. Hence one may try to deduce the value of neutron–matter radii from the determination of the over-all matter radii. We

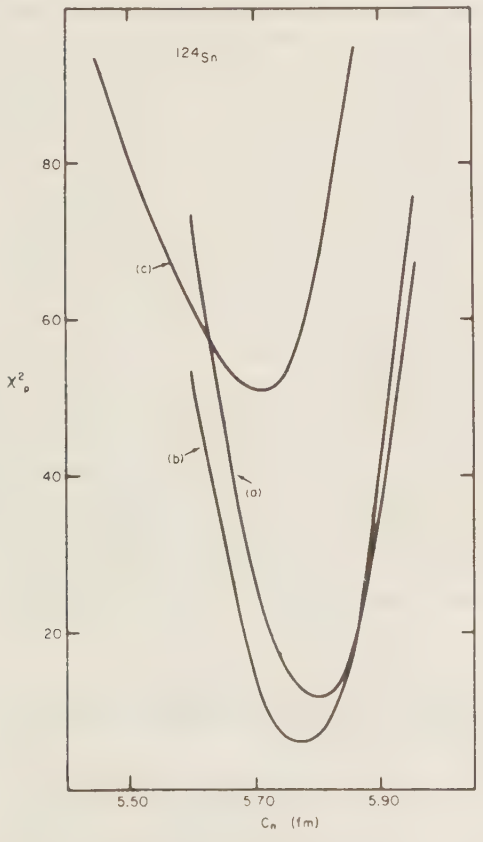

FIG. 5. χ^2_p versus c_n obtained by fitting the elastic scattering on ^{124}Sn to the theory outlined in text. The curves correspond to the angular ranges: (a) 0–20°; (b) 0–30°; (c) 0–42°.

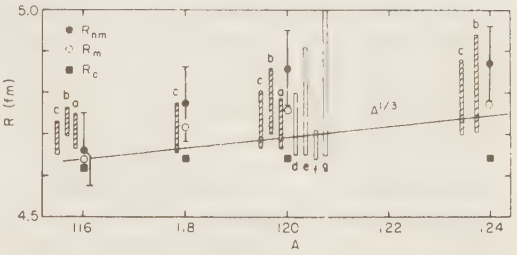

FIG. 6. Nuclear radii. Values extracted from this experiment: R_n and R_{nm}. The precisions indicated for R_n are the same as those for R_{nm}. Values extracted from other experimental and theoretical work are given by open and shaded rectangles, respectively. The precision of these results is not given. The bottom of each line indicates the R_c value, and the upper part indicates the R_{nm} value. The lengths of the line are to be compared to the differences between the full circles and the full squares. (a) Ref. 11; (b) Ref. 20; (c) Ref. 20; (d) Ref. 16; (e) Ref. 17; (f) Ref. 19; (g) Ref. 18.

assume a Fermi shape for the charge distribution whose parameters are defined with good accuracy by electron scattering. For the neutron–matter density a Fermi shape of the same diffuseness as that of the charge distribution was assumed. This is suggested by Hartree-Fock calculations, but has not been verified experimentally. The Fermi neutron-matter radius parameter c_n then remains the sole free parameter. An optical potential for each isotope is constructed as outlined previously. The fit of the elastic scattering experimental data by this potential defines, through use of a χ^2_p search routine, the parameters of the neutron-matter distribution and, consequently, rms neutron and matter radii:

$$\chi^2_p \equiv \frac{1}{N}\sum_{i=1}^{N}\left\{\left[\left(\frac{d\sigma}{d\Omega}\right)_{exp} - \left(\frac{d\sigma}{d\Omega}\right)_{th}\right] \Big/ \Delta\left(\frac{d\sigma}{d\Omega}\right)_{exp}\right\}^2 .$$

The errors incurred in determining the values of c_n are mainly due to the arbitrariness in selecting the angular range for the best-fit procedure. In Fig. 5 the variation of χ^2_p versus c_n for three angular ranges, (a) 0–20°, (b) 0–30°, and (c) 0–42°, is shown for ^{124}Sn. The positions of the χ^2_p minima for the three curves differ slightly (by 0.08 fm). For the four Sn isotopes, the angular range 0–20° was finally chosen for the analysis, since at larger angles the uncertainties mentioned in Sec. 2 render the significance of the fit ambiguous. In order to improve the precision obtained in the fitting procedure, the four-parameter Woods-Saxon potential mentioned in the previous section was used in the calculation in preference to the two-parameter (U_R, U_I) form. The four-parameter search of c_n was made for data lying in the 0–30 angular range. Smaller χ^2_p values were produced

than formerly, even though a set of values for radii of the neutron distributions were close to those obtained by the two-parameter form. If the total angular range had been employed, studies showed that the neutron-matter radius would have been modified by no more than 0.03 fm. The uncertainty introduced by the assumption that the diffuseness parameters a_n and a_p were equal did not prove important: A variation of ±10% for a_n produced a variation of 0.03 fm for the neutron radius.

In Fig. 6 and Table III the mean values obtained by the above methods are compared with the results of other analyses. Following general usage we define:

(a) The charge radius R_c: $R_c^2 = \int r^2 \rho_c(r) dr$. $\rho_c(r)$ is the charge distribution determined from electron scattering experiments.

(b) The proton distribution radius R_p: $R_p^2 = \int r^2 \rho_p(r) dr$. $\rho_p(r)$ is the point proton distribution density. $R_c^2 = R_p^2 + r_p^2$, where r_p is the rms charge radius of the proton ($r_p^2 = 0.64$ fm^2).

(c) The neutron distribution radius R_n: $R_n^2 = \int r^2 \rho_n(r) dr$. $\rho_n(r)$ is the point neutron distribution density of the nucleus.

(d) The neutron-matter radius R_{nm}: $R_{nm}^2 = R_n^2 + r_n^2$. We have assumed the neutron to have the same radius as the proton.

(e) The nuclear-matter radius R_m: $R_m^2 = [ZR_c^2 + (A-Z)R_{nm}^2]/A$.

Recalling that our effective interaction, parametrized by $\bar{U}_R$ (and hence μ[5] and $\bar{U}_I$, was determined with the use of "calibrating" *matter* densities, we note that its use at the present stage will in its turn allow us to determine the *matter* densities of the Sn nuclei. Only c_n, the neutron-*matter* radius parameter needs to be varied in the fitting procedure, and once this is determined from the best fit, R_{nm} is easily derived. [R_n can then be calculated from (c) above.]

The errors entering in the determination of R_{nm} include uncertainties which depend on the various assumptions made. The uncertainty of the parameters of the charge distribution and the assumption that the diffuseness parameters for the charge and the neutron-matter distributions are equal, the experimental uncertainties of the cross sections, the uncertainty in the range of the N-α interaction, the various choices of the angular regions considered (see Fig. 5) altogether contribute uncertainties in R_{nm} of about 1.3%. The parameter $\bar{U}_R$ is defined to within 5% which induces an additional relatively large uncertainty in R_{nm} of 1.6%. In contrast, a variation of 5% in $\bar{U}_I$ changes R_{nm} by only ±0.3%. (The imaginary potential plays a relatively minor role over tha angular ranges considered.) In sum, we estimate that the over-all errors in the determination of R_{nm} amount to approximately 2%. A quantitative study of these uncertainties has been made by Tatischeff, Brissaud, and Bimbot[9] for the nucleus ^{208}Pb.

For the proton distributions, Curtis's parameters[12] have been used. These are shown in Table IV along with c_n for the tin isotopes. The parameters determined by Barreau and Bellicard[13] and more recently by Khvastunov *et al.*[14] could also have been employed, but they do not differ appreciably from those of Curtis. The variations of the proton radii between the Sn isotopes have been measured with a great accuracy by Bhattacherjee, Boehm, and Lee[15] from analyses of electronic x-ray shifts. Values obtained are $\Delta(R_p^2)_{116-118} = 0.120$ fm^2, $\Delta(R_p^2)_{118-120} = 0.128$ fm^2, and $\Delta(R_p^2)_{120-124} = 0.166$ fm^2. The corresponding values of Curtis are 0.18, 0.19, and 0.28 fm^2, respectively. The differences between the two sets of values may seem significant, but correspond to differences in ΔR_p of about 0.01 fm if an average value for R_p is taken to be 4.55 fm. Considering the quoted uncertainty of 0.09 fm in R_{nm}, the implied errors in $\Delta(R_p^2)$ are inconsequential insofar as their effects upon R_{nm} are concerned.

Other methods have been used to determine neutron-matter radii.[11, 12, 16-20] The various results of these methods are tabulated in Table III. Greenlees, Pyle, and Tang[21] have analyzed proton elastic scattering data using a nuclear-matter distribution to calculate the real optical potential and a phenomenological imaginary potential. The calculation of the real potential did not include exchange or tensor terms. The (large) value found

TABLE III. Radius parameters for the tin isotopes. A comparison of experimental and theoretical values. R_c, R_{nm}, R_p, and R_n are charge, neutron-matter, proton, and neutron radii, respectively.

	Ref. 12	This experiment	Ref. 16		Ref. 17		Ref. 18		Ref. 19		Ref. 11		Ref. 20		Ref. 20	
A	R_c	R_{nm}	R_p	R_n	R_p	R_n	R_p	R_n	R_c	R_{nm}	R_p	R_n	R_p	R_n	R_p	R_n
116	4.60	4.68 ± 0.09	...	...	...	...	...	...	...	...	4.60	4.68	4.63	4.70	4.58	4.67
118	4.62	4.79 ± 0.09	...	...	...	...	...	...	...	...	...	...	...	...	4.59	4.71
120	4.64	4.87 ± 0.09	4.59	4.74 ± 0.19	4.59	4.85 ± 0.26	4.59	5.03	4.64	4.71	4.60	4.72	4.64	4.79	4.60	4.74
124	4.67	4.83 ± 0.09	...	...	...	...	...	...	...	...	...	...	4.65	4.87	4.63	4.81

TABLE IV. Parametrization of the nuclear-matter distribution for the tin isotopes. c_p, c_n, a_p, and a_n are radius and diffuseness parameters of Fermi density distributions. The values of c_p and a_p shown are the parameters of Curtis *et al.* (Ref. 12). The value of c_n is deduced from the α-particle scattering, with the assumption that $a_p = a_n$.

A	c_p (fm)	a_p (fm)	c_n (fm)
116	5.28	0.579	5.35
118	5.30	0.582	5.47
120	5.32	0.575	5.65
124	5.44	0.528	5.72

for R_n was recently reduced[16] so that the difference $R_n - R_p$ deduced became 0.15 ± 0.19 fm. Friedman[17] has used a method of analysis similar to that of Greenlees, Pyle, and Tang, but with a density-dependent nucleon-nucleon interaction. Batty and Greenlees[18] searched for an effective potential to fit the single-particle states of several nuclei and obtained neutron and proton distributions of ^{120}Sn. Nolen and Schiffer[19] deduced values for R_n from analyses of Coulomb displacement energies. They calculated the neutron excess with a Fermi distribution having the same diffuseness for the protons and neutrons of the core, and assumed also that the neutrons and protons of the core had the same radius. Campi-Benet's theoretical values[11] of R_n and R_p obtained from a Hartree-Fock calculation (Brink interactions), Beiner's values[20] obtained via a simplified pairing model, and other results of Beiner obtained upon imposing additional constraints on the matter distributions are also given in Table III.[22] From preliminary Hartree-Bogoliubov calculations, Gogny and Pradal[23] have deduced for the $A = 116$, 118, 120, and 124 tin isotopes the following results for $R_n - R_p$: 0.09, 0.10, 0.12, and 0.14 fm, respectively. Using a Fermi liquid model, Khrylin[24] has calculated the difference $R_n - R_p$ for ^{114}Sn and found it to be 0.12 fm.

Figure 5 shows that: (i) With the exception of the results of Ref. 19, our values are in agreement with the rest within the limits of uncertainty. (ii) Whereas the variation of the charge radii among the tin isotopes is small (true also for example for the calcium isotopes) the neutron radii appear to increase faster than $A^{1/3}$ for the isotopes $A = 116$, 118, and 120. (iii) The matter radii, R_m, within the limits of accuracy, increase as $A^{1/3}$. Statements (ii) and (iii) are in agreement with the conclusions of Ref. 19.

In addition to our own data we have analyzed 104-MeV α-particle scattering results of Hauser *et al.*[25] (See Table 8 of Ref. 1.) Taking the mean values $\bar{U}_R = 0.77$ and $\bar{U}_I = 0.42$, we obtain $R_{rm} = 4.83$ fm, which is close to the value of 4.86 fm found at 166 MeV. However, a rather large dispersion of the optimum values of U_I occurs for the data at 104 MeV. (It is still worse at lower energies.) It appears that the kind of calculation of an optical potential applied here seems to be better suited to the analysis of the α-particle scattering at higher energies.

4. STUDY OF THE FIRST 2^+ AND 3^- STATES

Using the DWBA and the optical potentials calculated as described in Sec. 3, inelastic scattering cross sections were generated so as to study the quasiparticle description of the tin isotopes. The calculation of the matter form factor $\langle f | V_{\text{eff}} | i \rangle$ has been discussed in Ref. 1. V_{eff} is taken to be the same effective interaction as that used for the elastic scattering calculations. Since there remain no adjustable parameters in the calculations, one can discuss without ambiguity the wave functions of the excited levels.

The validity of this procedure has been tested by comparing experimental and calculated inelastic cross sections in cases where the wave functions are considered to be reliable. Such a comparison appears to be satisfactory for the collective levels of ^{12}C (2^+, 4.43 MeV; 3^-, 9.64 MeV)[1], or for the collective 3^- level of ^{40}Ca.[26] The comparison is especially satisfactory for the first 2^+ level of ^{12}C with Bouten's wave function[26, 27] which incorporates the deformation of this nucleus. In each of these "test" cases the experimental and calculated values for inelastic α-particle cross sections, the

TABLE V. Features of the tested nuclear wave functions. CB and GGR refer to Refs. 29 and 30, respectively, of the text.

Model	Approximation	N-N force	Individual functions	Number of configurations: Neutrons 2^+	Neutrons 3^-	Protons 2^+	Protons 3^-
CB	Tamm-Dancoff	Tabakin	H 0 $b = 2.22$ fm	27	26	6	12
GGR	Random-phase	Inverse gap equation	H 0 $b = 2.27$ fm	17	14	2	10

electromagnetic transition rates, and the form factors from inelastic electron scattering experiments cross sections were compared simultaneously.

For the tin isotopes, several theoretical wave functions exist. The model of Arvieu *et al.*[28] (where only five neutron states have been considered) gives cross sections which are too small[1] by a factor of 13. In the present work the experimental results are therefore compared to theoretical predictions corresponding to the wave functions of Clement and Baranger (CB)[29] and Gillet, Giraud, and Rho (GGR).[30] Table V shows some characteristic features of these wave function calculations.

Proton Configurations

Calculated electromagnetic form factors and the experimental results of Curtis *et al.*[12] and of Barreau and Bellicard[13] are plotted in Figs. 7 and 8. The small differences in the position of the maxima of the form factors ($\Delta q \approx 0.1$ fm^{-1}) between experiment and theory result partially from the fact[31] that the electron scattering calculations are made with the plane-wave Born approximation and not with DWBA. For the 2^+ levels, the predicted form factor $|F(q)|^2_{th}$ remains essentially constant with atomic number A in both the CB and the GGR models. For the 3^- levels also $|F(q)|^2_{th}$ remains constant for both models, except in the case of ^{124}Sn where GGR predicts a form factor smaller than for the other isotopes by a factor of 2. For the 2^+ states (and the 3^- states in the case of small momentum transfers, i.e., $\Delta q < 0.6$ fm^{-1}), all the calculated values are smaller than the experimental ones. One may ascertain that for the 3^- states, the two models lead to form factors $|F(q)|^2$ proportional to each other. For 2^+ states this is not true, the smallness of $|F(q)|^2_{GGR}$ corresponding to the lack of deep proton configurations. Table V shows that only two proton configurations are taken into account in GGR, leading to a proton wave function whose collective character is completely inadequate. Principally for the 3^- levels, but also for the 2^+ levels, the experimental values of $|F(q)|^2$ for $q > 0.7$ fm^{-1} decrease from ^{116}Sn to ^{124}Sn. This may be related to the correspondingly small increase of R_p^2 and to the fact that the contribution of proton configurations becomes smaller when neutrons are added.

Similar information is obtained from electromagnetic transition rates, although the results obtained are not always unequivocal. Transition probabilities derived from inelastic electron scattering[12, 13] can be uncertain because of the method of analysis involved. For 2^+ states, values obtained by nuclear-resonance-fluorescence techniques[32, 33] are more reliable. The best results

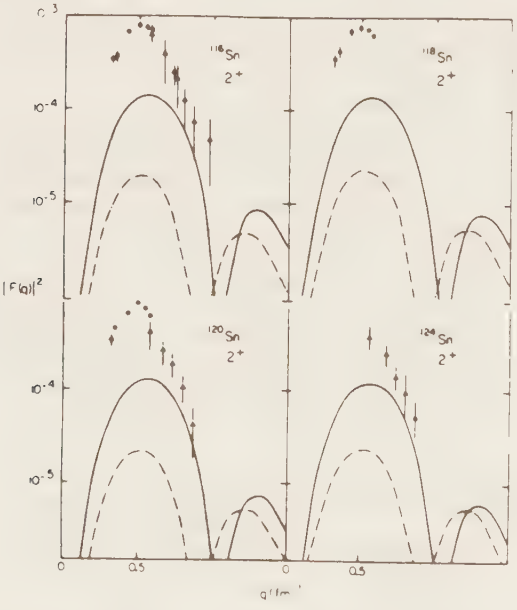

FIG. 7. Inelastic electron form factors for 2^+ levels. Barreau's results, ▲; Curtis's results, ●; curves obtained by use of GGR wave functions, ———; and CB wave functions, — — —.

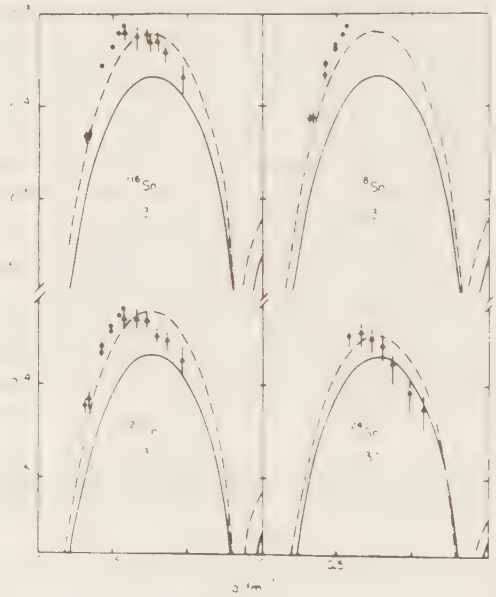

FIG. 8. Inelastic electron form factors for 3^- levels. Barreau's results, ▲; Curtis's results, ●; curves obtained by use of GGR wave functions, ———; and CB wave functions, — — — —.

TABLE VI. Electromagnetic transition rates for 2^+ states of tin isotopes.

2^+ levels A	$\left[\frac{1}{e^2}B(E2)\uparrow\right]_{th}$ GGR	CB	$\left[\frac{1}{e^2}B(E2)\uparrow\right]_{exp}$ References a	b	c	d	e	f
116	73	397	1455 ± 215	2900	1833	2200 ± 400	2350 ± 21	2070
118	82	381		2400	1722	2380 ± 206	2480	2280
120	83	361	1235 ± 205	2600	1729	2035 ± 390	2300	2200
124	89	345	1330 ± 225	2200			1840	2000

[a] See Ref. 13.
[b] See Ref. 34.
[c] See Ref. 12.
[d] See Refs. 32 and 33.
[e] See Ref. 35.
[f] See Ref. 36.

are those obtained from Coulomb-excitation experiments,[34] especially if the energy of the incident ion beam is sufficiently below the Coulomb barrier. For the 2^+ states, experimental results are given in Refs. 35 and 36. For the 3^- states, accurate values of $B(E3)$ do not exist. [From several values of $B(E3)$ corresponding to various higher energy transitions, the relevant values of $B(E3)$ were obtained by extrapolation.] It can be seen from Table VI[12, 13, 32-36] that for 2^+ levels the values of the $B(E2)$ corresponding to CB are in better agreement with experiment than those of GGR, although agreement with the experimental values in both cases is poor. For the 3^- levels (Table VII[12, 13, 37-39] GGR predicts results in better agreement with the experimental value.

A parameter $\lambda_p{}^2$ may be introduced in order to compensate pragmatically for the missing proton configurations. This coefficient is obtained by a comparison of the theoretical and experimental values of electromagnetic transition rates: $\lambda_p{}^2 \equiv B(E)_{exp}/B(E)_{th}$. For the 2^+ states of the tin isotopes, the mean value of λ_p is ≈5.4 for GGR, and ≈2.5 for CB. For the 3^- states, $\lambda_p \approx 1.2$ for GGR, and $\lambda_p \approx 2.2$ for CB.

TABLE VII. Electromagnetic transition rates for 3^- states of tin isotopes.

3^- levels A	$\left[\frac{1}{e^3}\frac{B(E3)\uparrow}{10^3}\right]_{th}$ GGR	CB	$\left[\frac{1}{e^3}\frac{B(E3)\uparrow}{10^3}\right]_{exp}$ References a	b	c	d	e
116	113	34	120 ± 14.7	160	74		570
118	122	34		170	112		
120	118	33.9	113 ± 13.8	130	103		
124	63	33.4	75 ± 10.7	160		250 ± 50 550 ± 110	600

[a] See Ref. 13.
[b] See Ref. 37.
[c] See Ref. 12.
[d] See Ref. 38.
[e] See Ref. 39.

Inelastic α-Particle Scattering: Sensitivity to Neutron Configurations

Experimental and theoretical results for inelastic α-particle scattering to the 2^+ and 3^- states of tin are given in Figs. 9 and 10. The relative variation with angle of the theoretical curves agrees well with the experimental points in all cases. This variation depends mainly on the optical potential and gives little information about the nuclear wave functions. The curves vary little for the different isotopes when the same nuclear model is used, except possibly for the case of the 3^- GGR model curves. [The same inconsistency for the 3^- GGR predictions can be made in connection with the $B(E3)$ values.]

If the experimental angular distributions at angles $\theta < 30°$ are considered for the 2^+ and 3^- states, the largest cross sections are obtained for ^{120}Sn and the smallest for ^{124}Sn. For angles $\theta > 32°$, distinctive differences appear: The distributions corresponding to ^{116}Sn and ^{118}Sn have different average slopes and a greater differential cross section than for the other two isotopes. In terms of the six-parameter Woods-Saxon optical potential obtained in the first part of this work, the different slopes of the angular distributions at larger angles correspond to the slight variation of V_R and W_I (see Fig. 4) from one isotope to another.

We have verified that when one arbitrarily increases the matter form factor, the cross section increases over the whole angular range, not just in a particular angular region. Because of the large value (2 fm) of the range of the α-nucleon effective interaction, the addition of a configuration at large radii modifies the magnitude of the form factor more than its shape, yielding an increase in the inelastic cross sections throughout the angular range. Therefore one is inclined to speculate that the behavior at large scattering angles is due to more complex reaction mechanisms,

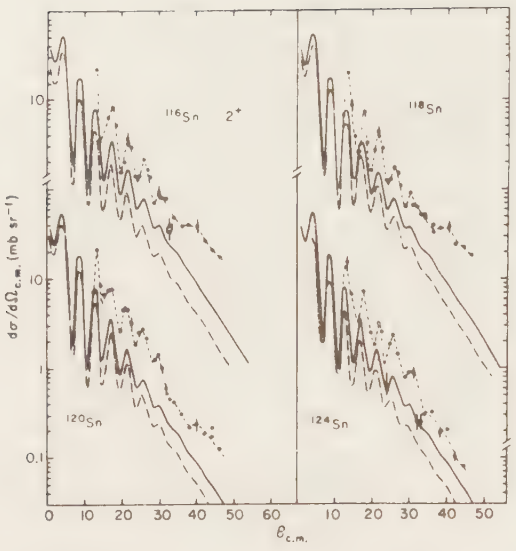

FIG. 9. α-particle inelastic scattering on 2^+ levels. Curves corresponding to GGR wave functions, ——; CB wave functions, ————.

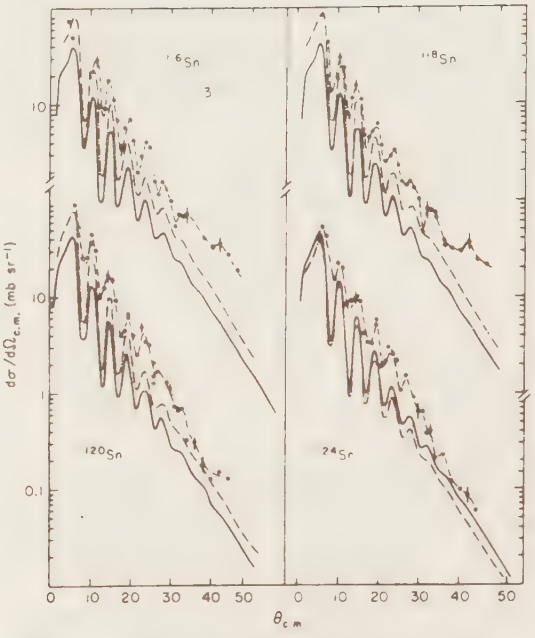

FIG. 10. α-particle inelastic scattering on 3^- levels. Curves corresponding to GGR wave functions, ——; CB wave functions, ————.

in particular multiple scattering, than are included in the DWBA. Notwithstanding, the variation of the experimental cross sections at large scattering angles when one goes from ^{116}Sn to ^{124}Sn is rather surprising.

Comparison to the Different Wave Functions

The GGR wave functions were obtained with the random-phase approximation (RPA). This approximation seems to have an important effect for 3^- states, but not for the neutron configurations of 2^+ states. The CB wave functions were obtained with the Tamm-Dancoff approximation. Therefore, better agreement to the experimental values of $B(E)$, $|F(q)|^2_{\text{incl}}$, and $d\sigma/d\Omega(\alpha)$ is obtained for the 3^- levels with GGR than with CB. The fact that the number of configurations, which all act coherently, has a greater effect in the CB than in the GGR case explains why the CB model gives better results for 2^+ states. The extension of configuration space in the CB model is due to the inclusion of $2\hbar\omega$ hole-particle excitations for protons. A question arises as to the relative importance of 2h-2p and 4h-4p proton configurations and 4 quasiparticle neutron configurations.

Just as for the λ_p^2 parameter, it is possible to define for the neutron configurations a normalization parameter λ_n^2, corresponding to a neutron configuration deficiency in the different wave functions, and a global normalization parameter λ^2 corresponding to a total deficiency. The values of these parameters which produce good agreement with all the experimental results are given in Table VII. These values, greater than unity, reflect the need for better excited state wave functions (more configurations, a deformed basis, etc.). This normalization procedure is not particularly precise (e.g., the normalization has been made for angles <30°); therefore, only mean values for the tin isotopes as a group are given. A similar discussion has been presented in connection with 155-MeV proton scattering,[40] with values of λ_n different from what is presented here, illustrating perhaps the limits of such a parametrization.

It can be seen in Table VIII that the neutron configurations in both the GGR and CB models are better described for 2^+ states than for 3^- states.

TABLE VIII. Normalization parameters describing excited state wave functions of tin. CB and GGR refer to the Refs. 29 and 30, respectively, of the text.

Levels	Models	Normalization constants λ_p	λ_n	λ
2^+	GGR	5.4	1.1	2.0
	CB	2.5	1.2	1.5
3^-	GGR	1.2	1.5	1.3
	CB	2.2	1.4	1.7

Very roughly one can say that the effect of omitting RPA correlations is compensated for by the increase in the number of configurations. (But note that the interactions used for the two wave functions are different.) The largest corrections (largest values of λ) are needed for the 2^+ states of the GGR model ($\lambda \approx 2$). It is interesting that the difference between E_{exp} and E_{th}, the experimental and theoretical values of the level energies is also greatest in this case.

Insofar as the 2^+ state predictions of the CB model, the total inelastic scattering cross sections decrease as A increases. This is due to a similar variation of differential cross sections at small angles.

If Woods-Saxon rather than harmonic-oscillator potentials had been used to generate the wave functions, the conclusions above would remain essentially the same. This point has been investigated[26] for the case of the ^{40}Ca 3^- level, where several wave functions generated in Woods-Saxon and harmonic-oscillator potentials are known.

5. CONCLUSION

The cross sections for the elastic and inelastic scattering of 166-MeV α particles have been measured on the tin isotopes of mass numbers 116, 118, 120, and 124. The method used to calculate optical potentials which describe the elastic scattering has been developed previously,[1] and appears to be more applicable than at lower α-particle energies because of the greater penetrability of 116-MeV α particles. For the tin isotopes, the sensitive region of the optical potential (for 166-MeV α scattering) is between 5 and 9 fm. Because of the large range (2 fm) of the effective interaction, the incident particle "sees" the nuclear density from $\approx$3 fm outward from the center of the nucleus. It is this fact that allows one to obtain the nuclear-matter radii with some precision. By using the charge densities determined from electron elastic scattering experiments, neutron-matter radii in the nuclei are extracted. The values found for these radii are similar to those calculated with other methods (e.g., via the energies of the isobaric analog states.)

The inelastic scattering data have been compared to theoretical predictions corresponding to the use of several nuclear models. This comparison leads to the conclusion that the importance of the protons in the wave functions used for these models is consistently underestimated. In order to account for the behavior of the inelastic cross sections at larger angles, more complex interaction processes than are included in the DWBA seem to be required. By incorporating our α-particle scattering results with those obtained from inelastic electron scattering and from electromagnetic-transition-rate studies, the neutron contributions to the wave functions have been extracted.

In the wave functions employed in this work, the closed shells are described by hole-particle excitations, the open shells by quasiparticle excitations. For doubly-closed-shell nuclei the electromagnetic properties are rather well obtained by the hole-particle models.[26] When a neutron shell is open, as in the case of the tin isotopes, the hole-particle excitations constructed on a spherical basis are not able to describe the electromagnetic properties well. ($\lambda_p > 1$.) Moreover, it is always that part of the wave function corresponding to the closed subshell which is not satisfactory, due to the insufficient collective character involved therein. This effect appears to be true for other nuclei also.[41]

The idea of this work is to use a consistent microscopic framework for the analysis of both elastic and inelastic scattering. The elastic scattering has been described in a microscopic model which has a rather simple parametrization. This parametrization then governs the behavior of the inelastic scattering, for chosen wave functions of the excited states. A comparison with measured cross-section data then provides a test of the wave functions chosen. The main questions are: How valid is the assumed interaction? Does lack of agreement to experimental data indicate insufficiently appropriate wave functions or is the interaction model at fault? If the interaction model employed here is deemed valid on the basis of its success in fitting the elastic scattering, we find the encouraging result that our analysis of inelastic scattering is sensitive to the kinds of wave functions chosen to describe the corresponding excited states.

ACKNOWLEDGMENTS

It is a pleasure to thank Professor M. Veneroni for his many suggestions and comments. We are greatly indebted to Professor E. Baranger and also to Professor V. Gillet and Dr. B. Giraud for communications of unpublished wave functions. We wish to thank X. Bayon, J. Y. Martel, and F. Reide for their help in the setup and use of experimental equipment and in fact we thank all the crew of the synchrocyclotron for their kind cooperation.

[1]B. Tatischeff and I. Brissaud, Nucl. Phys. A155, 89 (1970).
[2]G. Bruge, J. C. Faivre, H. Farragi, and A. Bussiere, Nucl. Phys. A146, 597 (1970).
[3]C. R. Bingham, M. L. Halbert, and A. R. Quinton, Phys. Rev. 180, 1197 (1969); N. Baron *et al.*, *ibid.* 146, 861 (1966).
[4]C. J. Batty, E. Friedman, and D. F. Jackson, Nucl. Phys. A175, 1 (1971), and references cited in this paper.
[5]M. K. Brussel and J. H. Williams, Phys. Rev. 106, 286 (1957).
[6]S. Hayakawa *et al.*, Phys. Letters 8, 330 (1964).
[7]A. M. Bernstein and W. A. Seidler, Phys. Letters 34B, 569 (1971).
[8]A. M. Bernstein, in *Advances in Nuclear Physics*, edited by M. Baranger and E. Vogt (Plenum, N.Y., 1970), Vol. 3, p. 325.
[9]B. Tatischeff, I. Brissaud, and L. Bimbot, Phys. Rev. C 5, 234 (1972).
[10]That is, by convolution of the Hartree-Fock nucleon distribution with a Gaussian nucleon form factor.
[11]X. Campi-Benet, private communication.
[12]T. H. Curtis, R. A. Eisenstein, D. W. Madsen, and C. K. Bockelman, Phys. Rev. 184, 1162 (1969).
[13]P. Barreau and J. B. Bellicard, Phys. Rev. Letters 19, 1444 (1967).
[14]V. M. Khvastunov *et al.*, Nucl. Phys. A146, 15 (1970).
[15]S. K. Bhattacherjee, F. Boehm, and P. Lee, Phys. Rev. 188, 1919 (1969).
[16]C. W. Greenlees, W. Makofske, and G. J. Pyle, Phys. Rev. C 1, 1145 (1970).
[17]E. Friedman, Phys. Letters 29B, 213 (1969).
[18]C. J. Batty and G. W. Greenlees, Nucl. Phys. A133, 673 (1969).
[19]J. A. Nolen and J. P. Schiffer, Ann. Rev. Nucl. Sci. 19, 471 (1969).
[20]M. Beiner, in *Theory of Nuclear Structure, Trieste Lectures, 1969* (International Atomic Energy Agency, Vienna, Austria, 1970), p. 903; and private communication.
[21]C. W. Greenlees, G. J. Pyle, and Y. C. Tang, Phys. Rev. 171, 1115 (1968).
[22]We would like to thank Dr. M. Beiner, Dr. X. Campi-Benet, Dr. D. Gogny, and Dr. J. Pradal for communication of unpublished results.
[23]D. Gogny and J. Pradal, private communication.
[24]B. A. Khrylin, Yadern. Fiz. 6, 949 (1967) [transl.: Soviet J. Nucl. Phys. 6, 691 (1968).
[25]G. Hauser *et al.*, Nucl. Phys. A128, 81 (1969).
[26]B. Tatischeff *et al.*, Phys. Rev. C 4, 494 (1971).
[27]M. Bouten and P. van Leuven, Ann. Phys. (N.Y.) 43, 421 (1967); and private communication.
[28]R. Arvieu, E. Baranger, M. Veneroni, M. Baranger, and V. Gillet, Phys. Letters 4, 119 (1963).
[29]D. M. Clement and E. Baranger, Nucl. Phys. A120, 25 (1968); T. T. S. Kuo, E. Baranger, and M. Baranger, *ibid.* 81, 241 (1966); E. Baranger, in *Advances in Nuclear Physics*, edited by M. Baranger and E. Vogt (Plenum, N. Y., 1971), Vol. 4, p. 261.
[30]V. Gillet, B. Giraud, and M. Rho, Phys. Rev. 178, 1695 (1969); V. Gillet and B. Giraud, private communication.
[31]J. F. Ziegler and G. A. Peterson, Phys. Rev. 165, 1337 (1968).
[32]N. Lingappa, E. Kondaiah, C. Badrinathin, M. D. Despande, and M. Balakrishnan, Nucl. Phys. 38, 146 (1962).
[33]H. Hrastnik, V. Knapp, and M. Vlatković, Nucl. Phys. 89, 412 (1966).
[34]D. S. Andreev, V. D. Vasil'ev, G. M. Gusinskii, K. I. Erokina, and I. Kh. Lemberg, Izv. Akad. Nauk SSSR Ser. Fiz. 25, 832 (1961) [transl.: Bull. Acad. Sci. USSR, Phys. Ser. 25, 1842 (1961)].
[35]P. H. Stelson, F. K. McGowan, R. L. Robinson, W. T. Milner, and R. O. Sayer, Phys. Rev. 170, 1172 (1968).
[36]P. H. Stelson and F. K. McGowan, Phys. Rev. 110, 489 (1958).
[37]D. G. Alkazov *et al.*, Izv. Akad. Nauk SSSR Ser. Fiz. 28, 232 (1964) [transl.: Bull. Acad. Sci. USSR, Phys. Ser. 28, 149 (1964)].
[38]J. M. Lagrange, Centre National de la Recherche Scientifique Report No. 3709, 1970 (unpublished).
[39]O. Hansen and O. Nathan, Nucl. Phys. 42, 197 (1963).
[40]V. Comparat, 3e cycle thesis, University of Paris, 1970 (unpublished).
[41]C. Schaeffer, Centre à l'Energie Atomique Report No. CEA F4000, 1969 (unpublished).

PHYSICAL REVIEW C VOLUME 4, NUMBER 2 AUGUST 1971

Study of the First 3⁻ Levels of ^{40}Ca and ^{208}Pb Nuclei

B. Tatischeff, L. Bimbot, I. Brissaud, V. Comparat, and A. Willis
Institut de Physique Nucléaire, Orsay, France
and
M. K. Brussel
University of Illinois, Urbana, Illinois 61801
(Received 22 March 1971)

Differential cross sections for the inelastic scattering of 166-MeV α particles from the 3⁻ levels of ^{40}Ca and ^{208}Pb are presented. A distorted-wave Born-approximation microscopic analysis is made utilizing an effective α-nucleon interaction previously determined from a study of elastic scattering. In considering the results obtained, various aspects of nuclear structure implicit in the calculations of microscopic wave functions are implicated: the effective nucleon-nucleon interaction, the importance of nucleon correlations, and the extent of the configuration space. Electromagnetic transition probabilities and inelastic electron scattering form factors calculated with the microscopic wave functions used in the α-particle analysis are compared with experimental results. No effective charge is required to obtain agreement.

The microscopic description of the collective first excited states for closed-shell (or subshell) nuclei has been known for some years. However, the results of calculations that have been made rest on theoretical variables or assumptions whose influence on the calculations has not always been clear. Among the theoretical uncertainties are the following: (1) the choice of nucleon-nucleon interactions; (2) the single-particle wave-function basis to be used for both occupied and unoccupied states; (3) the energies and number of configuration states to be chosen (hole or particle states); (4) the type of approximation to be used [random-phase approximation (RPA), Tamm-Dancoff approximation (TDA), ...].

When numerous wave functions describing a particular excited state exist, a comparison between the experimental results and predictions based upon the theoretical variables can allow one to discern the relative importance of these variables. The comparison made in this paper employs the following experimentally determined quantities: (a) the electromagnetic transition rates, $B(E)$; (b) the inelastic electron scattering form factors, $|F(q)|_{\text{inel}}^2$; and (c) the inelastic α-particle cross sections measured with incident 166-MeV α particles, $d\sigma/d\Omega(\alpha)$.

Calculations corresponding to nuclei having a single shell closing (e.g., Ni, Zr, Sn) have been less successful in describing the excited states than those for double shell closings (e.g., ^{12}C, ^{40}Ca, ^{208}Pb). In these calculations, the ^{40}Ca 3⁻ ($T=0$) level at 3.73 MeV is probably the most studied, and it was a natural candidate for study here. In the same vein of trying to probe the validity of the theoretical calculations, results for the 3⁻ (2.62-MeV) level of ^{208}Pb will also be presented.

The inelastic scattering of 166-MeV α particles cited here was performed at the Institut de Physique Nucléaire synchrocyclotron of Orsay. The experimental methods employed have been described elsewhere,[1,2] as have some preliminary results.[3] The analysis of the inelastic cross-section measurements is made via the distorted-wave Born-approximation (DWBA) method using our computer code ODABAL. The optical potential employed therein is derived[4,5] from a nuclear-matter density and an average effective α-nucleon interaction which accounts for the elastic scattering of 166-MeV α particles on various nuclei. The same average effective interaction is employed to calculate the inelastic scattering form factor. This is consistent with the assumption that exchange and multiple-scattering effects (not included here) are the same in both cases. No adjustable parameters are introduced into the calculation. The validity of our analysis has been tested for the (light) nucleus ^{12}C, whose neutron and proton configurations probably play equivalent roles in the description of the excited states. A satisfying aspect of the analysis is that when it predicts values of $B(E)$ and $|F(q)|_{\text{inel}}^2$ in accord with experiment[6] it also leads to good agreement for the 166-MeV inelastic α-particle scattering cross section, $d\sigma/d\Omega(\alpha)$, to the 2⁺ (4.43-MeV) state.[7]

The wave functions used in the present analysis and the calculated electromagnetic transition rates are given in Table I.[8-21] The inelastic electron scattering form factors are presented in

TABLE I. Properties of excited-level wave functions and electromagnetic transition rates.

Nucleus	Theoretical model	E_{th} (MeV)	Single-particle wave functions	Force	Approximation	$(1/e^2)B(E)\uparrow$ (e^2 fm^6) Theor.	Exp.
^{40}Ca	Dieperink, Leehouts, and Brussard [a]	2.8	H. O. $b=1.87$ fm	Tabakin	RPA	28 000	14 000 [a]
							17 150 [g]
3.73-MeV level	Gillet and Sanderson [b]	3.83	H. O. $b=1.89$ fm	CAL	RPA	12 100	21 100 [h]
	Stamp and Mayers [c]	3.78	W. S. one potential	Yukawa, range 1.25 fm	RPA	6 240	15 700 [i]
							16 600 [j]
	Perez [d]	4.	W. S. many potentials	Yukawa, range 1.54 fm	TDA	3 940	24 900 [k]
							16 100 [l]
^{208}Pb	Gillet, Green, and Sanderson [e]	2.74	H. O. $b=2.325$ fm	COP	RPA	$2.33\ 10^5$	$7.2\ (10^5)$ [m]
2.62-MeV level	Gillet, Giraud, and Rho [f]	1.94	H. O. $b=2.50$ fm	IGE	RPA	$5.76\ 10^5$	$5.8\ (10^5)$ [n]

[a] Reference 8.
[b] Reference 9.
[c] Reference 10.
[d] Reference 11.
[e] Reference 12.
[f] Reference 13.
[g] Reference 14.
[h] Reference 15.
[i] Reference 16.
[j] Reference 17.
[k] Reference 18.
[l] Reference 19.
[m] Reference 20.
[n] Reference 21.

Fig. 1,[8-13, 15, 20, 22, 23] and the inelastic α-particle cross sections are shown in Fig. 2.

Cross sections in Fig. 2 have not been given for scattering angles less than 8°. These are omitted because our experimental energy resolution ($\Delta E \sim 0.9$ MeV) was insufficient to distinguish the 3⁻, 3.73-MeV level of ^{40}Ca from the 2^+, $T=0$ level at 3.90 MeV, and the latter is expected to be more highly excited than the 3⁻ level at small angles ($\Delta q < 0.7$ fm^{-1}).[22]

RESULTS FOR THE 3⁻ LEVEL of ^{40}Ca, 3.73 MeV

The four models studied,[8-11] (Table I) all describe the wave function of the excited state in terms of nine coherent particle-hole configurations built upon the ground state. (All the $1\hbar\omega$ excitations are included.) Except in the case of the model of Stamp and Mayers[10] (denoted SM) each single-particle energy is equal to the experi-

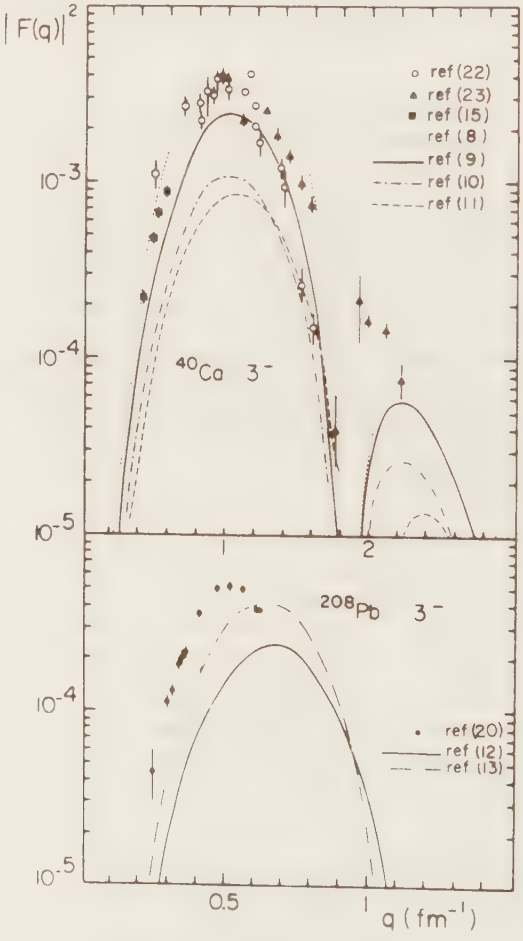

FIG. 1. Form factors for inelastic electron scattering.

mental value.

The model of Dieperink, Leenhouts, and Brussaard[8] yields values for $B(E)$, $|F(q)|_{\text{inel}}^2$, and $d\sigma/d\Omega(\alpha)$ which are all larger than the data indicate, perhaps due to the fact that the Tabakin interaction employed there is too strong.

The model of Gillet and Sanderson[9] (GS) leads to results for the ground state somewhat smaller than the data indicate. A previous calculation of GS,[24] using a wave function obtained with a different two-body interaction COP[12] and with a harmonic-oscillator parameter of 2.08 fm, predicted[25] a value of $|F(q)|_{\text{inel}}^2$ in slightly better agreement with the data than what we are presenting. However, the present calculation[9] employs a more general two-body interaction CAL[12] which permits a description of the excited states of different nuclei.

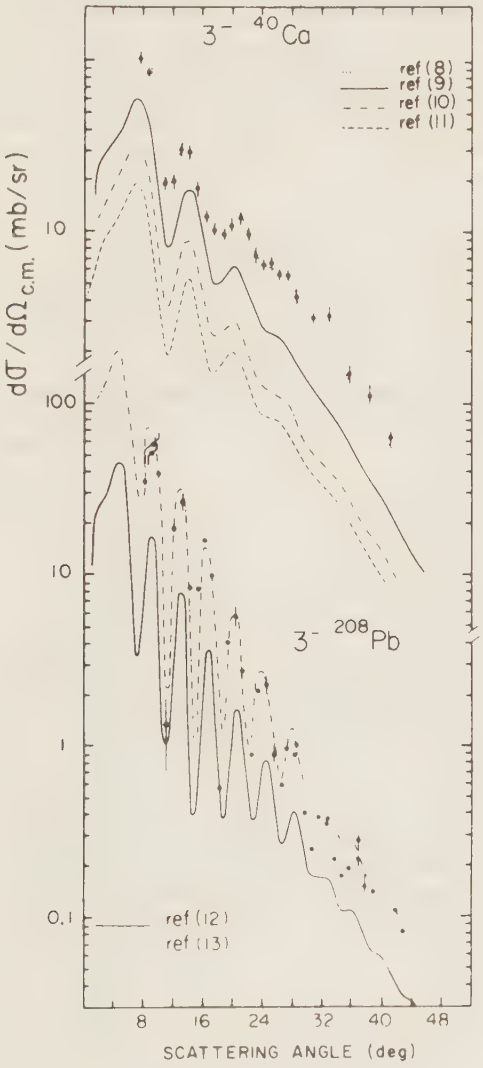

FIG. 2. Differential cross sections for 166-MeV α-particle inelastic scattering.

The two other models used in this work[10, 11] to generate experimental predictions employ Woods-Saxon (W.S.) single-particle wave functions rather than the harmonic-oscillator (H.O.) wells used in Refs. 8 and 9 above. Whereas Perez[11] employs a different well for each shell so as to have correct single-particle energies, SM[10] employ a single well, and so obtain slightly inaccurate single-particle energies. (The energy separation between the hole and particle states is somewhat small, which favors collective effects.) The results of Perez[11] are systematically too small, because of the use of TDA instead of RPA. In both models[10, 11] the interaction chosen leads to wave functions less collective than those of GS.[9] In addition, the ground-state correlations which appear in the weighting of the configurations are much less important in the wave functions of SM than in those of GS. The tails of the wave functions are less important for the latter than for the former. Whereas the inversion of their relative magnitude occurs at 5 fm for the $2p$ shell, it occurs at 6 fm for the $1d$ shell. The region effective for the scattering of α particles of 166 MeV on ^{40}Ca is approximately from 3 to 9 fm, so partial compensation is produced by this effect. The same comment holds for comparison of the $B(E)$ due to the long range of the operator r^L [the ratios of values between GS and SM at cross-section maxima are: (a) for $B(E)$, 1.94; (b) for inelastic α scattering, 2.1; (c) for $|F(q)|_{\text{inel}}^2$, 2.3[26]]. Note that the theoretical energy predicted for the level is not a sufficient criteria for goodness of the wave function: The more collective the wave function is, the lower is the corresponding energy.

3^- LEVELS OF ^{208}Pb

In Table I are presented results obtained with two models denoted by GGS[12] and GGR.[13] A comparison with the experimental $B(E)$ is also given. Figure 2 shows the associated theoretical and experimental cross sections. The model of GGS[12] is derived with the effective two-body interaction COP which yields cross sections which are too small for ^{12}C.[1] All $1\hbar\omega$ configurations are included (21 proton and 24 neutron configurations). The model GGR[13] was derived with the inverse-gap-equation method. The parameters for the two-body interaction were obtained from experimental spectra of neighboring odd nuclei. In GGR the neutrons are treated in the quasiparticle formalism. This allows for the introduction of four additional

configurations corresponding to excitations between "occupied" states $[2f_{7/2}^{-1} - 1i_{13/2}; 1h_{9/2}^{-1} - 1i_{13/2}]$ and "unoccupied" states $[1i_{11/2}^{-1} - 1j_{15/2}; 2g_{9/2}^{-1} - 1j_{15/2}]$. As a consequence, these two effects (different forces and additional configurations) give a form factor for the inelastic α scattering for neutron configurations which is larger for the model of GGR than for that of GGS. (The ratio is 1.22 at 7 fm.) The same is true for the proton configurations even though in GGS four supplementary configurations occur from the formation of a hole in the $1g_{9/2}$ shell. These excitations ($2\hbar\omega$) play no significant role. GGS does not account well for the experimental results for $B(E)$, $|F(q)|_{\text{inel}}^2$, and $d\sigma/d\Omega(\alpha)$, whereas GGR agrees rather well with these quantities. Again it is found that these results are obtained with too small a theoretical energy. A small displacement in the position of the maxima ($\Delta q = 0.1$ fm^{-1}) between the experimental and calculated curves, Fig. 1, is due to the fact that the calculations have been made in the Born approximation. A distorted-wave calculation would increase the theoretical cross sections by a factor of 1.23. The resulting agreement appears rather good.

In summary, the similar correspondences of $B(E)$, $|F(q)|_{\text{inel}}^2$, and $d\sigma/d\Omega(\alpha)$ between theory and experiment in all the cases we have treated leads us to draw the following conclusions: (1) It is necessary to use RPA and a good two-body force (not so strong as the Tabakin force). (2) It is necessary to employ a large number of configurations. (3) It is not necessary to use an effective charge in calculating electromagnetic transition rates. Finally, (4) it is not necessary to use Woods-Saxon single-particle wave functions when particles of intermediate penetrability are involved, though this may be modified when levels are excited by low-energy particles (with strong absorption).

We wish to thank Dr. V. Gillet and Dr. B. Giraud for their communication of unpublished wave functions, and Dr. M. Beiner for the computer code which calculated wave functions in a Woods-Saxon well.

---

[1]B. Tatischeff and I. Brissaud, Nucl. Phys. A155, 89 (1970).

[2]I. Brissaud, B. Tatischeff, L. Bimbot, M. K. Brussel, V. Comparat, and A. Willis, to be published.

[3]I. Brissaud and B. Tatischeff, in Proceedings of the Nuclear Physics Conference, Surrey, G. B. (April, 1970).

[4]D. Jackson, *Nuclear Reactions* (Methuen and Company, Ltd., London, 1970).

[5]A. M. Bernstein, in *Advances in Nuclear Physics*, edited by M. Baranger and E. Vogt (Plenum Press, Inc., New York, 1969).

[6]M. Bouten and P. Van Leuven, Ann. Phys. (N.Y.) 43, 421 (1967).

[7]I. Brissaud *et al.*, to be published.

[8]A. E. L. Dieperink, H. P. Leenhouts, and P. J. Brussaard, Nucl. Phys. A116, 556 (1968).

[9]V. Gillet and A. E. Sanderson, Nucl. Phys. A91, 292 (1967).

[10]A. P. Stamp and D. F. Mayers, Nucl. Phys. 82, 296 (1966).

[11]S. M. Perez, Nucl. Phys. A136, 599 (1969).

[12]V. Gillet, A. M. Green, and E. A. Sanderson, Nucl. Phys. 88, 321 (1966); Phys. Letters 2, 44 (1964).

[13]V. Gillet, B. Giraud, and M. Rho, Phys. Rev. 178, 1695 (1969); V. Gillet and B. Giraud, private communication.

[14]T. Hertel and T. W. Tetz-Schmidt, Nucl. Data A2, 347 (1966).

[15]R. A. Eisenstein *et al.*, Phys. Rev. 188, 1815 (1969).

[16]E. P. Lippincott and A. M. Bernstein, Phys. Rev. 163, 1170 (1967).

[17]W. S. Gray *et al.*, Nucl. Phys. 67, 542 (1965).

[18]J. Lindskog *et al.*, in *Alpha-, Beta-, and Gamma-Ray Spectroscopy*, edited by K. Siegbahn (North-Holland Publishing Company, Amsterdam, The Netherlands, 1965), p. 1599.

[19]D. Newton *et al.*, Nuclear Phys. Laboratory, Internal Report No. 58/64, University of Oxford.

[20]J. F. Ziegler and G. A. Peterson, Phys. Rev. 165, 1337 (1968).

[21]A. R. Barnett and W. R. Phillips, Phys. Rev. 186, 1205 (1969).

[22]D. Blum, Ph.D. thesis, University of Paris, 1965 (unpublished); D. Blum, P. Barreau, and J. Bellicard, Phys. Letters 4, 109 (1963).

[23]M. Croissiaux *et al.*, Phys. Rev. 137, B865 (1965).

[24]V. Gillet and A. E. Sanderson, Nucl. Phys. 54, 472 (1964).

[25]V. Gillet and M. A. Melkanoff, Phys. Rev. 133, B1190 (1964).

[26]Note that if one changes the Woods-Saxon potentials, the result changes greatly. Thus, with the weights of Gillet and a potential taking good account of the properties of spherical nuclei (from ^{40}Ca to ^{208}Pb) one obtains a value for $B(E)$ equal to 22 900 e^2fm^4.

2.L

Nuclear Physics A210 (1973) 397—420; © *North-Holland Publishing Co., Amsterdam*

Not to be reproduced by photoprint or microfilm without written permission from the publisher

STUDY OF MICROSCOPIC WAVE FUNCTIONS OF NUCLEAR LEVELS THROUGH INELASTIC SCATTERING OF 166 MeV α-PARTICLES

L. BIMBOT †, B. TATISCHEFF, I. BRISSAUD, Y. LE BORNEC,
N. FRASCARIA and A. WILLIS

Institut de Physique Nucléaire, B.P. no. 1, 91 – Orsay, France

Received 26 June 1972
(Revised 18 April 1973)

Abstract: The inelastic cross sections of 166 MeV α-particles have been measured for the first collective levels of 22 nuclei. The experimental angular distributions are presented and compared, when possible, with DWBA calculations using microscopic wave functions. The importance of the choice of the optical potential, of the exchange term and of the Coulomb interaction, and the validity of the microscopic wave functions are discussed.

E

NUCLEAR REACTIONS ^{12}C, ^{24}Mg, ^{28}Si, ^{32}S, ^{40,44,48}Ca, ^{48}Ti, ^{56}Fe, ^{58,60,62}Ni, ^{68}Zn, ^{88}Sr, ^{90}Zr, ^{92}Mo, ^{116,118,120,124}Sn, ^{140}Ce, ^{208}Pb(α, α′), E_α = 166 MeV; measured $\sigma(E_\alpha, \theta)$; α-N interaction, phenomenological and calculated optical potentials used with DWBA; microscopic wave functions tested.

1. Introduction

In the past few years there has been a great development in microscopic model calculations and there exist now a large number of nuclear wave functions which may be tested directly. The usual tests of validity are the comparison of calculated values of the electromagnetic transition rate $B(E\lambda)$ and of the inelastic electron scattering form factor $|F(q)|^2_{el.}$ with experimental results. These two last quantities depend on proton configurations only and the inelastic particle scattering is now currently used to give additional information on neutron configurations [1-6]). The calculations are carried out in the DWBA framework [7]). The microscopic analysis is an extension of the method using macroscopic models to extract β_l deformation parameters [7, 8]). The inelastic particle scattering form factor is calculated with nuclear wave functions and an effective interaction between the projectile and one nucleon of the target [9-11]). A good determination of the effective interaction is required.

For low-energy protons the N-N interaction has central, *L-S*, and tensor terms. The last two are supposed to be negligible but the central force contains spin and isospin components. Thus several constants have to be adjusted, generally to reproduce the nucleon-nucleon phase shifts [6]). Moreover the one-particle exchange

† This work is part of the thesis of L. Bimbot.

term has been found to be too important to be neglected at these energies ($\leqq$ 100 MeV) and can be calculated only to a rough approximation [12]), introducing other uncertainties in the conclusions about the microscopic wave functions. At medium proton energy DWIA may be used [13]) to avoid these difficulties with the nucleon-nucleon interaction, but the approximations generally included [14]) (zero-range approximation for example) affect the validity of these calculations and for heavy nuclei [15]) a disagreement is observed in the slopes of experimental and theoretical differential cross sections.

A better approach to this problem seems to be the inelastic α-particle scattering at medium energy. For the α-particle ($S = 0, T = 0$) the effective interaction $V_{\alpha N}^{\text{eff}}$ can be reduced to a central term with neither spin nor isospin component. Owing to this important simplification the effective interaction can be deduced from a fit to experimental results of elastic α-particle scattering at the same energy for a large number of nuclei spanning the periodic table [16]) and no new parameter is introduced for inelastic scattering analysis. The exchange effects and the multiple scattering are probably small at this relatively high energy (166 MeV) but however these complex mechanisms are supposed to be taken into account through the determination of the effective interaction (this implies that their effects are the same in elastic and inelastic processes).

The effective interaction $V_{\alpha N}^{\text{eff}}$ being assumed to be reliable, we can use it to check any microscopic wave functions. Preliminary results have proved the validity of this method [2]). Thus a systematic study of the (α, α') reaction has been undertaken on the low-lying collective levels of 22 nuclei having a level density small enough to be resolved with our present instrumentation. In most of cases at least one shell was closed and there exist microscopic calculations for the states investigated.

The most often used wave functions are those of Gillet *et al.* [17]). All the even single-closed-shell nuclei (except the $N = 82$ isotones) are involved. The parameters of the residual Gaussian interaction and the single-particle energies are determined by the inverse-gap-equations (IGE) method. The microscopic description of the excited state is obtained by applying the RPA method on the BCS ground state deduced from IGE results. The configuration space corresponds to one particle and one hole in the closed shell and two quasiparticles in the open shell. Thus the core polarization is introduced as well for proton ($Z = 28, 50, 82$ isotopes) as for neutron ($N = 50$ isotones) and it is interesting to compare the importance of this effect on inelastic electron and α-particle scattering. A quantitative estimation of the quality of the fits is given to explain the disagreements eventually observed. When different calculations exist for the same level we have presented the best of the others to be compared with this model.

For ^{12}C, the wave functions of Bouten *et al.* [18]) calculated with a Volkov interaction in a projected Hartree-Fock formalism and those of Gillet and Vinh Mau [19]) which give a particle-hole description are tested. For the deformed ^{28}Si and ^{32}S nuclei we have considered the wave functions of Eisenberg [20]) corresponding to particle-hole

configurations with the Tamm-Dancoff approximation (TDA). For the double-closed-shell nuclei ^{40}Ca and ^{208}Pb, and for tin isotopes, we have previously done precise studies [2, 3]) and we present here only some new results obtained with the best nuclear wave functions and including the exchange effect and the Coulomb interaction. Table 1 shows the levels studied.

TABLE 1

Levels studied in 166 MeV inelastic α-particle scattering

	J^π	E_x (MeV)		J^π	E_x (MeV)		J^π	E_x (MeV)
^{12}C	2^+	4.43	^{58}Ni	2^+	1.45	^{116}Sn	2^+	1.27
	3^-	9.64					3^-	2.24
^{24}Mg	2^+	1.37	^{60}Ni	2^+	1.33	^{118}Sn	2^+	1.22
	(2^+4^+)	4.12		3^-	4.04		3^-	2.30
^{28}Si	2^+	1.78	^{62}Ni	2^+	1.17	^{120}Sn	2^+	1.18
				3^-	3.77		3^-	2.40
^{32}S	2^+	2.24	^{68}Zn	2^+	1.08	^{124}Sn	2^+	1.13
				3^-	2.76		3^-	2.53
^{40}Ca	3^-	3.73	^{88}Sr	2^+	1.83	^{140}Ce	2^+	1.60
	5^-	4.48		3^-	2.74			≈ 2.50
^{44}Ca	2^+	1.16	^{90}Zr	2^+	2.18	^{208}Pb	3^-	2.62
	3^-	3.31		3^-	2.75			
^{48}Ca	2^+	3.83	^{92}Mo	2^+	1.54			
	3^-	4.50		3^-	2.88			
^{48}Ti	2^+	0.98						
^{56}Fe	2^+	0.84						

2. Experimental method

Alpha-particles were accelerated by the IPN synchrocyclotron at Orsay. The scattered particles were analysed with the $R = 170$ cm spectrometer and detected in the focal plane by a 17-plastic-scintillator hodoscope [21]) covering a useful energy range of about 4 MeV. The total energy resolution (FWHM) was about 900 keV. The angular resolution ($\Delta\theta \approx 0.7°$) was due to the beam size on the target (8 mm wide, 15 mm high), the angular aperture of the primary beam focused on the target and the solid angle of the scattered beam determined by the entrance slits of the magnetic spectrometer.

Coincidence with a large plastic scintillator behind the hodoscope was used to minimize the background. Other particles produced by transfer reactions were suppressed by a discrimination of energy loss in the small plastic scintillators. A typical experimental spectrum is shown in fig. 1.

The last few measurements were made with the $R = 125$ cm magnetic spectrometer. Chromatic correction [22]) and the use of a spark chamber in the spectrograph focal plane gave a resolution of about 450 keV.

The solid angles and efficiency of the detection systems were obtained by α-scattering

on a proton target and comparison with the inverse reaction ^{4}He(p, p)^{4}He studied at 39.8 MeV by Brussel *et al.* [23]) and at 55 MeV by Hayakawa [24]). Target thicknesses [16]) were from 1 to 125 mg/cm^2 and were easily measurable. For $\theta \geqq 10°$ the beam current was monitored in a Faraday cup; for $\theta < 10°$ an induction ring in front of the target was used. The absolute cross sections are accurate to $\pm$ 15 % for well-separated peaks.

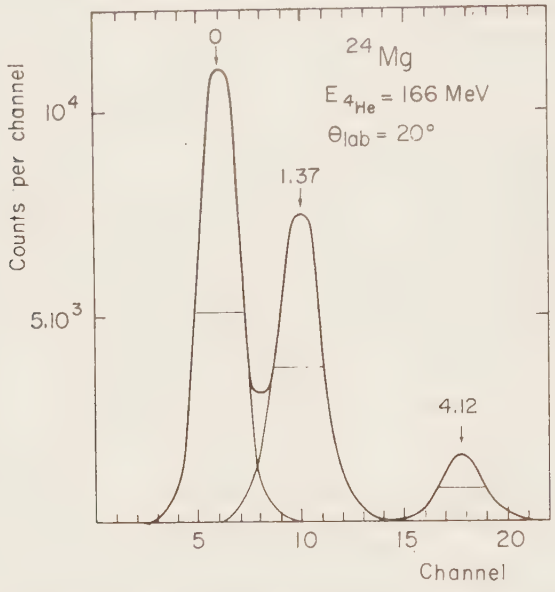

Fig. 1. Typical spectrum of 166 MeV α-particle scattering on ^{24}Mg showing the 3 levels 0^+, 2^+, 4^+. The resolution in the focal plane of the spectrometer was about 900 keV.

Measurements were made in 1° intervals at extremely forward angles and in 2° steps at more backward angles where there was less structure.

3. Analysis

The calculations are carried out in the DWBA framework. The inelastic scattering differential cross section is given [7]) by

$$\frac{\mathrm{d}\sigma}{\mathrm{d}\Omega}(\theta) = \left(\frac{\mu}{2\pi\hbar^2}\right)^2 \frac{k_\mathrm{f}}{k_\mathrm{i}} \sum_{M_\mathrm{f}} |T_\mathrm{if}^{M_\mathrm{f}}|^2$$

for target nuclei of zero spin. Here

$$T_\mathrm{if}^{M_\mathrm{f}} = \int \mathrm{d}\boldsymbol{r}\, \chi_\mathrm{f}^-(\boldsymbol{k}_\mathrm{f}, \boldsymbol{r}) \langle \mathrm{f}|V_\mathrm{eff}|\mathrm{i}\rangle \chi_\mathrm{i}^+(\boldsymbol{k}_\mathrm{i}, \boldsymbol{r}),$$

where $|i\rangle$ and $|f\rangle$ are the initial and final states of the target nucleus, χ_i^+ and χ_f^- are respectively the incoming and outgoing wave solutions of the Schrödinger equation for the optical potential, and $\langle f|V_{eff}|i\rangle$ is the form factor.

Thus the distorted wave functions and V_{eff} must be known if we want to try different nucleon wave functions.

3.1. EFFECTIVE INTERACTION AND FORM FACTOR

From the analysis of the elastic scattering data it is possible to determine an effective α-nucleon interaction $V_{\alpha N}^{eff}$ [refs. [3, 9, 16])]. The real part of the optical potential is expressed as:

$$V_{opt}^{R}(r_\alpha) = u_R \int \rho(r) V_{\alpha N}(r, r_\alpha) \mathrm{d}r. \tag{1}$$

Here $\rho(r)$ is the nuclear matter density of the nucleus and $u_R V_{\alpha N}(r, r_\alpha)$ is the real part of the effective interaction normalized by the parameter u_R to simulate rescattering and higher-order terms. The imaginary part of the potential is chosen to be proportional to the real part:

$$V_{opt}^{I}(r_\alpha) = i \frac{u_I}{u_R} V_{opt}^{R}(r_\alpha). \tag{2}$$

A choice of nuclei for which $\rho(r)$ is known allows the determination of u_R and u_I through optimization of the cross sections calculated using the optical potential. The averages of these values $\overline{u_R}$ and $\overline{u_I}$ give the normalization of the effective interaction,

$$V_{\alpha N}^{eff} = (\overline{u_R} + i\overline{u_I}) V_{\alpha N}(r, r_\alpha).$$

Adopting the effective interaction of Bernstein [27]),

$$V_{\alpha N}(r, r_\alpha) = V_0 \exp(-|r - r_\alpha|^2/\mu^2),$$

where $V_0 = -37$ MeV and $\mu = 2$ fm, we obtain:

$$\overline{u_R} = 0.70, \qquad \overline{u_I} = 0.35.$$

The interaction $V_{\alpha N}^{eff}$ is thus completely determined and an optical potential, which we will call the microscopic optical potential, can be calculated from relations (1) and (2).

This procedure does not take account explicitly of the exchange of nucleons between the incident particle and the target. The exact calculation is not possible but Schaeffer [12]) has proposed an approximated method allowing a rough evaluation of a one-nucleon exchange term. This has been relatively successfully applied by Satchler [11]) in the inelastic α-scattering of about 40 MeV. Following this method we added a Gaussian pseudo-potential to the previously determined effective interaction:

$$V'_{\alpha N} = -40 \exp(-|r - r_\alpha|^2/(1.31)^2).$$

[This term of course is not exactly simulated by $\overline{u_R}$ because it does not have the same range as $V_{\alpha N}$.]

When the total effective interaction $V_{\alpha N}+V'_{\alpha N}$ is normalized to give the best fit to the elastic scattering data we obtain the values:

$$\overline{u_{R\,ex}} = 0.64, \qquad \overline{u_{I\,ex}} = 0.34.$$

The importance of this effect can be seen in the uppermost part of fig. 2. For the 3^- level of ^{62}Ni three curves are drawn corresponding to the same nuclear model [quasiparticle wave functions of Gillet *et al.* [17])] and to the microscopic optical

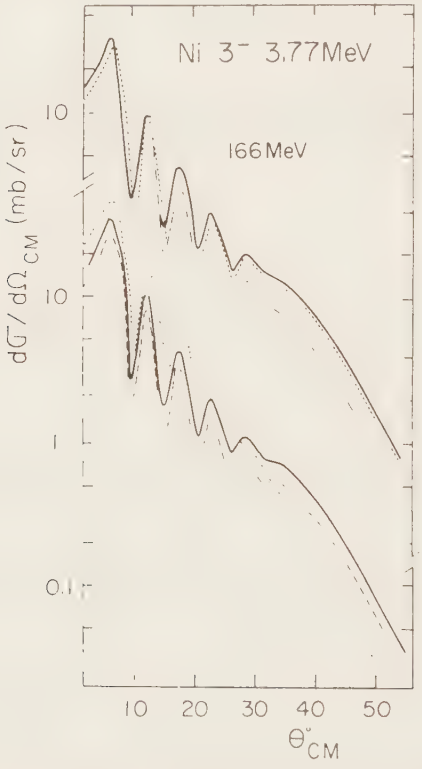

Fig. 2. Importance of the introduction of an exchange term and a Coulomb interaction for the 3^- 3.77 MeV level of ^{62}Ni (see text). In the lower part, only the exchange term is included, and the optical potential is changed.

potential. If one looks beyond 30° the lowest curve corresponds to a computation without exchange terms while the uppermost curve takes account of particle exchange in the way described above. That the difference between the two results increases with angle can be understood by the observation that the exchange term has a smaller

range than the principal part of the interaction so that their sum is not greatly modified at large radii (which corresponds classically to forward-angle scattering). For the 2^+ level of ^{12}C the introduction of an exchange term increases the cross section by about 35 %. The contribution is less important than at lower energy [4]).

TABLE 2

Optical model parameters

	V (MeV)	r_R (fm)	a_R (fm)	W (MeV)	r_I (fm)	a_I (fm)	χ^2/N
^{12}C (a)	100.9	1.21	0.76	14.7	1.86	0.48	2.50
(b)	85.0	1.34	0.70	17.7	1.77	0.52	3.20
^{28}Si	109.7	1.25	0.81	24.6	1.63	0.51	0.55
^{32}S	116.8	1.22	0.82	20.4	1.67	0.52	2.57
^{40}Ca	112.9	1.24	0.79	20.7	1.62	0.55	4.15
^{48}Ca	106.9	1.29	0.77	21.5	1.59	0.65	0.70
^{58}Ni	107.4	1.27	0.75	22.6	1.59	0.50	3.72
^{60}Ni	103.8	1.28	0.71	25.3	1.51	0.63	2.08
^{62}Ni	115.7	1.20	0.80	21.6	1.53	0.64	2.70
^{88}Sr	116.0	1.27	0.76	22.6	1.50	0.76	1.35
^{90}Zr	118.4	1.24	0.79	21.7	1.54	0.59	1.88
^{92}Mo	120.5	1.22	0.81	21.1	1.54	0.60	2.20
^{116}Sn	121.5	1.21	0.84	21.9	1.51	0.63	5.07
^{118}Sn	125.6	1.19	0.86	21.6	1.52	0.62	4.35
^{120}Sn	119.4	1.26	0.76	30.7	1.43	0.70	6.10
^{124}Sn	119.3	1.26	0.77	28.8	1.45	0.67	3.88
^{208}Pb	119.9	1.26	0.74	21.3	1.45	0.80	1.32

Parameters of the Woods-Saxon optical potential

$$V_{opt} = -V[1+\exp(r-r'_R)/a_R)]^{-1} - iW[1+\exp(r-r'_I)/a_I]^{-1},$$

with $r'_R = r_R A^{\frac{1}{3}}$ and $r'_I = r_I A^{\frac{1}{3}}$. Potentials depths are in MeV; radii and diffusenesses are in fm. The quantity

$$\frac{\chi^2}{N} = \frac{1}{N}\sum_N \left\{ \left| \left(\frac{d\sigma}{d\Omega}\right)_{exp.} - \left(\frac{d\sigma}{d\Omega}\right)_{th.} \right|^2 \Big/ \left(\Delta \frac{d\sigma}{d\Omega}\right)^2_{exp} \right\}$$

gives the validity of the fits.

Assuming that the nuclear effective interaction is now determined we can calculate the form factor for inelastic α-scattering. A more accurate value is obtained for proton configurations by adding the Coulomb interaction. It has been shown [25]) that a constant interaction inside 1 fm and corresponding to a term equal to 2.88 MeV/r beyond 1 fm gives a good approximation (this is consistent with the hypothesis of a uniform charged sphere). This interaction has been introduced in our computer code. The effect is not important as can be seen in the uppermost part of fig. 2 by comparison of the middle curve with the uppermost one. The Coulomb interaction being repulsive the cross section is somewhat reduced. The effect is more important at forward angles and, for the 3^- level of ^{208}Pb, the calculated cross section is reduced by about 30 % at the first maximum but only by 8 % beyond 30°.

3.2. DISTORTED WAVE OPTICAL POTENTIAL

By means of the relations (1) and (2) the optical potential and the effective interaction are determined in a mutually consistent fashion. However, it is also possible and of interest to study the effect of using different optical potentials for the determination of the distorted wave functions while keeping the same form factor.

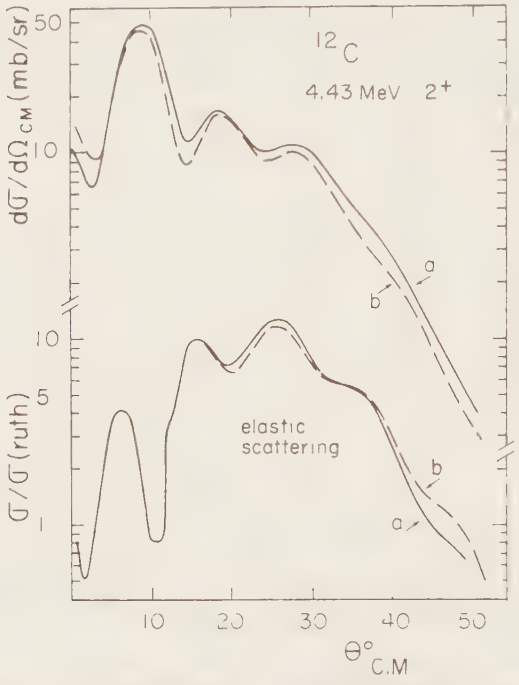

Fig. 3. Importance of the optical potential in elastic and inelastic α-particle scattering on the 2^+ 4.43 MeV state of ^{12}C. Curve (a) is for $V = 100.9$ MeV and curve (b) is for $V = 85$ MeV. The inelastic values are obtained with the wave functions of Gillet *et al.* [26]). The exchange term and the Coulomb interaction are included.

In the previous work of Tatischeff and Brissaud [1]), results for distorted waves produced by the microscopic potential and by a six-parameter macroscopic potential of Woods-Saxon shape were compared for the 2^+ and 3^- levels of ^{12}C and for the 2^+ level of natural Sn. Significant differences appear for the levels of ^{12}C when the optical potential is changed.

In this present work we give a more detailed and extensive study of this effect. A Woods-Saxon shape optical potential (WS potential) is determined by fitting elastic scattering data for all the nuclei for which the analysis of excited states is possible. The results are shown in table 2. The two different solutions obtained from ^{12}C elastic scattering are used for the computation of the inelastic scattering cross

sections for the 2^+, 4.43 MeV excited level. The results shown in fig. 3 indicate that the inelastic scattering is very sensitive to changes in the optical potential. [In both cases particle-hole wave functions of Gillet *et al.* [19]) were used.]

The modifications in theoretical cross section caused by changing the optical potential have also been studied for the 3^- level of ^{62}Ni. The lower part of fig. 2 shows the results obtained with the same form factor [from quasiparticle wave functions of Gillet *et al.* [17])] for three different optical potentials. The solid line is for the WS potential of table 2, the dotted line is for the microscopic potential and the dashed line is for an "average" WS potential, the parameters of which are the average values of the parameters of table 2 ($\overline{V} = -114$ MeV, $\overline{r_R} = 1.22$ fm, $\overline{a_R} = 0.79$ fm; $\overline{W} = -21.1$ MeV, $\overline{r_I} = 1.59$ fm and $\overline{a_I} = 0.60$ fm). The great difference between the two WS curves made us abandon this last average potential.

We will therefore present the results for the individual WS potentials, which should be the most correct, and the results given by the microscopic potential, which should be the most consistent because this potential is calculated with the same interaction for all nuclei.

In the figures there will generally be two curves : a solid line for calculations including the Coulomb interaction and the exchange term and using the Woods-Saxon optical potentials of table 2; and a dashed line for calculations done with the microscopic optical potential with neither an exchange term nor a Coulomb interaction. The latter curves are shown only in order to emphasize the magnitude of the effects discussed above. Although the conclusions would not be strongly modified if the dashed lines were considered, it is the solid-line curves which correspond to the best calculations.

4. Discussion of the results

4.1. GENERAL

The main features already observed in the inelastic scattering of low-energy α-particles [7,26–28]) are reproduced. The frequency of the oscillations increases with the target nucleus mass and the 2^+ and 3^- levels of the same nucleus follow the Blair phase rule in the diffraction region. The oscillations are always well described by the microscopic calculations – independently of the validity of the model tested – because they are only due to a geometric effect (nuclear radius) and not to details of nuclear structure. Fig. 4 shows different form factors calculated for ^{12}C. There are great differences between them, but if we exclude the imaginary part of the macroscopic form factor (the role of which is weak in a macroscopic analysis), both the microscopic form factors (for 2^+ and 3^- levels) and the real macroscopic form factor (derived from optical potential and corresponding to a first order collective excitation) have a very similar shape beyond $r_\alpha \approx 4$ fm. Because the α-particles are strongly absorbed, the inelastic scattering is not sensitive to a variation of form factor to within about 4 fm and the inelastic differential cross sections are well described by

these models with a normalization parameter β in the macroscopic analysis.

Generally, the solid line, corresponding to the WS optical potential, shows more oscillations beyond 30° than the dashed line, corresponding to the microscopic optical potential (the imaginary part of which is strong inside the nucleus). These oscillations are not often observed as can be seen for the 3^- (2.28 MeV) level of

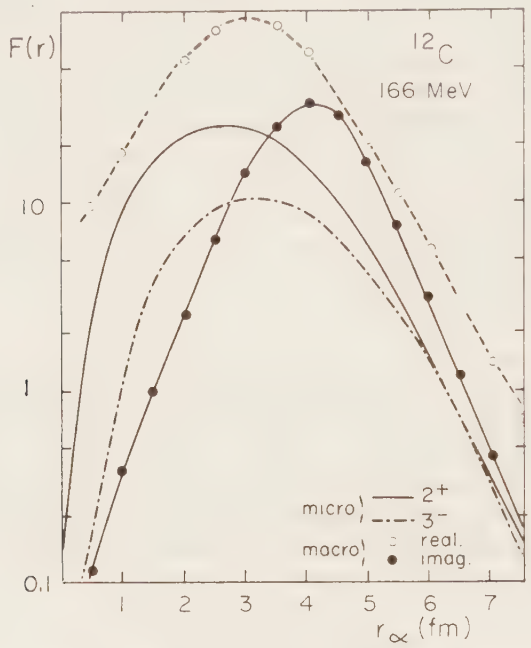

Fig. 4. Inelastic α-particle scattering form factors for ^{12}C. The microscopic form factors are calculated with the particle-hole wave functions of Gillet *et al.* [26]) for the 2^+ and 3^- levels. The macroscopic real and imaginary form factors are calculated with the collective model of Bassel *et al.* [7]).

^{92}Mo (fig. 11). Thus it might appear that the microscopic optical potential is more appropriate to the DWBA description of inelastic scattering. However some rescattering terms, which are not included in DWBA, may be more important at these angles than at smaller ones and account for the discrepancy between experiment and calculation, preventing any conclusion about the validity of each of these optical potentials.

4.2. LEVELS OF ^{12}C

Fig. 5 shows the angular distributions for the 2^+ and 3^- levels of ^{12}C with the inelastic electron scattering form factor measurements of Crannel *et al.* [29]). The curves represent our calculations.

For the 2^+ level, two wave functions have been tested. The calculations of Bouten *et al.* [18]) are done with a Volkov interaction in a projected Hartree-Fock model. This wave function gives a very good value of $B(\mathrm{E2})\uparrow$: $40\,e^2 \cdot \mathrm{fm}^4$ compared with $42\,e^2 \cdot \mathrm{fm}^4$ for the experimental value [30]). The results obtained for $|F(q)|^2_{\mathrm{el.}}$ and $(\mathrm{d}\sigma/\mathrm{d}\Omega)_{\alpha\alpha'}$ (curves (a) of fig. 5) are also in good agreement with the experimental

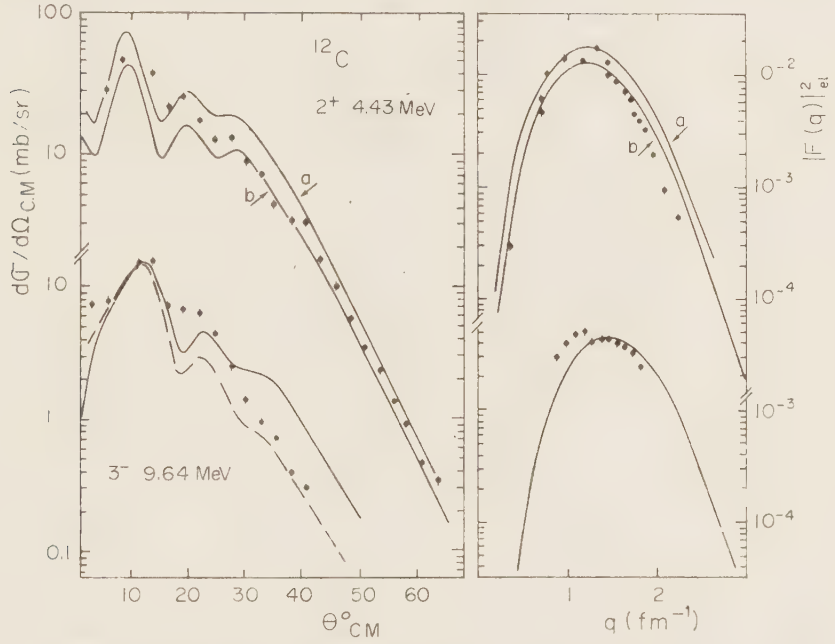

Fig. 5. Differential cross sections of 166 MeV α-particle inelastic scattering and form factors of inelastic electron scattering $|F(q)|_{\mathrm{el.}}^2$ for 2^+ and 3^- levels of ^{12}C.

values, giving nearly the right values for the maxima. Another wave function calculated by Gillet and Vinh Mau [26]) with a particle-hole model gives theoretical estimates of $|F(q)|^2_{\mathrm{el.}}$ and $(\mathrm{d}\sigma/\mathrm{d}\Omega)_{\alpha\alpha'}$ which are somewhat small (curves (b)). The theoretical value of $B(\mathrm{E2})\uparrow = 30.5\,e^2 \cdot \mathrm{fm}^4$ is also quite low.

For the 3^- level only the wave function of Gillet and Vinh Mau [26]) was tried. The theoretical value $B(\mathrm{E3})\uparrow = 343\,e^2 \cdot \mathrm{fm}^6$ is greater than the experimental value [31]) of $118\,e^2 \cdot \mathrm{fm}^6$. The calculated $|F(q)|^2_{\mathrm{el.}}$ and $(\mathrm{d}\sigma/\mathrm{d}\Omega)_{\alpha\alpha'}$ fit the experimental results reasonably. This has already been observed by Gillet and Melkanoff [32]) for $|F(q)|^2_{\mathrm{el.}}$.

4.3. LEVELS OF ^{24}Mg, ^{28}Si AND ^{32}S

Fig. 6 shows the experimental results for levels of ^{24}Mg, ^{28}Si and ^{32}S. The wave functions obtained with a deformed projected Hartree-Fock model [33]) have been

tested for 155 MeV proton scattering [13]). That model being different from the particle-hole and quasiparticle models used in this work, the corresponding wave functions have not been tested. There is no particle-hole wave function for ^{24}Mg since it has no closed shell (or subshell). For the first 2^+ levels of ^{28}Si and ^{32}S (1.78

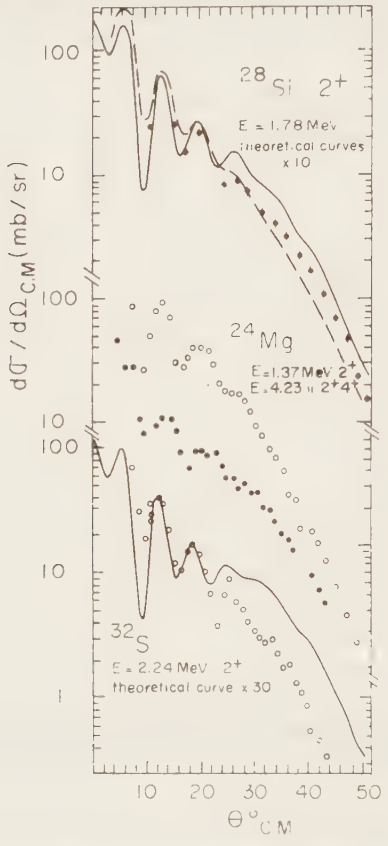

Fig. 6. Differential cross sections for 166 MeV α-particle inelastic scattering on ^{28}Si, ^{24}Mg and ^{32}S. The solid line corresponds to the calculation with the macroscopic optical potential; the Coulomb interaction and exchange term are included. The dashed curve is for the microscopic optical potential with neither the exchange term nor the Coulomb interaction.

and 2.24 MeV respectively) we have done calculations with the wave functions of Eisenberg [20]) obtained by TDA particle-hole calculations. Since the results for wave functions corresponding to $V_0 = -50$ MeV and $V_0 = -55$ MeV are almost indiscernible, only the values from $V_0 = -50$ MeV have been plotted in fig. 6. For ^{28}Si the fit is good if the curves are multiplied by a factor of 10. This normalization

is consistent with the factor 8 found for protons [13]). The comparison of the calculated $|F(q)|^2_{el.}$ with experiment [34, 35]) gives a factor of 9. An average experimental B(E2) value is found [36–38]) to be 7.2 times larger than the calculated value. For ^{32}S the situation is a little more complicated. If we choose $b = 1.7$ fm for the harmonic oscillator parameter [value used in the model calculation [20])], then the following

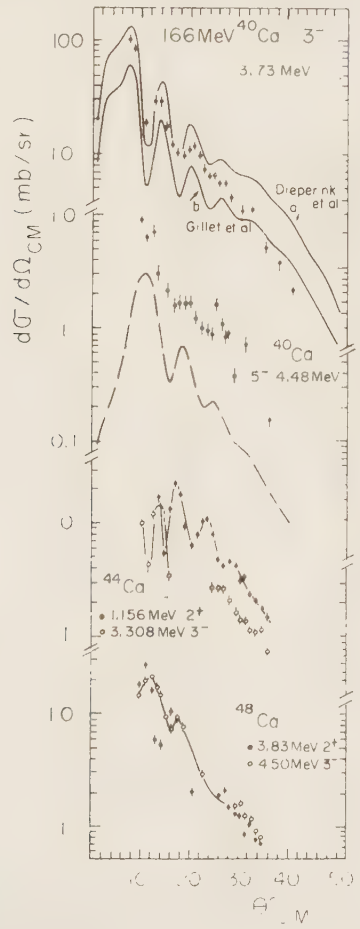

Fig. 7. Experimental and theoretical results for Ca isotopes. For ^{40}Ca the conventions are the same as in fig. 6. For ^{44}Ca and ^{48}Ca, the curves are drawn to guide the eye.

normalizations between experiments and calculations appear : 30 for α-particle scattering, 15 for B(E2) and 12 for $|F(q)|^2_{el.}$. This dispersion corresponds to the fact that, in addition to the deficiency of the model, we obtain with that value of b a bad

fit to the form factor shifted toward the small r-values (the large q-values). If we choose $b = 1.87$ fm [which corresponds to the charge rms radius [39])] then more consistent normalizations appear : 14.7 for α-particle scattering, 11 for $|F(q)|^2_{el.}$ and 10 for B(E2).

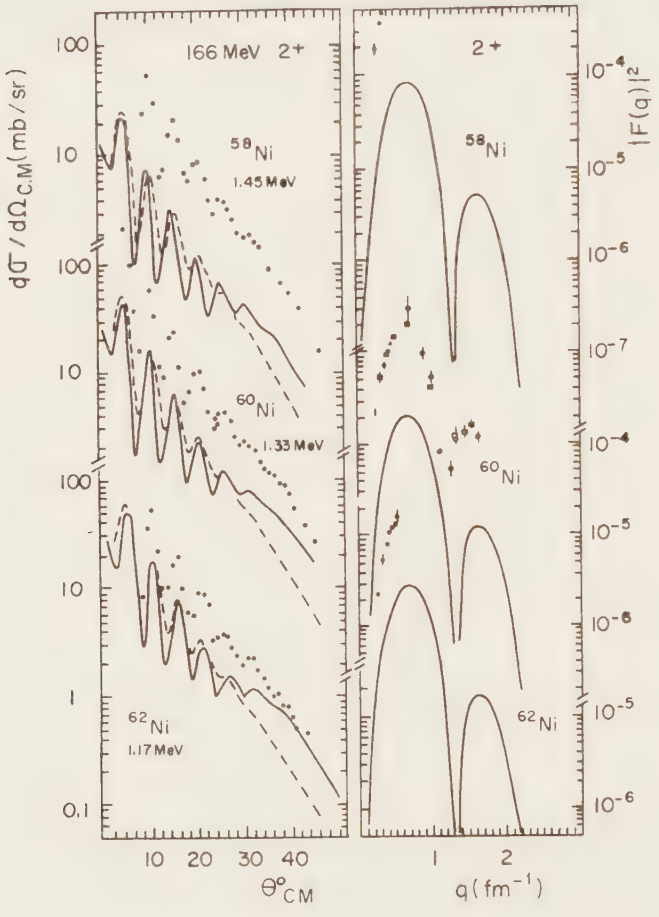

Fig. 8. Results for the 2^+ levels of Ni isotopes. Differential cross sections of 166 MeV α-particle inelastic scattering and form factors of inelastic electron scattering (same conventions as in fig. 6).

These results corroborate the well-known fact that TDA gives insufficiently collective wave functions and that protons and neutrons play equivalent roles in the excited states of $N = Z$ nuclei.

4.4. CALCIUM ISOTOPE LEVELS

Experimental and calculated results are shown in fig. 7. The 3^- level of ^{40}Ca has been studied in detail previously [2]); the computations were performed with the microscopic optical potential but with neither the exchange term nor the Coulomb interaction. Rejecting the wave functions of Stamp and Meyer [40]) and of Perez [41]) which really yield too small values, new calculations have been done: the result of Dieperink [42]) gives too large cross sections while that of Gillet and Sanderson [43]) with a CAL interaction shows cross sections which are too small.

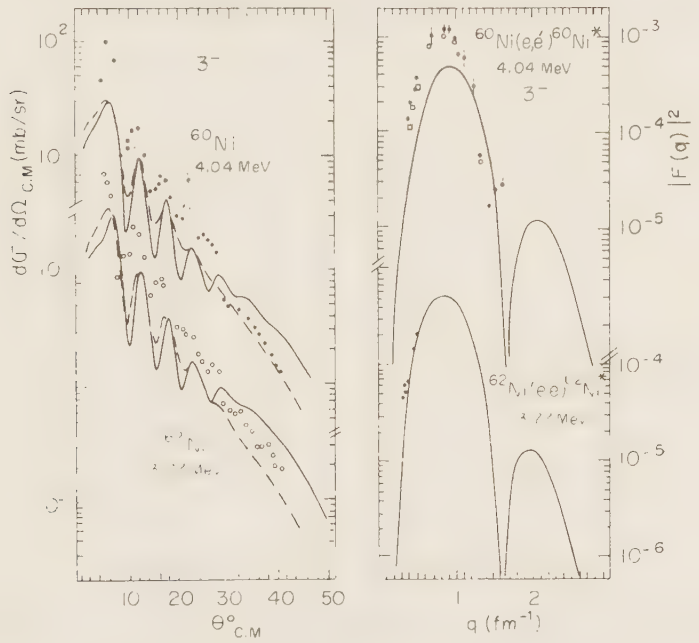

Fig. 9. The 3^- states of Ni isotopes. The conventions are those of fig. 6.

The dashed curve for the 5^- level of ^{40}Ca is that calculated with the model of Gillet and Sanderson.

Strongly excited states of ^{44}Ca and ^{48}Ca have been resolved in our most recent experiment ($\Delta E \approx 400$ keV). These levels have already been studied at a lower energy [44]). Angular distributions of the 2^+ $T = 0$ (1.156 MeV) level and the 3^- $T = 0$ (3.308 MeV) level of ^{44}Ca, and of the 2^+ $T = 0$ (3.83 MeV) level and the 3^- $T = 0$ (4.503 MeV) level of ^{48}Ca, are plotted in fig. 7. The lack of experimental points around 20° c.m. is due to ^{12}C and ^{16}O contamination in the ^{44}Ca and ^{48}Ca targets. The first maximum in the experimental angular distribution of the 3^- level

of ^{48}Ca is large and shows a shift from the predictions of the Blair phase rule. This was also the case at a lower energy in the work of Peterson [45]).

4.5. LEVELS OF Ni ISOTOPES

Measurements were performed with the three $^{58, 60, 62}$Ni isotopes. The 3^- level of ^{58}Ni could not be seen because our first experimental set-up did not detect sufficiently high excitation energies (4.50 MeV). Figs. 8 and 9 show respectively the

TABLE 3

Normalization factors for proton (λ_p), neutron (λ_n) and total (λ) amplitudes deduced from $B(E\lambda)_{exp.}$[a]) and (α, α') experiments and corresponding to GGR wave functions [17]) for nuclei with one closed shell

	J^π	E_x (MeV)	$B(E\lambda)_{exp.}$	$B(E\lambda)_{th.}$	$B_{th.}/B_{s.p.}$	λ_p	λ	λ_n
^{58}Ni	2^+	1.45	730	38.4	0.58	4.4	2.6	1.9
^{60}Ni	2^+	1.33	800	93.1	1.33	3.0	1.9	1.4
	3^-	4.04	22 000	8 140	5.42	1.7	1.5	1.4
^{62}Ni	2^+	1.17	890	128	1.76	2.6	1.7	1.4
	3^-	3.77	20 150	8 590	5.36	1.5	1.6	1.6
^{88}Sr	2^+	1.84	1 000	307	2.65	1.8	2.8	5.9
	3^-	2.74	80 600	45 300	14.05	1.3	1.4	1.5
^{90}Zr	2^+	2.18	450	155	1.29	1.7	3.5	8.8
	3^-	2.75	95 000	60 200	17.85	1.3	1.3	1.4
^{92}Mo	2^+	1.54	1 170	336	2.73	1.9	2.5	4.4
	3^-	2.88		77 500	22.00	1.0	1.2	1.5
^{116}Sn	2^+	1.27	2 120	73	0.44	5.4	2.1	1.2
	3^-	2.24	120 000	113 000	20.00	1.0	1.3	1.5
^{118}Sn	2^+	1.22	2 300	82	0.48	5.3	1.9	1.0
	3^-	2.30	110 000	122 000	21.00	1.0	1.3	1.7
^{120}Sn	2^+	1.18	2 200	83	0.47	5.2	2.0	1.2
	3^-	2.40	113 000	118 000	19.50	1.0	1.6	2.4
^{124}Sn	2^+	1.13	2 150	89	0.48	4.9	1.9	1.2
	3^-	2.53	76 000	63 000	9.80	1.1	2.1	3.3
^{208}Pb	3^-	2.62	650 000	576 000	32.00	1.1	1.0	1.0

[a]) Mean values corresponding to various experiments [30, 46, 49, 50, 55–62]). The λ_n are extracted from results taking into account WS optical potentials and exchange and Coulomb interactions.

experimental angular distributions of the 2^+ levels of $^{58, 60, 62}$Ni and the 3^- levels of $^{60, 62}$Ni together with the form factors determined from inelastic electron scattering [46, 47]). The curves show calculations using the wave functions of Gillet *et al.* [17]) corresponding to a RPA formalism using two-quasiparticle excitations for the open shell and particle-hole excitations for the core. (For the remainder of this work these wave functions will be referred to as GGR wave functions.)

The calculated $|F(q)|^2_{el.}$ are better for the 3^- states than for the 2^+ levels. The experimental points for both always lie above the calculated curves showing that the proton core is not described by a sufficient number of configurations. Confirmation is given by a comparison of the calculated electromagnetic transition rates with

the measured values (see table 3). Following the method described in the thesis of Schaeffer [4]) one can introduce a normalization coefficient λ_p so that:

$$\lambda_p^2 = B(E)_{exp.}/B(E)_{th.} \quad \text{or} \quad \lambda_p^2 = |F(q)|^2_{exp.}/|F(q)|^2_{th.}$$

at q_{max}, i.e. the value of q giving the first maximum of $|F(q)|^2$. Thus a value $\lambda_p > 1$ corresponds to a lack of proton configurations in the tested model. In the same way

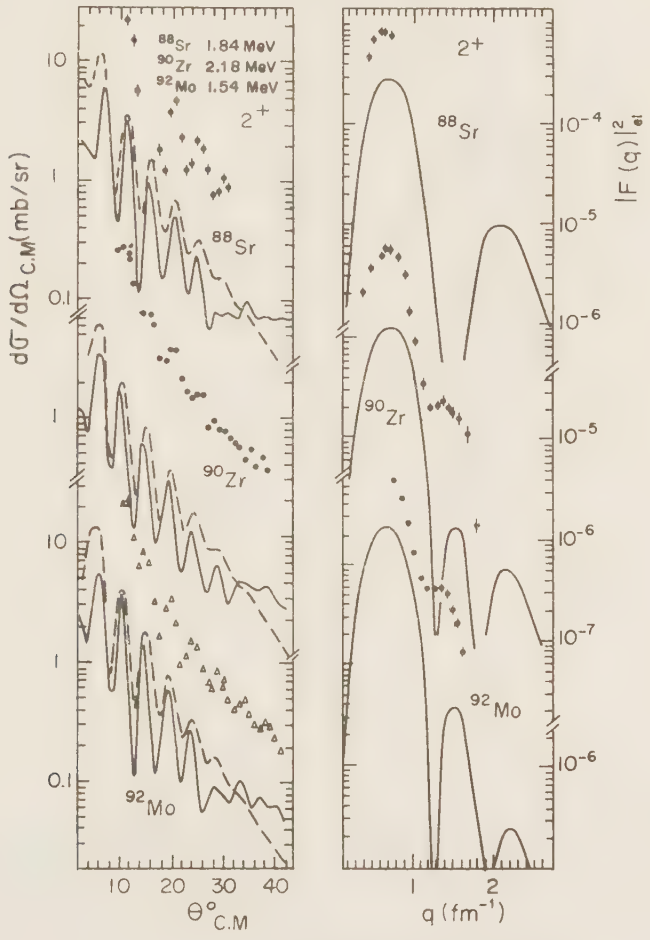

Fig. 10. The 2^+ levels of $N = 50$ nuclei using the conventions of fig. 6.

for α-particle inelastic scattering a total normalization coefficient λ is introduced as $\lambda^2 = (d\sigma/d\Omega)_{exp.}/(d\sigma/d\Omega)_{th.}$. If A_n and A_p are taken to be form factors corresponding respectively to neutron and proton configurations, one has $\lambda(A_n + A_p) = \lambda_n A_n + \lambda_p A_p$,

and λ_n can be deduced from (α, α') experiments allowing a quantitative test of neutron configurations of the studied model. It is obvious that such a relationship between λ, λ_n and λ_p is not rigorous. It assumes that the total neutron and proton form factors act coherently (which is true). It assumes also that these form factors

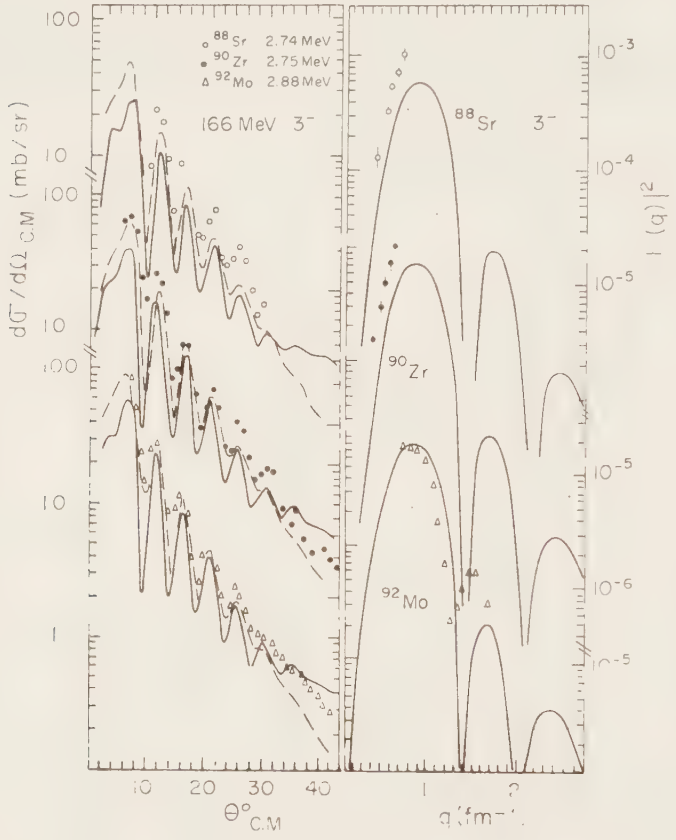

Fig. 11. The 3^- states of $N = 50$ nuclei with the conventions of fig. 6.

are proportional [which is only roughly true although the rather large value of the range of the α-particle-nucleon interaction (2 fm) has as a consequence a bringing together of the two form factors]. Thereby the λ_n values are given with an uncertainty of about $\pm$ 20 %.

The results corresponding to a computation with the WS optical potential are given in table 3. For the 2^+ state of $^{58, 60, 62}$Ni the deficiencies in proton configurations are given by $\lambda_p = 4.4$, 3.0 and 2.6 respectively while λ_n are 1.9, 1.4 and 1.4 for the neutron configurations. Thus for 2^+ levels it is clear that the model does not

include a sufficient number of proton core configurations. For the 3^- levels λ_p and λ_n are close. By comparison with the reduced transition rates obtained from lower-energy α-particle scattering [48]) the values $\lambda_p = 1.8$ and 1.1 are obtained for the 2^+ and 3^- levels of ^{60}Ni. All these results are in fairly good agreement with those obtained in the same way from (p, p′) experiments [4]).

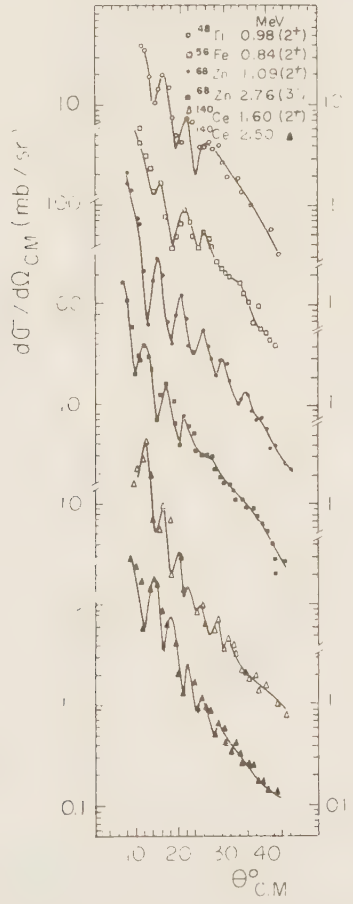

Fig. 12. Excited levels of ^{48}Ti, ^{56}Fe, ^{68}Zn and ^{140}Ce. The lines are drawn between the experimental points to guide the eye.

4.6. LEVELS OF $N = 50$ NUCLEI

The first 2^+ and 3^- levels of ^{88}Sr, ^{90}Zr and ^{92}Mo have been studied. The experimental results and the calculation with the GGR wave functions are shown in fig. 10 (for the 2^+ levels) and fig. 11 (for the 3^- levels). Calculated $|F(q)|^2_{el.}$ and experimental

results [49-51]) are also plotted in these figures. Once more there is a very good fit for the 3^- states but not for the 2^+ levels. The model wave functions do not now contain a sufficient number of neutron configurations (see λ_n in table 3) and it is again the closed-shell contribution which is underestimated. Similar results have been obtained from proton inelastic scattering [4, 5]).

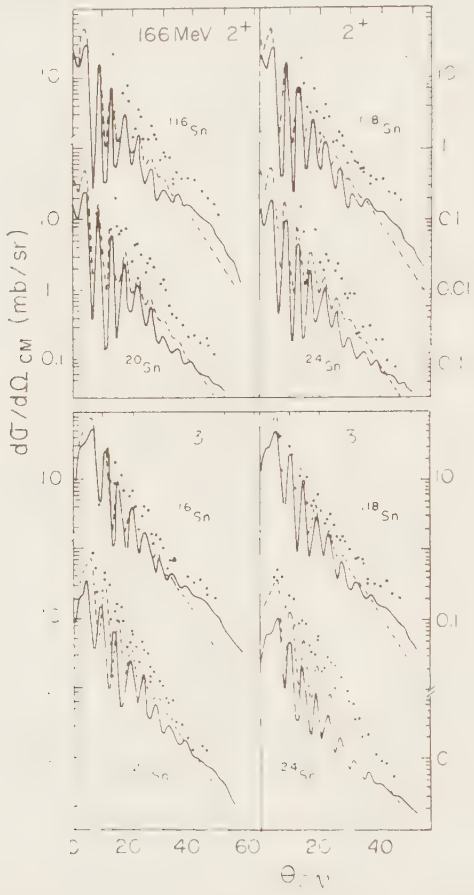

Fig. 13. Differential cross sections of α-particle inelastic scattering on the first 2^+ and 3^- levels of ^{116,118,120,124}Sn measured at 166 MeV. The full and dashed lines correspond respectively to the macroscopic and microscopic optical potentials.

4.7. INTERMEDIATE NUCLEI

The results corresponding to some levels of nuclei far from closed shells and for which there are no calculated microscopic wave functions are plotted in fig. 12.

A solid line is drawn between the experimental points to guide the eye. These include the nuclei ^{48}Ti, ^{56}Fe, ^{68}Zn and ^{140}Ce.

4.8. TIN ISOTOPE LEVELS

The first 2^+ and 3^- levels of ^{116,118,120,124}Sn have been investigated. A detailed discussion of the results has been presented previously [3]) together with the results on $|F(q)|^2_{el.}$ and $B(E\lambda)$. The cross sections calculated from the model of Arvieu *et al.* [52]), in which there are only excited neutron configurations, are much too small.

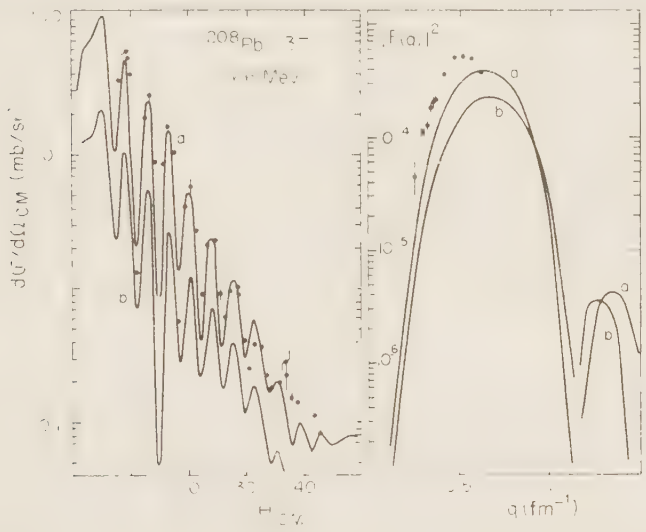

Fig. 14. Results obtained for the 3^- state of ^{208}Pb. Curves (a) are for the GGR model [17]) and curves (b) are for the Gillet *et al.* [15]) model. The electron scattering experimental points are taken from a publication of Ziegler *et al.* [56]).

Proton configurations checked by comparison of experiment with calculated values of reduced electromagnetic transition rates or with inelastic electron scattering form factors are found to be better using the model of Clement and Baranger [53]) for the 2^+ levels. For the 3^- levels the predictions of the model of Gillet *et al.* [17]) are best. Neutron configurations are better for the 2^+ than for the 3^- states. The λ_p and λ_n values (obtained from the macroscopic optical potential with exchange term and Coulomb interaction) are given in table 3 and show a defect in the description of the closed shell.

The experimental points for the 2^+ levels and the 3^- levels are shown in fig. 13 together with new computations including the exchange term and the Coulomb interaction with the macroscopic optical potential. Only the best results, those using Clement-Baranger wave functions for the 2^+ levels and GGR wave functions for

the 3^- levels, are plotted. The solid and dashed lines are obtained from macroscopic and microscopic optical potentials respectively (in the latter case, as previously, without exchange and Coulomb interaction terms). A phase shift sometimes appears between these two curves. This is particularly obvious for the 3^- level of ^{120}Sn (fig. 13). At 10° c.m. the calculated cross section corresponding to the WS optical potential presents a maximum quite in contradiction with the experimental data, while the microscopic optical potential gives a much better prediction.

On the other hand, the minima obtained with the WS potential are more marked than those obtained with the microscopic potential but the experimental angular resolution ($\Delta\theta \approx 0.7°$) is too poor to determine which theoretical result is the best.

4.9. THE ^{208}Pb NUCLEUS

Two different models of Gillet *et al.* [17, 54]) have been tested and the results have been discussed in a previous publication [2]). The curves obtained for $|F(q)|^2_{\text{el.}}$ and $(\mathrm{d}\sigma/\mathrm{d}\Omega)_{\alpha\alpha'}$ (fig. 14) show that the good fit previously given by the GGR quasiparticle model (curve (a)) is not destroyed by including an exchange term. Moreover the agreement with experimental data becomes better at large angles. The particle-hole model of Gillet *et al.* [54]) (curve (b)) still provides calculated cross sections which are too small. Experimental results of $|F(q)|^2_{\text{el.}}$ are extracted from ref. [56]).

5. Summary

The inelastic differential cross sections measured with 166 MeV α-particles have been used to test microscopic nuclear wave functions of the first collective states of several nuclei. The effective α-nucleon interaction is deduced from elastic scattering at the same energy. For 2^+ and 3^- states of ^{12}C and for the 3^- level of ^{40}Ca there exist satisfactory wave functions which give good agreement with the experimental $B(\mathrm{E}\lambda)$ and $|F(q)|^2_{\text{el.}}$ values. The good fits obtained for the inelastic α-particle scattering without any new parameter provide further confirmation of the method despite the approximations used: the Gaussian shape of the α-nucleon interaction, the normalization of $V^{\text{eff}}_{\alpha\text{N}}$ by means of $\overline{u_{\text{R}}}$ and $\overline{u_{\text{I}}}$ to simulate antisymetry and rescattering, the use of the same $V^{\text{eff}}_{\alpha\text{N}}$ to study the inelastic scattering for all the states of all nuclei investigated, and the choice of the optical potential.

Moreover these calculations have allowed an additional test of neutron configurations. For deformed nuclei such as ^{28}Si and ^{32}S, TDA calculations [20]) are found to give a bad description of collective states (a well-known fact) and the results differ from experimental data by one order of magnitude. For closed-shell nuclei the good results previously obtained [2]) have been improved at large angles by including an approximated exchange term. For doubly even one-closed-shell nuclei the most often used wave functions are those of Gillet *et al.* [17]) which give encouraging results. They take account of the core polarization through 1-particle-1-hole configurations. For the 3^- states the results are satisfactory but this model fails for the

2^+ states. The closed-shell configurations are found to be underestimated. To increase the core contribution it would be necessary to introduce 2p-2h and 4p-4h in the description of the ground and excited states of the nuclei studied. This is not yet possible but the method and the experimental results presented here would allow a valuable test for such further calculations.

It is a pleasure to thank the persons who have made this work possible: Dr. E. Baranger, M.-C. Bouten, V. Gillet, B. Giraud and M. Rho for the communication of unpublished wave functions; Messrs M. Bayon, J.-Y. Martel and F. Reide for the electronics and all the synchrocyclotron crew for their friendly cooperation. Special thanks are due to Dr. J. L. Foster for his help in the writing of this manuscript.

References

1) B. Tatischeff and I. Brissaud, Nucl. Phys. **A155** (1970) 89
2) B. Tatischeff, L. Bimbot, I. Brissaud, V. Comparat, A. Willis and M. K. Brussel, Phys. Rev. **C4** (1971) 494
3) I. Brissaud, B. Tatischeff, L. Bimbot, V. Comparat, A. Willis and M. K. Brussel, Phys. Rev. C6 (1972) 595
4) R. Schaeffer, thesis, Orsay, 1969; internal report CEA R 4000; Nucl. Phys. **A135** (1969) 231
5) J. Picard *et al.*, Nucl. Phys. **A128** (1969) 481;
J. Picard, thesis, Orsay, 1968; internal report CEA R 3856
6) Y. Terrien, Nucl. Phys. **A199** (1973) 65
7) R. H. Bassel *et al.*, Phys. Rev. **128** (1962) 2693
8) N. Austern and J. S. Blair, Ann. of Phys. **33** (1965) 15
9) C. G. Morgan and D. F. Jackson, Phys. Rev. **188** (1969) 1758
10) D. F. Jackson, Nuclear reactions (Methuen, London, 1970)
11) G. R. Satchler, Particles and Nuclei **2** (1971) 265
12) R. Schaeffer, Nucl. Phys. **A158** (1970) 321
13) A. Willis, B. Geoffrion, N. Marty, M. Morlet, C. Rolland and B. Tatischeff, Nucl. Phys. **A112** (1968) 417
14) V. Comparat, thesis, Orsay, 1970, unpublished
15) A. Willis, B. Geoffrion, N. Marty, M. Morlet, C. Rolland and B. Tatischeff, J. de Phys. **30** (1969) 13
16) I. Brissaud, Y. Le Bornec, B. Tatischeff, L. Bimbot, M. K. Brussel and G. Duhamel, Nucl. Phys. **A191** (1972) 145
17) V. Gillet, B. Giraud and M. Rho, Phys. Rev. **178** (1969) 1695, and to be published
18) M. Bouten and P. van Leuven, Ann. of Phys. **43** (1967) 421;
M. C. Bouten and M. Bouten, private communication
19) V. Gillet and N. Vinh Mau, Nucl. Phys. **54** (1964) 321
20) J. M. Eisenberg, private communication;
S. A. Farris and J. M. Eisenberg, Nucl. Phys. **88** (1966) 241
21) Y. Le Bornec, thesis, Orsay, 1971, unpublished
22) N. Frascaria, thesis, Orsay, 1969, unpublished
23) M. K. Brussel and J. H. Williams, Phys. Rev. **106** (1957) 286
24) S. Hayakawa *et al.*, Phys. Lett. **8** (1964) 330
25) Nguyen Van Giai, thesis, Orsay, 1972, unpublished
26) C. R. Bingham, H. L. Halbert and R. H. Bassel, Phys. Rev. **148** (1966) 1174; Nucl. Phys. **A143** (1970) 373
27) A. M. Bernstein, Advances in nuclear physics, vol. 3, ed. M. Baranger and E. Vogt (Plenum, New York, 1970)

28) G. Bruge, J. C. Faivre, H. Faraggi and A. Bussiere, Nucl. Phys. **A146** (1970) 597
29) H. Crannell *et al.*, Phys. Rev. **121** (1961) 283
30) P. H. Stelson and L. Grodzins, Nucl. Data Tables **1** (1965) 21
31) S. J. Skorka *et al.*, Nucl. Data **A2** (1966) 347
32) V. Gillet and M. A. Melkanoff, Phys. Rev. **133** (1964) B1190
33) G. Ripka, thesis, Orsay, 1968; internal report CEA R 3404
34) G. A. Savitskii *et al.*, Sov. J. Phys. **8** (1969) 376
35) Y. Horizawa *et al.*, Phys. Lett. **36B** (1971) 9
36) J. R. MacDonald *et al.*, Nucl. Phys. **A108** (1968) 6
37) S. J. Skorka and T. W. Retz-Schmidt, Nucl. Phys. **46** (1963) 225
38) D. S. Andreyev *et al.*, Nucl. Phys. **19** (1960) 411
39) G. C. Li and I. Sick, J. de Phys. **C5B** (1971) 275;
G. C. Li, I. Sick and M. R. Yearian, Phys. Lett. **37B** (1971) 282
40) A. P. Stamp and D. F. Meyer, Nucl. Phys. **82** (1966) 296
41) S. M. Perez, Nucl. Phys. **A136** (1969) 599
42) A. E. L. Dieperink, H. P. Leenhouts and P. J. Brussaard, Nucl. Phys. **A116** (1968) 556
43) V. Gillet and E. A. Sanderson, Nucl. Phys. **A91** (1967) 292
44) E. P. Lippincott and A. M. Bernstein, Phys. Rev. **163** (1967) 1170
45) R. J. Peterson, Phys. Rev. **140** (1965) B1479
46) M. A. Duguay *et al.*, Phys. Rev. **163** (1967) 1259
47) Y. Torizuka *et al.*, Phys. Rev. **185** (1969) 1499
48) M. Inoue, Nucl Phys. **A119** (1968) 449
49) J. B. Bellicard *et al.*, Nucl. Phys. **A143** (1970) 213
50) G. A. Peterson and J. Alster, Phys. Rev. **166** (1968) 1136
51) Phan Xuan Ho, J. B. Bellicard, Ph. Leconte and I. Sick, Proc. European Conf. on nuclear physics, Aix en Provence (1972) 167; and to be published
52) R. Arvieu, Ann. de Phys. **8** (1963) 407;
R. Arvieu, E. Baranger, M. Veneroni, M. Baranger and V. Gillet, Phys. Lett. **4** (1963) 119
53) D. M. Clement and E. Baranger, Nucl. Phys. **A120** (1968) 25;
T. T. S. Kuo, E. Baranger and M. Baranger, Nucl. Phys. **81** (1966) 241
54) V. Gillet, A. M. Green and E. A. Sanderson, Nucl. Phys. **88** (1966) 321
55) C. R. Gruhn *et al.*, Phys. Rev. Lett. **23** (1969) 1175
56) J. F. Ziegler and G. A. Peterson, Phys. Rev. **165** (1968) 1337
57) A. R. Barnett and W. R. Phillips, Phys. Rev. **186** (1969) 1205
58) P. Barreau and J. B. Bellicard, Phys. Rev. Lett. **19** (1967) 1444
59) T. H. Curtis, R. A. Eisenstein, D. W. Madsen and C. R. Bockelman, Phys. Rev. **184** (1969) 1162
60) J. Heisenberg *et al.*, Nucl. Phys. **A164** (1971) 353
61) F. R. Metzger, Phys. Rev. **103** (1956) 983; Nucl. Phys. **A158** (1970) 88, **A173** (1971) 141
62) P. H. Stelson and E. K. MacGowan, Nucl. Phys. **32** (1962) 258, **A108** (1968) 6

IV.4 - RESULTATS OBTENUS AVEC LE MODELE DE DIAGONALISATION EXACTE DANS UN ESPACE DE MODELE EN COUCHE.

La fonction d'onde d'Einsenberg (24) calculée dans un modèle particule-trou avec l'approximation de T.D.A. pour le niveau 2^+ E = 1.78 MeV du ^{28}Si a été testée. La courbe théorique se trouve en dessous de l'expérience d'un facteur 10 par suite du manque de collectivité de l'approximation utilisée. Les calculs faits avec le modèle de diagonalisation pour le ^{28}Si et le ^{24}Mg (25) sont présentés sur la figure 1.L'accord est excellent avec l'expérience comme le laisse supposer le bon accord entre les taux de transition électromagnétique et le bon fit des diffusions inélastiques d'électrons (28). Les noyaux

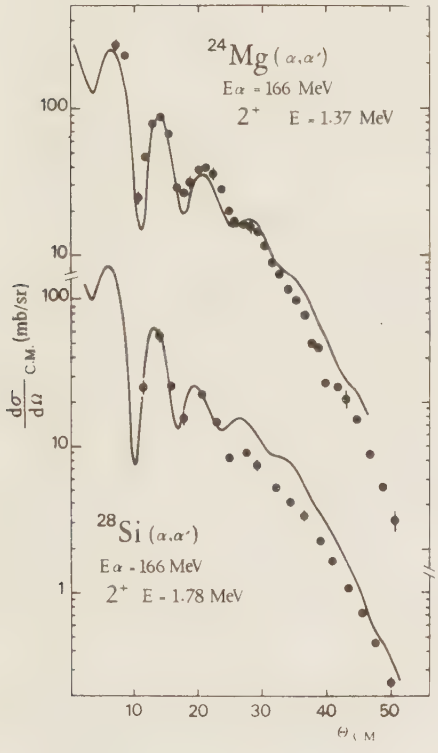

Figure 1 - Résultats obtenus avec le modèle de diagonalisation dans l'espace (sd) du modèle en couches pour les premiers niveaux excités du ^{24}Mg et du ^{28}Si.

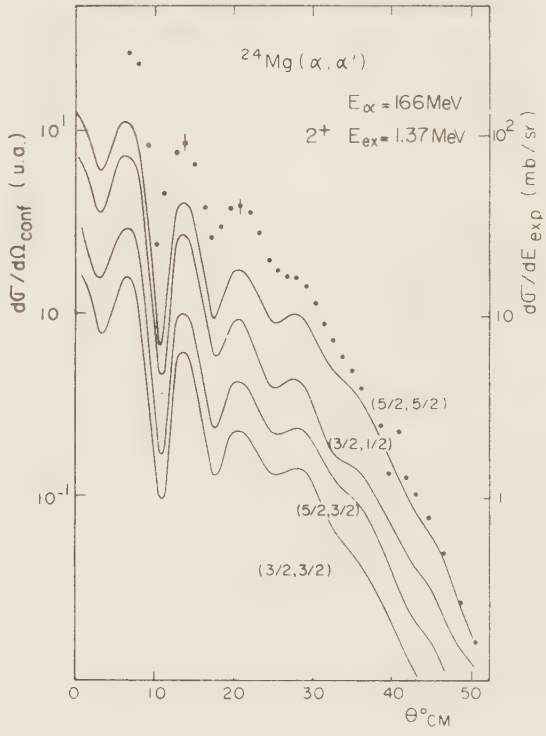

Figure 2 - Exemple des contributions individuelles de configurations intervenant dans un calcul de diagonalisation dans l'espace (sd) du modèle en couches.

de la couche (sd) sont décrits à partir d'un coeur inerte d'^{16}O.Pour le ^{24}Mg il intervient donc 8 repartitions possibles des 8 particules restantes dans les couches d5/2, s1/2 et d3/2. La figure 2 montre les résultats obtenus pour 4 configurations choisies arbitrairement. Les formes des distributions angulaires,surtout dans la zone diffractionnelle, sont toujours bien rendues. Il en est de même pour les quatre autres configurations. Notre méthode n'est donc sensible qu'aux poids et cohérence de chaque configuration. Cela est moins vrai aux grands angles mais c'est alors le principe de calcul DWBA qui devient incertain.

Dans ce modèle de diagonalisation il faut pour obtenir de bons résultats sur les propriétés électromagnétiques des noyaux dans la couche (sd) introduire des charges effectives de 1.5 pour les protons et 0.5 pour les neutrons. Cela peut se justifier par des considérations de polarisation (9), c'est-à-dire d'influence des nucléons du coeur sur les autres nucléons.

Dans les modèles de quasi-particules ou particule-trou par contre ces phénomènes sont supposés correspondre à des configurations faisant intervenir le coeur fermé. De même pour la diffusion inélastique de particule α il faut renormaliser d'une façon comparable pour reproduire les résultats expérimentaux. Le très bon accord obtenu prouve pour ce modèle que l'interaction résiduelle entre nucléons semble bien adaptée à cette région, que les estimations des polarisations sont correctes et que le calcul de diagonalisation exact donne de bonnes fonctions d'onde du fondamental et du premier état excité. Il serait intéressant de pouvoir étendre cette étude aux niveaux plus profonds.

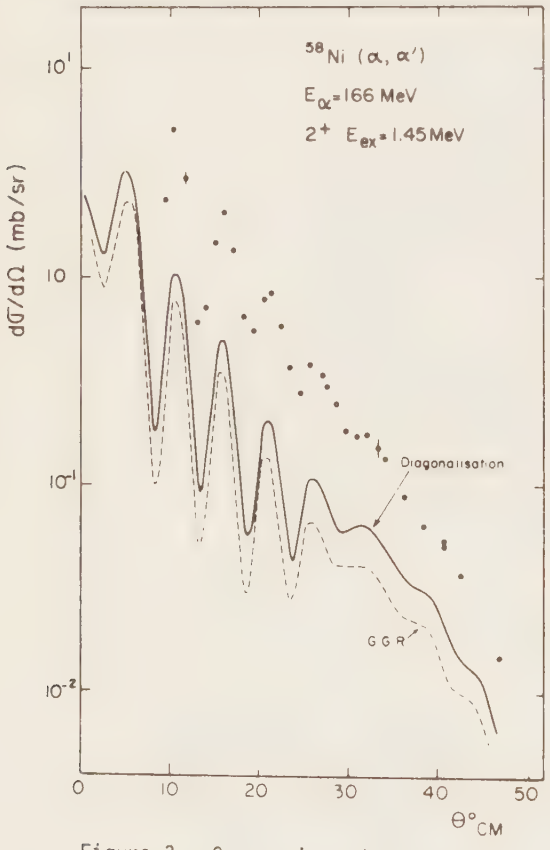

Figure 3 - Comparaison du modèle de diagonalisation et du modèle de quasi-particules traité par RPA, dans le cas du premier niveau excité du ^{58}Ni.

Pour le ^{58}Ni la situation est plus complexe. Le choix de l'espace du modèle en couches adéquat est important et le problème reste ouvert. Une étude précise de Zuker et Pasquini (19) montre qu'une diagonalisation dans l'espace formé des simples couches f7/2 et p3/2 semble être une très bonne approche pour la description de la transition entre le premier 2^+ et le fondamental mais cet espace est certainement trop restreint et une meilleure signification physique est obtenue en ajoutant à cet espace les possibilités de 3p-1h correspondant à 3 particules réparties dans les couches p3/2 , p1/2 et f5/2 avec un trou dans la couche f7/2 . Cet espace de 3p-1h donnant d'ailleurs à lui seul des fonctions raisonnables reproduisant le 1/3 des propriétés de transition si l'on utilise des charges effectives de 1.5 pour les protons et 0.5 pour les neutrons. Les fonctions d'onde correspondant à cet espace ont été introduites dans nos calculs avec les mêmes charges effectives et le résultat est présenté sur la figure 3. Le désaccord entre expérience et théorie est du même ordre que celui observé pour le taux de transition électromagnétique. Une légère amélioration est obtenue par rapport au résultat du calcul de RPA avec la méthode IGE (14) qui est aussi tracé sur la figure 3 mais il faut noter que dans ce calcul il n'y a aucune charge effective , les effets de polarisation étant supposés partiellement inclus dans les corrélations introduites par la R.P.A.

CONCLUSION

Parmi les réactions nucléaires, les diffusions élastiques et inélastiques sont certainement celles dont le mécanisme est relativement le plus simple. Ceci permet de développer plus loin les calculs et l'analyse des expériences que nous avons réalisées s'est donc montrée très enrichissante. Nous avons pu dans un premier temps établir une interaction effective α-nucléon pour des α de 166 MeV qui reproduit bien la diffusion élastique pour tous les noyaux à cette énergie. L'utilisation de cette interaction dans les calculs de sections efficaces inélastiques dans le cadre de la DWBA microscopique a permis une étude comparée de nombreux modèles nucléaires existants, apportant des informations intéressantes sur le rôle des configurations de neutrons, plus difficile à atteindre que celui des protons qui peut être étudié à partir des propriétés électromagnétiques du noyau. L'analyse précise du phénomène de diffusion inélastique et nos essais de calculs ont mis en évidence les résultats suivants :

i) La forme vers l'avant des sections efficaces différentielles de diffusion inélastique de particules α de 166 MeV n'est pas très caractéristique du modèle nucléaire à cause de la forte absorption des α et la structure nucléaire ne peut être testée que par la valeur absolue obtenue pour ces sections efficaces. Il en est évidemment de même à énergie plus basse. Il est possible qu'avec des α de plus grande énergie - moins absorbés - il devienne possible d'observer des variations de forme des sections efficaces pour différents modèles.

ii) Les valeurs absolues calculées varient par contre notablement d'un modèle à l'autre permettant des comparaisons directes parfois mal aisées à cause des différents paramètres intervenant dans les calculs.

L'introduction de différentes fonctions d'onde dans le calcul du facteur de forme a permis de tirer les conclusions suivantes :

i) Pour le ^{12}C la fonction d'onde de Bouten et al. (27) qui donne une très bonne valeur du taux de transition électromagnétique $B(E2)_{\downarrow}$ et du facteur de forme de diffusion inélastique d'électrons pour le 2^+ à 4.43 MeV restitue aussi très bien la diffusion inélastique d'α en valeur absolue, alors que la fonction d'onde de Gillet et N.Vinh Mau (26) donne pour ce 2^+ une valeur légèrement inférieure et pour le 3^- à 9.64 MeV un accord moyen avec l'expérience.

ii) Pour le ^{40}Ca la fonction d'onde de Gillet et Sanderson (20) utilisant l'approximation de RPA semble être une très bonne approche de la réalité. Les grandeurs examinées le prouvent. Ce modèle utilise une interaction (CAL) de forme gaussienne avec des fonctions d'onde de particule individuelle d'oscillateur harmonique . Les autres modèles existants pour le ^{40}Ca nous ont permis de comparer l'importance des divers ingrédients entrant dans les calculs :

1 - L'intensité de l'interaction nucléon-nucléon puisque le calcul de Dieperink et al.(21) utilisant le potentiel de Tabakin donne des résultats systématiquement trop grands du fait de la trop grande force de cette interaction.

2 - Le type de fonctions d'onde de particule individuelle . Les modèles de Stamp et Mayers (22) et de Perez (23) utilisent des fonctions d'onde d'orbite individuelle de type Saxon-Woods. Nous avons utilisé les mêmes fonctions d'onde dans le calcul du facteur de forme microscopique et montré ainsi que l'augmentation de section efficace qui serait attendue pour une réaction uniquement de surface n'apparaît pas à notre énergie.

3 - Les approximations de calcul puisque l'approximation de TDA utilisée par Perez (23) s'est révélée insuffisamment collective alors que la RPA donne dans le cas des fonctions d'onde de Gillet et al.(20) des résultats très acceptables.

iii) Pour le ^{208}Pb les deux modèles que nous avons comparés permettent de conclure que le nombre de configurations joue un grand rôle et qu'il est possible d'obtenir dans un formalisme de quasi-particules traité en RPA de très bonnes fonctions d'onde dispensant de l'emploi de charges effectives. La collectivité est augmentée par les corrélations introduites par la RPA dans le coeur fermé et qui jouent de façon cohérente. L'intensité de l'interaction nucléon-nucléon du modèle est déterminée par la méthode d'inversion des équations du gap à partir de données expérimentales.

iiii) Pour les isotopes de l'étain, la comparaison des modèles de Clément et Baranger (18) et de Gillet et al.(14) redonne les mêmes résultats à savoir l'avantage de la RPA sur la TDA, la meilleure détermination de l'interaction nucléon-nucléon par la méthode de l'IGE (bien que le potentiel Tabakin, s'il est renormalisé donne aussi de bons résultats (16, 19, 25)) et l'influence du nombre de configurations.

iiiii) Pour les isotopes $Z = 28$ et les isotones $N = 50$ les fonctions d'onde de Gillet et al.(14) ont donné de très bons résultats pour les états 3^- et de moins bons résultats pour les états 2^+ . La carence venait toujours de la description particule-trou de la couche fermée (protons pour les $^{58,60,62}Ni$ et neutrons pour le ^{88}Sr, le ^{90}Zr et le ^{92}Mo). Une extension récente des configurations permises pour ces particules ou ces trous a conduit à de très bons résultats pour l'analyse des réactions pp' à 35 MeV (7) ainsi qu'une amélioration des calculs de taux de transition électromagnétiques pour ces niveaux 2^+. Les mêmes observations seraient valables en diffusion (α,α') et permettent de supprimer les différences entre les niveaux 2^+ et 3^- sans faire appel à des configurations compliquées 4p-4t par exemple. Cependant un problème de convergence se pose si on autorise trop de couches pour former des états particule-trou ou de quasi-particules et l'on arrive à dépasser les valeurs expérimentales des observables. Cela peut être dû soit à une incertitude sur la force résiduelle nucléon-nucléon qui devient alors difficile à évaluer soit aux configurations plus complexes négligées qui devraient alors avoir une contribution destructive.

Donc d'une façon générale pour les noyaux à une ou deux couches fermées les premiers niveaux collectifs sont bien décrits dans un formalisme de trou-particule et de quasi-particule sans avoir besoin de charge effective en utilisant seulement un espace de configurations suffisamment grand et en faisant intervenir largement le coeur fermé.

Pour les noyaux de la couche (sd) il est nécessaire d'utiliser un autre modèle car on s'écarte trop des couches fermées pour que le modèle précédent soit justifiable. Un calcul de diagonalisation dans un espace de modèle en couches donne des résultats en très bon accord avec l'expérience pour les premiers niveaux 2^+ du ^{24}Mg et du ^{28}Si à condition d'introduire une charge effective pour toutes les quantités mesurées : taux de transition, facteurs de forme de diffusion inélastique d'électrons et sections efficaces différentielles de diffusion inélastique de particules α . C'est encourageant mais cela montre qu'il reste d'importants problèmes à résoudre:

1) Quelle est l'interaction entre nucléons qu'il faut introduire avant diagonalisation ?

2) Comment interviennent les couches "gelées", ou plus précisément quelle est la polarisation induite dans l'espace actif par les couches inactives, ou encore quel est l'effet de troncature de l'espace de diagonalisation ; comment cela peut-il jouer sur les différents processus étudiés et une normalisation par une charge effective multiplicative est-elle adaptée ?

3) Peut-on étendre ce calcul à des noyaux plus lourds en utilisant des méthodes de diagonalisation partielle qui permettent de calculer certains niveaux sans avoir besoin de construire des matrices de taille prohibitive et quelle est l'influence de ces techniques sur la description des niveaux ?

Il semble que la méthode d'analyse exposée ici, basée essentiellement sur la valeur absolue des sections efficaces différentielles de diffusion inélastique de particules α permette de tester rapidement ce genre de recherche avant d'avoir à améliorer et affiner le formalisme décrivant le processus de diffusion. Cependant compte tenu des approximations que contient notre analyse nous ne pourrons examiner que les caractéristiques des modèles apportant des variations notables de section efficace.

Côté expérimental enfin les recherches d'amélioration doivent porter sur la résolution en énergie afin de pouvoir étudier des niveaux plus profonds et moins collectifs des noyaux légers ou avoisinant les couches magiques, et peut être aussi dans un stade ultérieur faire des mesures précises sur quelques noyaux déformés en espérant d'ici là un progrès comparable des modèles nucléaires.

BIBLIOGRAPHIE

(1) A.BERNSTEIN, Advances in nuclear physics Vol.3(1969) 325 ed. M. Baranger et E. Vogt (Plenum, New York)

(2) R.H. BASSEL et al. Phys. Rev. 128(1962) 2693

(3) V. GILLET, Elements de physique nucléaire théorique. Cours CEN SACLAY (1964-65), Ecole d'Eté de Varenna (1965)

(4) D.F. JACKSON and V.K. KEMBHAVI, Phys. Rev. 178(1969) 1626

(5) R. SCHAEFFER, Thèse Orsay, Rapport CEA R4000(1969), Nucl. Phys. A135(1969) 231

(6) G.R. SATCHLER, Particles and Nuclei 2(1971) 265

(7) Y. TERRIEN, Nucl. Phys. A199(1973) 65 , Thèse Orsay (1973)

(8) Y. LE BORNEC, Thèse 3ème cycle Orsay (1971)

(9) N. FRASCARIA, Thèse 3ème cycle Orsay (1969)

(10) M.K. BRUSSEL and J.H. WILLIAMS, Phys. Rev. 106(1957) 286

(11) S. HAYAKAWA et al., Phys. Lett. 8(1964) 330

(12) N.K. GLENDENNING and M. VENERONI, Phys. Rev. 144(1966) 839

(13) R.SCHAEFFER, Nucl.Phys. A158(1970) 321

(14) V. GILLET, B. GIRAUD and M. RHO, Phys. Rev.178(1969) 1695

(15) J.B. FRENCH et al. Advances in nuclear physics, Vol.3(1969) 193

(16) E.U. BARANGER, Advances in nuclear physics Vol.4(1971) 261

(17) V. GILLET, A.M. GREEN and E.A. SANDERSON, Nucl. Phys. 88(1966) 321

(18) D.M. CLEMENT and E. BARANGER , Nucl. Phys. A120(1968) 25 ; T.T.S. KUO, E. BARANGER and M. BARANGER, Nucl. Phys. 81(1966) 241

(19) A.P. ZUKER et E. PASQUINI, Communication privée et Journées d'Etudes de Physique Théorique , AUSSOIS 1973 (à paraître)

(20) V. GILLET and A.E. SANDERSON, Nucl. Phys. A91(1967) 292

(21) A.E.L. DIEPERINK et al., Nucl. Phys. A116(1968) 556

(22) A.P. STAMP and D.F. MAYERS, Nucl. Phys. 82(1966) 296

(23) S.M. PEREZ, Nucl. Phys. A136(1969) 599

(24) J.M. EISENBERG, communication privée.
S.A. FARRIS and J.M. EISENBERG, Nucl. Phys. 88(1966) 241

(25) A.P. ZUKER et M. SOYEUR, communication privée ; Phys. Lett. 41B (1972) 135 ; M. SOYEUR, La Toussuire (1973)

(26) V. GILLET and N. VINH MAU, Nucl. Phys. 54(1964) 321

(27) M. BOUTEN and P. VAN LEUVEN, Ann. of Phys. 43(1967) 421
M.C. BOUTEN and M. BOUTEN, communication privée

(28) G. RIPKA, Lectures at the International Conference on Nuclear Structure Studies using Electron Scattering and Photo-reactions Sendai, Japan (1972)

(29) B. MOTTELSON, Scuola "Enrico Fermi" corso XV(1960) 44

(30) WONG et al. Nucl. Phys. A91 (1967) 433

(31) L. REICHSTEIN et Y.C. TANG, Nucl. Phys. A 139(1969) 144

DEUXIÈME THÈSE

Propositions données

Vu et approuvé :

Orsay, le 13 Novembre 19 73

Le Vice-Président du Centre d'Orsay :

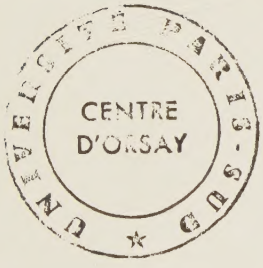

M. STEINBERG.